

# **COMPLEX WAVELET TRANSFORMS AND THEIR APPLICATIONS**

By

**Panchamkumar D SHUKLA**

For

**Master of Philosophy (M.Phil.)**

**2003**



Signal Processing Division  
Department of Electronic and Electrical Engineering  
University of Strathclyde  
Glasgow G1 1XW  
Scotland  
United Kingdom

# **COMPLEX WAVELET TRANSFORMS AND THEIR APPLICATIONS**

**A DISSERTATION  
SUBMITTED TO THE SIGNAL PROCESSING DIVISION,  
DEPARTMENT OF ELECTRONIC AND ELECTRICAL ENGINEERING  
AND THE COMMITTEE FOR POSTGRADUATE STUDIES  
OF THE UNIVERSITY OF STRATHCLYDE  
IN PARTIAL FULFILMENT OF THE REQUIREMENTS  
FOR THE DEGREE OF  
MASTER OF PHILOSOPHY**

By  
**Panchamkumar D SHUKLA**  
**October 2003**

The copyright of this thesis belongs to the author under the terms of the United Kingdom Copyright Act as qualified by University of Strathclyde Regulation 3.49. Due acknowledgement must always be made of the use of any material contained in, or derived from, this thesis.

© Copyright 2003

Dedicated to

my parents

**Rajeshwari and Dilip**

and to my wife

**Krupa**

## **Declaration**

I declare that this Thesis embodies my own research work and that is composed by myself. Where appropriate, I have made acknowledgements to the work of others.

Panchamkumar D SHUKLA

## Acknowledgements

First of all, I am very much thankful to my supervisor, Prof. John Soraghan, for his excellent guidance, support and patience to listen. His always-cheerful conversations, a friendly behaviour, and his unique way to make his students realise their hidden research talents are extraordinary. I heartily acknowledge his constant encouragements and his genuine efforts to explore possible funding routes for the continuation of my research studies. I am also thankful to him for giving me an opportunity to work as a Teaching Assistant for MSc courses.

My sincere acknowledgements to Dr. Kingsbury (Cambridge University), Prof. Selesnick (Polytechnic University, NY, USA) and Dr. Fernandes (Rice University, USA) for their useful suggestions on complex wavelets transforms, and answering my queries. I also acknowledge Dr. P. Wolfe (Cambridge University) for giving useful information about applying wavelets in audio signals processing. I extend my thanks to my senior research colleague Mr. Akbar for his encouragement and tips regarding statistical validation of my results.

I will always remember my friends Chirag, Ratnakar, Satya, (Flatmates), and Nandu, Santi, Stefan, Fadzli etc. (from Signal Processing Group) that I have made during my stay in Glasgow, and with whom I have cherished some joyous moments and refreshing exchanges.

I wish to extend my utmost thanks to my relatives in India, especially my parents, and parents' in-law for their love and continuous support. Finally, my thesis would have never been in this shape without lovely efforts from my wife Krupa. Her invaluable companionship, warmth, strong faith in my capabilities and me has always helped me to be assertive in difficult times. Her optimistic and enlightening boosts have made this involved research task a pleasant journey.

# Abstract

Standard DWT (Discrete Wavelet Transform), being non-redundant, is a very powerful tool for many non-stationary Signal Processing applications, but it suffers from three major limitations; 1) shift sensitivity, 2) poor directionality, and 3) absence of phase information. To reduce these limitations, many researchers developed real-valued extensions to the standard DWT such as WP (Wavelet Packet Transform), and SWT (Stationary Wavelet Transform). These extensions are highly redundant and computationally intensive. Complex Wavelet Transform (CWT) is also an alternate, complex-valued extension to the standard DWT. The initial motivation behind the development of CWT was to avail explicitly both magnitude and phase information. This thesis presents a detailed review of Wavelet Transforms (WT) including standard DWT and its extensions. Important forms of CWTs; their theory, properties, implementation, and potential applications are investigated in this thesis.

Recent developments in CWTs are classified into two important classes first is, Redundant CWT (RCWT), and second is Non-Redundant CWT (NRCWT). The important forms of RCWT include *Kingsbury's* and *Selesnick's* Dual-Tree DWT (DT-DWT), whereas the important forms of NRCWT include *Fernandes's* and *Spaendonck's* Projection based CWT (PCWT), and Orthogonal Hilbert transform filterbank based CWT (OHCWT) respectively. All recent forms of CWTs try to reduce two or more limitations of standard DWT with limited (or controllable) redundancy, or without any redundancy. Potential applications such as Motion estimation, Image fusion/registration, Denoising, Edge detection, and Texture analysis are suggested for further investigation with RCWT. Directional and phase based Compression is suggested for investigation with NRCWT.

Denoising and Edge detection applications are investigated with DT-DWTs. Promising results are compared with other DWT extensions, and with the classical approaches. After thorough investigations, it is proposed that by employing DT-DWT for Motion estimation and NRCWT for Compression might significantly improve the performance of the next generation video codecs.

# Acronyms

1-D	One Dimensional
2-D	Two Dimensional
FT	Fourier Transform
DFT	Discrete Fourier Transform
FFT	Fast Fourier Transform
WT	Wavelet Transform
DWT	Discrete Wavelet Transform
MRA	Multi-Resolution Analysis
PR	Perfect Reconstruction
WP	Wavelet Packet Transform
SWT	Stationary Wavelet Transform
TFR	Time Frequency Representation
STFT	Short Time Fourier Transform
AWT	Analog (Continuous) Wavelet Transform
CoWT	Continuous (Analog) Wavelet Transform
CWT	Complex Wavelet Transform
FIR	Finite Impulse Response
GUI	Graphical User Interface
SDW	Symmetric Daubechies Wavelets
RCWT	Redundant Complex Wavelet Transform
NRCWT	Non Redundant Complex Wavelet Transform
DT-DWT	Dual Tree Discrete Wavelet Transform
DT-DWT(K)	Kingsbury's Dual Tree Discrete Wavelet Transform
DT-DWT(S)	Selesnick's Dual Tree Discrete Wavelet Transform
DDWT	Double Density Discrete Wavelet Transform
DDTWT	Double Density Discrete Wavelet Transform
CDDWT	Complex Double Density Wavelet Transform
PCWT	Projection based Complex Wavelet Transform

PCWT-CR	Projection based Complex wavelet Transform with Controllable Redundancy
PCWT-NR	Projection based Complex wavelet Transform with No Redundancy
OHCWT	Orthogonal Hilbert Transform Filterbank based Complex Wavelet Transform
MSE	Mean Square Error
RMSE	Root Mean Square Error
SNR	Signal to Noise Ratio
PSNR	Peak Signal to Noise Ratio
SURE	Stein's Unbiased Risk Estimator
MRI	Magnetic Resonance Imaging
SAR	Synthetic Aperture Radar
HMM	Hidden Markov Model
STSA	Short Time Spectrum Attenuation
STWA	Short Time Wavelet Attenuation
MZ-MED	Mallat and Zong's Multiscale Edge Detection
ECG	Electrocardiogram
FMED	Fuzzy Multiscale Edge Detection
FWOMED	Fuzzy Weighted Offset Multiscale Edge Detection
DBFMED	Dual Basis Fuzzy Multiscale Edge Detection
CMED	Complex Multiscale Edge Detection
IMED	Imaginary Multiscale Edge Detection
FCMED	Fuzzy Complex Multiscale Edge Detection
SFCMED	Spatial Fuzzy Complex Multiscale Edge Detection
NFCMED	Non-decimated Fuzzy Complex Multiscale Edge Detection
CBIR	Content Based Image Retrieval
MSD	Mean Square Distance
FOM	Figure of Merit

# Table of Contents

<b>Declaration</b>	v
<b>Acknowledgement</b>	vi
<b>Abstract</b>	vii
<b>Acronyms</b>	viii
<b>Table of Contents</b>	x
<b>List of Figures</b>	xiv
<b>List of Table</b>	xviii
<b>1. Introduction</b>	1
1.1 Introduction.....	1
1.2 Motivation and Scope of Research.....	2
1.3 Organisation of Thesis.....	3
<b>2. Wavelet Transforms (WT)</b>	5
2.1 Introduction.....	5
2.1.1 Wavelet Definition.....	5
2.1.2 Wavelet Characteristics.....	6
2.1.3 Wavelet Analysis.....	6
2.1.4 Wavelet History.....	6
2.1.5 Wavelet Terminology.....	7
2.2 Evolution of Wavelet Transform.....	8
2.2.1 Fourier Transform (FT).....	8
2.2.2 Short Time Fourier Transform (STFT).....	8
2.2.3 Wavelet Transform (WT).....	10
2.2.4 Comparative Visualisation.....	11
2.3 Theoretical Aspects of Wavelet Transform.....	15
2.3.1 Continuous Wavelet Transform (CoWT).....	15
2.3.2 Discrete Wavelet Transform (DWT).....	16

<b>2.4 Implementation of DWT.....</b>	<b>18</b>
2.4.1 Multiresolution Analysis (MRA).....	18
2.4.2 Filterbank Implementation.....	20
2.4.3 Perfect Reconstruction (PR).....	22
<b>2.5 Extensions of DWT.....</b>	<b>24</b>
2.5.1 Two Dimensional DWT (2-D DWT).....	25
2.5.2 Wavelet Packet Transform (WP).....	29
2.5.3 Stationary Wavelet Transform (SWT).....	32
<b>2.6 Applications of Wavelet Transforms.....</b>	<b>33</b>
<b>2.7 Limitations of Wavelet Transforms.....</b>	<b>33</b>
<b>2.8 Summary.....</b>	<b>36</b>
<b>3. Complex Wavelet Transforms (CWT).....</b>	<b>38</b>
3.1 Introduction.....	38
3.2 Earlier Work.....	39
3.3 Recent Developments.....	40
3.4 Analytic Filter.....	43
3.5 Redundant Complex Wavelet Transforms (RCWT).....	45
3.5.1 Introduction.....	45
3.5.2 Filterbank Structure of Dual-Tree DWT based CWT.....	46
3.5.3 Kingsbury's Dual-Tree DWT (DT-DWT(K)).....	49
3.5.4 Selesnick's Dual-Tree DWT (DT-DWT(S)).....	56
3.5.5 Properties of DT-DWT.....	58
3.6 Non-Redundant Complex wavelet Transforms (NRCWT).....	61
3.6.1 Introduction.....	61
3.6.2 Projection based CWT (PCWT).....	62
3.6.2.1 Generic Structure.....	62
3.6.2.2 Theory of Complex Projection .....	63
3.6.2.3 Realisation of Complex Projection.....	64
3.6.2.4 Non-redundant Complex Projection.....	67
3.6.3 PCWT with Controllable Redundancy (PCWT-CR).....	69
3.6.4 PCWT with No-Redundancy (PCWT-NR).....	70

3.6.5 Orthogonal Hilbert Transform- Filterbank based CWT (OHCWT) .....	72
<b>3.7 Advantages and Applications of CWT.....</b>	<b>74</b>
<b>3.8 Summary.....</b>	<b>76</b>
<b>4. Application I – Denoising</b>	<b>80</b>
<b>4.1 Introduction.....</b>	<b>80</b>
<b>4.2 Wavelet Shrinkage Denoising.....</b>	<b>81</b>
4.2.1 Basic Concept.....	81
4.2.2 Shrinkage Strategies.....	82
<b>4.3 1-D Denoising.....</b>	<b>83</b>
4.3.1 Signal and Noise Model.....	83
4.3.2 Shrinkage Strategy.....	84
4.3.3 Algorithm.....	84
4.3.4 Performance Measure.....	85
4.3.5 Results and Discussion.....	85
<b>4.4 Audio Signal Denoising.....</b>	<b>92</b>
4.4.1 WT for Audio Signals.....	92
4.4.2 Denoising Model.....	92
4.4.3 Shrinkage Strategies.....	93
4.4.4 Performance Measure.....	94
4.4.5 Results and Discussion.....	94
<b>4.5 2-D Denoising.....</b>	<b>98</b>
4.5.1 Image and Noise Model.....	98
4.5.2 Shrinkage Strategy.....	98
4.5.3 Algorithm.....	98
4.5.4 Performance Measure.....	99
4.5.5 Results and Discussion.....	99
<b>4.6 Conclusion.....</b>	<b>117</b>
<b>5. Application II - Edge Detection</b>	<b>118</b>
<b>5.1 Introduction.....</b>	<b>118</b>

<b>5.2 Edge Detection Approaches.....</b>	<b>119</b>
5.2.1 Classical Approaches.....	119
5.2.2 Multiscale Approaches.....	120
<b>5.3 1-D Edge Detection.....</b>	<b>121</b>
5.3.1 Review of Existing Approaches.....	121
5.3.2 Edge Model.....	122
5.3.3 Multiscale Decomposition.....	122
5.3.4 FMED (Fuzzy Multiscale Edge Detection) Algorithms.....	123
5.3.5 CMED (Complex Multiscale Edge Detection) Algorithms.....	126
5.3.6 Performance Measure.....	127
5.3.7 Results and Discussion.....	128
<b>5.4 2-D Edge Detection.....</b>	<b>137</b>
5.4.1 Basic Approach.....	137
5.4.2 Algorithms.....	138
5.4.2.1 WT based Algorithm.....	138
5.4.2.2 CWT based Algorithm.....	138
5.4.3 Performance Measure.....	139
5.4.4 Results and Discussion.....	140
<b>5.5 Conclusion.....</b>	<b>142</b>
<b>6. Conclusions and Future Scope</b>	<b>143</b>
<b>6.1 Conclusions.....</b>	<b>143</b>
<b>6.2 Future Scope.....</b>	<b>146</b>
<b>Appendix A</b>	<b>148</b>
<b>Appendix B</b>	<b>150</b>
<b>Appendix C</b>	<b>152</b>
<b>References</b>	<b>153</b>

# List of Figures

Figure 2.1	Representation of a wave (a), and a wavelet (b).....	5
Figure 2.2	(a) Uniform division of frequency with constant bandwidth in STFT, (b) logarithmic division of frequency with constant-Q in WT.....	10
Figure 2.3	Comparative visualisation of time-frequency representation of an arbitrary non-stationary signal in various transform domains.....	12
Figure 2.4	Two signals $x_1(t)$ and $x_2(t)$ and their FFTs.....	13
Figure 2.5	Spectrograms and scalograms of signals $x_1(t)$ and $x_2(t)$ .....	14
Figure 2.6	Standard DWT on dyadic time-scale grid.....	17
Figure 2.7	Nested vector spaces spanned by scaling and wavelet basis.....	18
Figure 2.8	Two-channel, three-level analysis filterbank with 1-D DWT.....	21
Figure 2.9	Two-channel, three-level synthesis filterbank with 1-D DWT.....	21
Figure 2.10	A simple 2-channel filterbank model.....	22
Figure 2.11	Single level analysis filterbank for 2-D DWT.....	25
Figure 2.12	Multilevel decomposition hierarchy of an image with 2-D DWT..	26
Figure 2.13	Frequency plane partitioning with 2-D DWT.....	27
Figure 2.14	(a) Test image ‘Pattern’, (b) single level 2-D DWT decomposition of the same.....	28
Figure 2.15	Wavelet packet transform:(a) binary-tree decomposition, (b) time-frequency tiling of basis.....	30
Figure 2.16	Vector subspaces for WP.....	31
Figure 2.17	Uniform frequency division for WP.....	31
Figure 2.18	Flexible representation with WP: either with boxes or with circles	31
Figure 2.19	Three level decomposition with SWT.....	32
Figure 2.20	Shift-sensitivity of standard 1-D DWT.....	34
Figure 2.21	Directionality of standard 2D DWT.....	35
Figure 2.22	Presentation of (a) real, and (b) analytic wavelets.....	36
Figure 3.1	Hilbert Transform in (a) polar form, (b) frequency domain.....	43
Figure 3.2	Spectral representation of (a) original signal $f(t)$ , (b) analytic signal	

$x(t)$ .....	44
Figure 3.3 Interpretation of an analytic filter by 2-real filters.....	45
Figure 3.4 (a) Analysis filterbank for 1-D DT-DWT, (b) synthesis filterbank for 1-D DT-DWT.....	47
Figure 3.5 Filterbank structure for 2-D DT-DWT.....	48
Figure 3.6 Filterbank structure of <i>tree-a</i> of figure 3.5.....	49
Figure 3.7 Analysis tree using odd-even filters.....	50
Figure 3.8 Analysis tree using Q-shift filters.....	50
Figure 3.9 Modelling of DT-DWT(K) filter structure for deriving the shift-invariance constraints.....	51
Figure 3.10 Shift-invariance property of 1-D DT-DWT.....	59
Figure 3.11 Directionality of 2-D DT-DWT.....	59
Figure 3.12 3-D representation of 12 wavelets of DT-DWT.....	60
Figure 3.13 A complex wavelet as a quadrature combination of real and imaginary wavelets for 1-D DT-DWT.....	61
Figure 3.14 Generic implementation of PCWT.....	63
Figure 3.15 Realisable complex projection in softy-space.....	65
Figure 3.16 $ H^+(\omega) $ , the magnitude response of complex projection filter $h^+$ ....	66
Figure 3.17 Relation between function spaces.....	66
Figure 3.18 Non-redundant complex projection.....	67
Figure 3.19 The relationship between non-redundant mapping $\tilde{H}^+$ and Softy-space mapping $h^+$ .....	68
Figure 3.20 Implementation of realisable PCWT: PCWT-CR.....	69
Figure 3.21 Realisation of non-redundant mapping.....	70
Figure 3.22 3-band filterbank structure for 1-D OHCWT.....	72
Figure 3.23 Single level analysis filterbank equivalence of 1-D OHCWT for real signal as shown in figure (3.22).....	73
Figure 3.24 Three possible ways of implementing CWT for natural signals.....	79
Figure 4.1 Thresholding functions; (a) linear, (b) hard, (c) soft.....	82
Figure 4.2 (a) Denoising of signal ‘blocks’ with standard DWT, WP and SWT, (b) Denoising of signal ‘blocks’ with redundant CWT, DT-DWT(S) and DT-DWT(K).....	90
	91

Figure 4.3	Block diagram of STWA (short time wavelet attenuation) method..	92
Figure 4.4	Spectrograms of audio signals with standard DWT based denoising.....	96
Figure 4.5	Spectrograms of audio signals with DT-DWT(K) based denoising..	97
Figure 4.6	Conventional filtering methods for denoising of ‘Lenna’ image with reference to tables (4.7) and (4.8).....	107
Figure 4.7	Wavelet Transform based methods for denoising of ‘Lenna’ image with reference to tables (4.7) to (4.9).....	108
Figure 4.8	Threshold vs MSE for determination of optimum threshold value for all wavelet based methods. Image for denoising is ‘Lenna’ with reference to table (4.9).....	109
Figure 4.9	Conventional filtering methods for denoising of ‘Lenna’ image with reference to tables (4.10) and (4.11).....	110
Figure 4.10	Wavelet Transform based methods for denoising of ‘Lenna’ image with reference to tables (4.10) to (4.12).....	111
Figure 4.11	Threshold Vs MSE for determination of optimum threshold value for all wavelet based methods. Image for denoising is ‘Lenna’ with reference to table (4.12).....	112
Figure 4.12	DWT based denoising of ‘Lenna’ image using hard and soft thresholding with reference to tables (4.10) to (4.12).....	113
Figure 4.13	SWT based denoising of ‘Lenna’ image using hard and soft thresholding with reference to tables (4.10) to (4.12).....	114
Figure 4.14	DT-DWT(K) based denoising of ‘Lenna’ image using hard and soft thresholding with reference to tables (4.10) to (4.12).....	115
Figure 4.15	DT-DWT(S) based denoising of ‘Lenna’ image using hard and soft thresholding with reference to tables (4.10) to (4.12).....	116
Figure 5.1	Generalised step edge model.....	122
Figure 5.2	Cubic spline smoothing function $\phi(t)$ and its derivative $\psi(t) = d/dt(\phi(t))$ .....	123
Figure 5.3	1-D edge detection with FMED (‘cubic’) with $\sigma=0.6$ and $A=5$ .....	133
Figure 5.4	$J$ level wavelet coefficients (left) and their only positive parts (right) with FMED(‘cubic’) under the noise of $\sigma=0.6$ and slope of	

$\Delta=5$ .....	133
Figure 5.5 $J$ level fuzzy subsets (left) and their corresponding 2 to $J$ level fuzzy intersection (right) for the computation of minimum fuzzy set (right top) employing FMED ('cubic') under the noise of $\sigma =0.6$ and slope of $\Delta=5$ .....	134
Figure 5.6 1-D edge detection with CMED: $\sigma=0.6$ and $\Delta=5$ .....	134
Figure 5.7 $J$ level of decimated real and imaginary coefficients with CMED: $\sigma=0.6$ and $\Delta=5$ .....	135
Figure 5.8 $J$ level of decimated original and modified (inverted and left cyclic shift of 1 sample for levels 2 to $J$ ) real coefficients with CMED: $\sigma=0.6$ and $\Delta=5$ .....	135
Figure 5.9 $J$ level of interpolated modified real and original imaginary coefficients with CMED: $\sigma=0.6$ and $\Delta=5$ .....	136
Figure 5.10 $J$ level of complex magnitude coefficients (left) and fuzzy subsets of complex magnitudes (right). Top left shows detected edge with complex magnitude (at level 5) and top right shows detected edge with fuzzy subset (at level 5) employing CMED: $\sigma=0.6$ and $\Delta=5$ ...	136
Figure 5.11 2-D edge detection with conventional edge operators.....	140
Figure 5.12 2-D edge detection with wavelet based methods.....	141

# List of Tables

Table 3.1	Classification of complex wavelet transforms.....	42
Table 3.2	Comparative summary of complex wavelet transforms.....	78
Table 4.1	Effect of thresholding criteria for 1-D denoising.....	87
Table 4.2	Effect of different SNRi and MSEi for 1-D denoising.....	88
Table 4.3	Effect of low SNRi for 1-D denoising.....	89
Table 4.4	Effect of long-tap filters for 1-D denoising.....	89
Table 4.5	Effect of more number of decomposition levels for 1-D denoising.	89
Table 4.6	The MSE and SNR of denoised audio signal.....	95
Table 4.7	MSE for various denoising methods ( $\sigma=10$ ).....	101
Table 4.8	PSNR for various denoising methods ( $\sigma=10$ ).....	102
Table 4.9	Optimum threshold value for various denoising methods ( $\sigma=10$ )..	103
Table 4.10	MSE for various denoising methods ( $\sigma=40$ ).....	104
Table 4.11	PSNR for various denoising methods ( $\sigma=40$ ).....	105
Table 4.12	Optimum threshold value for various denoising methods ( $\sigma=40$ )..	106
Table 5.1	RMSE of various 1-D edge detection algorithms with $\Delta=0$ .....	130
Table 5.2	RMSE of various 1-D edge detection algorithms with $\Delta=1$ .....	130
Table 5.3	RMSE of various 1-D edge detection algorithms with $\Delta=3$ .....	131
Table 5.4	RMSE of various 1-D edge detection algorithms with $\Delta=5$ .....	131
Table 5.5	% Hit of various 1-D edge detection algorithms in varying slope and AWGN noise conditions.....	132

# Chapter 1:

## Introduction

### 1.1 Introduction

Fourier Transform (FT) with its fast algorithms (FFT) is an important tool for analysis and processing of many natural signals. FT has certain limitations to characterise many natural signals, which are non-stationary (e.g. speech). Though a time varying, overlapping window based FT namely STFT (Short Time FT) is well known for speech processing applications, a new time-scale based Wavelet Transform (WT) is a powerful mathematical tool for non-stationary signals.

WT uses a set of damped oscillating functions known as wavelet basis. WT in its continuous (analog) form is represented as CoWT. CoWT with various deterministic or non-deterministic basis is a more effective representation of signals for analysis as well as characterisation. Continuous wavelet transform (CoWT) is powerful in singularity detection. A discrete and fast implementation of CoWT (generally with real valued basis) is known as the standard DWT (Discrete Wavelet Transform).

With standard DWT, signal has a same data size in transform domain and therefore it is a non-redundant transform. Standard DWT can be implemented through a simple filterbank structure of recursive FIR filters. A very important property; Multiresolution Analysis (MRA) allows DWT to view and process

---

---

different signals at various resolution levels. The advantages such as non-redundancy, fast and simple implementation with digital filters using micro-computers, and MRA capability popularised the DWT in many signal processing applications since last decade. Many researches have successfully applied and proved the advantages of DWT for signal denoising and compression in a number of diverse fields.

## 1.2 Motivation and Scope of Research

Though standard DWT is a powerful tool for analysis and processing of many real-world signals and images, it suffers from three major disadvantages, (1) Shift-sensitivity, (2) Poor directionality, and (3) Lack of phase information. These disadvantages severely restrict its scope for certain signal and image processing applications (e.g. edge detection, image registration/segmentation, motion estimation).

Other extensions of standard DWT such as Wavelet Packet Transform (WP) and Stationary Wavelet Transform (SWT) reduce only the first disadvantage of shift-sensitivity but with the cost of very high redundancy and involved computation. Recent research suggests the possibility of reducing two or more above-mentioned disadvantages using different forms of Complex Wavelet Transforms (CWT) [93,98,101,103] with only limited (and controllable) redundancy and moderate computational complexity.

The objectives of research in this thesis include:

1. Review of Wavelet Transforms: History, Theory, Various forms of WTs and their properties, and Applications.
2. Thorough study of Complex Wavelet Transforms (CWT): History, Theory, Various forms, Properties, and Investigations for potential applications.

- 
- 3. Comprehensive and collective analysis of recently proposed CWTs, and a comparison with existing forms of WTs.
  - 4. Implementation: Practical realisation of various CWTs and WTs through individual Matlab simulations. Review of selected applications like denoising and edge detection. Individual implementation of selected application with suitable WTs and CWTs. Incorporating novel ideas culminating in the original and novel outcomes. Statistical validation of original results.
  - 5. Comparative study: Critical evaluation of the original results obtained from individual implementations of existing and novel algorithms for selected applications using various forms of WTs and CWTs.

### **1.3 Organisation of Thesis**

The thesis is organised in to six chapters as follows:

Chapter 1 is an introduction with the comprehensive description of the central theme of this research. A systematic organisation of thesis is also presented.

Chapter 2 is a detailed review of Wavelet Transforms (WT). A brief history, evolution and fundaments of wavelet transforms are presented. The structure of fast and reversible implementation of standard DWT (Discrete wavelet Transform) through filterbank is explained. Concept of separable and multidimensional DWT as an extension of 1-D DWT is described. Other important variants of WTs like SWT (Stationary wavelet Transforms) and WP (Wavelet Packet Transforms) with their properties are reviewed. Finally, the applications and limitations of the popular standard DWT are enlisted.

Chapter 3 is the heart of this thesis. It presents a thorough study of CWT (Complex wavelet Transforms). The history, evolution and recent advances in the field of CWTs are comprehensively analysed. Recent developments and newer

extensions of CWTs with their theories, structures and properties are critically explored. Advantages and limitations of various CWTs are analysed through individual implementations and simulations. Potential applications of various forms of CWTs are suggested after thorough investigations.

Chapter 4 and chapter 5 are about practical implementations and simulations carried out with various WTs (reviewed in chapter 2) and CWTs (investigated in chapter 3). Key signal and image processing applications such as Denoising and Edge-detection are thoroughly reviewed. In chapter 4, Denoising application is explored in both 1-D and 2-D cases with WTs, and redundant CWTs (i.e. DT-DWT).

In chapter 5, Edge-detection application is explored in similar manner. Individual simulations with WTs and CWTs algorithms are carried out for the mentioned applications and performances are compared with other conventional algorithms. Some novel ideas are incorporated in existing algorithms and available results are presented after statistical validation.

Chapter 6 is the summary of investigation on ‘complex wavelet transforms and their applications’. The advantages and limitations of CWTs over other WTs for the selected applications (namely denoising and edge-detection) are concluded. Future directions are given for further investigations using CWTs in other relevant applications (such as Motion estimation and Compression for video coding).

# Chapter 2:

## Wavelet Transforms (WT)

### 2.1 Introduction

#### 2.1.1 Wavelet Definition

A ‘wavelet’ is a small wave which has its energy concentrated in time. It has an oscillating wavelike characteristic but also has the ability to allow simultaneous time and frequency analysis and it is a suitable tool for transient, non-stationary or time-varying phenomena [1,2].

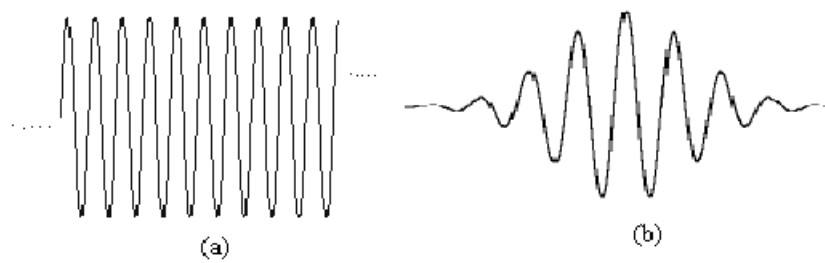


Figure 2.1: Representation of a wave (a), and a wavelet (b)

### 2.1.2 Wavelet Characteristics

The difference between wave (sinusoids) and wavelet is shown in figure (2.1). Waves are smooth, predictable and everlasting, whereas wavelets are of limited duration, irregular and may be asymmetric. Waves are used as deterministic basis functions in Fourier analysis for the expansion of functions (signals), which are time-invariant, or stationary. The important characteristic of wavelets is that they can serve as deterministic or non-deterministic basis for generation and analysis of the most natural signals to provide better time-frequency representation, which is not possible with waves using conventional Fourier analysis.

### 2.1.3 Wavelet Analysis

The wavelet analysis procedure is to adopt a wavelet prototype function, called an ‘analysing wavelet’ or ‘mother wavelet’. Temporal analysis is performed with a contracted, high frequency version of the prototype wavelet, while frequency analysis is performed with a dilated, low frequency version of the same wavelet [12]. Mathematical formulation of signal expansion using wavelets gives Wavelet Transform (WT) pair, which is analogous to the Fourier Transform (FT) pair. Discrete-time and discrete-parameter version of WT is termed as Discrete Wavelet Transform (DWT). DWT can be viewed in a similar framework of Discrete Fourier Transform (DFT) with its efficient implementation through fast filterbank algorithms similar to Fast Fourier Transform (FFT) algorithms [1].

### 2.1.4 Wavelet History

Wavelet theory has been developed as a unifying framework only recently, although similar ideas and constructions took place as early as the beginning of the century [3,4]. The idea of looking at a signal at various scales and analyzing it with various resolutions has in fact emerged independently in many different fields of mathematics, physics and engineering. In mid-eighties, researchers of the ‘French school’ [5-7] built strong mathematical foundation around the subject and named

their work ‘ondelettes’ (wavelets). Brief history of early research on wavelets can be found in [8]. A very good overview of the philosophy of wavelet analysis and history of its development is given in [9]. Introductory tutorial articles on wavelets are [10-13]. Readable books on wavelet theory and applications are [1,2,14-25].

### 2.1.5 Wavelet Terminology

The applications of wavelets to signal processing can be attributed to [26-27]. Wavelet theory is closely related to filter bank theory [15,28]. In [28] the concept of Multiresolution Analysis (MRA) was introduced leading to an implementation of DWT with octave-band filterbank, while [26] showed that under certain condition filter bank converges to orthonormal wavelet bases. Generation of various wavelet families (Daubechies, Coiflets, Symlets etc.) through modifications in parameterization of wavelets availed some useful properties such as compact-support, symmetry, regularity, and smoothness [24].

The wavelet systems with biorthogonality gives flexibility [29,30], overcompleteness removes certain disadvantages of DWT [24,31], and Perfect Reconstruction (PR) filterbank implementation is utmost essential for retrieval of original signal [15,32-33]. Wavelet Packet Transform (WP) is an efficient decomposition of filterbank [65-68]. All these newer techniques have broaden the scope of wavelets in various signal and image processing applications [11,20,34-36].

Section 2.2 leads towards the evolution of wavelet transform through various time-frequency representations. Section 2.3 describes the theoretical aspects of the WT in continuous and discrete domains, whereas section 2.4 deals with the implementation aspects of the WT. Section 2.5 introduces the useful extensions of generic WT in discrete domain. Sections 2.6 and 2.7 are about the applications and limitations of various WTs. Section 2.8 is a summary highlighting the need for an alternate form of WT namely Complex Wavelet Transform (CWT).

## 2.2 Evolution of Wavelet Transform

The need of simultaneous representation and localisation of both time and frequency for non-stationary signals (e.g. music, speech, images) led toward the evolution of wavelet transform from the popular Fourier transform. Different ‘time-frequency representations’ (TFR) are very informative in understanding and modelling of WT [37-39].

### 2.2.1 Fourier Transform (FT)

Fourier transform is a well-known mathematical tool to transform time-domain signal to frequency-domain for efficient extraction of information and it is reversible also. For a signal  $x(t)$ , the FT is given by:

$$X(f) = \int_{-\infty}^{\infty} x(t) e^{-j2\pi f t} dt \quad (2.1)$$

Though FT has a great ability to capture signal’s frequency content as long as  $x(t)$  is composed of few stationary components (e.g. sine waves). However, any abrupt change in time for non-stationary signal  $x(t)$  is spread out over the whole frequency axis in  $X(f)$ . Hence the time-domain signal sampled with Dirac-delta function is highly localised in time but spills over entire frequency band and vice versa. The limitation of FT is that it cannot offer both time and frequency localisation of a signal at the same time.

### 2.2.2 Short Time Fourier Transform (STFT)

To overcome the limitations of the standard FT, *Gabor* [39] introduced the initial concept of Short Time Fourier Transform (STFT). The advantage of STFT is that it uses an arbitrary but fixed-length window  $g(t)$  for analysis, over which the actual nonstationary signal is assumed to be approximately stationary. The STFT decomposes such a pseudo-stationary signal  $x(t)$  into a two dimensional time-

frequency representation  $S(\tau, f)$  using that sliding window  $g(t)$  at different times  $\tau$ . Thus the FT of windowed signal  $x(t) g^*(t-\tau)$  yields STFT as:

$$\text{STFT}_x(\tau, f) = \int_{-\infty}^{\infty} x(t) g^*(t-\tau) e^{-j2\pi f t} dt \quad (2.2)$$

Filterbank interpretation is an alternative way of seeing ‘windowing of the signal’ viewpoint of STFT [41,42]. With the modulated filterbank, a signal can be seen as passing through a bandpass filter centred at frequency  $f$  with an impulse response of the window function modulated to that frequency. The division of frequency is uniform as shown in figure (2.2 a).

From this dual interpretation, a possible drawback related to time-frequency resolution of STFT can be shown through ‘Heisenberg’s uncertainty principle’ [2,43,44]. For a window  $g(t)$  and its Fourier transform  $G(f)$ , both centred around the origin in time as well as in frequency, that is satisfying  $\int |t| |g(t)|^2 dt = 0$  and  $\int |f| |G(f)|^2 df = 0$ . Then the spreads in time and frequency are defined as:

$$\begin{aligned} \Delta_t^2 &= \frac{\int_{-\infty}^{\infty} t^2 |g(t)|^2 dt}{\int_{-\infty}^{\infty} |g(t)|^2 dt} \\ \Delta_f^2 &= \frac{\int_{-\infty}^{\infty} f^2 |G(f)|^2 df}{\int_{-\infty}^{\infty} |G(f)|^2 df} \end{aligned} \quad (2.3)$$

Thus, the time-frequency resolution for STFT is lower bounded by their product as:

$$\text{Time-Bandwidth product} = \Delta_t \Delta_f \geq \frac{1}{4\pi} \quad (2.4)$$

Once a window has been chosen for STFT, the time-frequency resolution is fixed over the entire time-frequency plane because the same window is used at all frequencies. There is always a trade off between time resolution and frequency resolution in STFT.

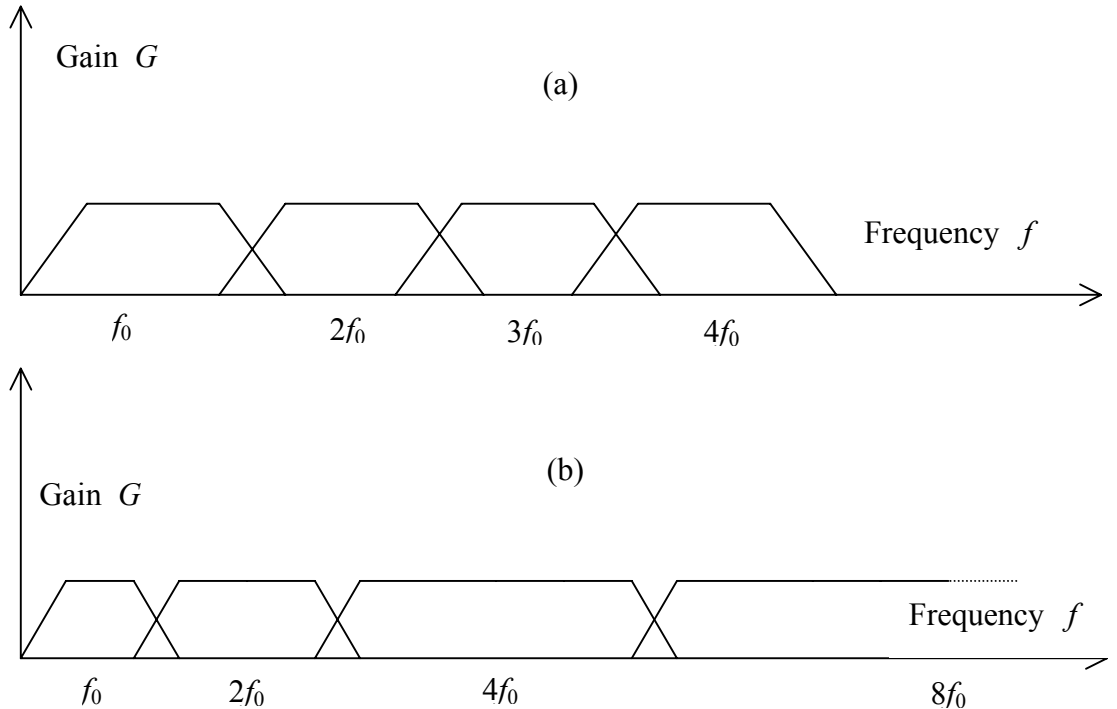


Figure 2.2: (a) Uniform division of frequency with constant bandwidth in STFT, (b) logarithmic division of frequency with constant-Q in WT

### 2.2.3 Wavelet Transform (WT)

Fixed resolution limitation of STFT can be resolved by letting the resolution  $\Delta_t$  and  $\Delta_f$  vary in time-frequency plane in order to obtain Multiresolution analysis. The Wavelet Transform (WT) in its continuous (CoWT) form provides a flexible time-frequency window, which narrows when observing high frequency phenomena and widens when analyzing low frequency behaviour. Thus time resolution becomes arbitrarily good at high frequencies, while the frequency resolution becomes arbitrarily good at low frequencies. This kind of analysis is suitable for signals

composed of high frequency components with short duration and low frequency components with long duration, which is often the case in practical situations [11].

When analysis is viewed as a filterbank, the WT, generally termed as standard Discrete Wavelet Transform (DWT), is seen as a composition of bandpass filters with constant relative bandwidth (constant-Q) such that  $\Delta_f/f$  is always constant. As  $\Delta_f$  changes with frequencies, corresponding time resolution  $\Delta_t$  also changes so as to satisfy the uncertainty condition. The frequency responses of bandpass filters are logarithmically spread over frequency as shown in figure (2.2 b). A generalisation of the concept of changing resolution at different frequencies is obtained with so-called Wavelet Packet Transform (WP) [67], where arbitrary time-frequency resolutions are chosen depending on the signal. More detailed description about the WT is given in subsequent sections of this chapter.

#### 2.2.4 Comparative Visualisation

A comprehensive visualization of various time-frequency representations, shown in figure (2.3), demonstrates the time-frequency resolution for a given signal in various transform domains with their corresponding basis functions [1].

The time-frequency representation problem is illustrated with Matlab simulations in figure (2.4) and figure (2.5) using two signals  $x_1(t)$  and  $x_2(t)$ . The signals are analysed through their corresponding FTs with FFTs, through STFTs with spectrograms, and through their CoWTs with scalograms [25]. Signal  $x_1(t) = \sin(2\pi 10t) + \sin(2\pi 35t) + \sin(2\pi 50t)$  is a stationary signal composed of three sinusoids of 10Hz, 35Hz, and 50Hz. Signal  $x_2(t)$  is non-stationary, which contains the same three distinct frequency components but over three adjoining time slots such that only one frequency component is present in a particular time interval. In both cases, the FFT picks up frequency contents very well but it fails to demonstrate the time varying nature of signal  $x_2(t)$ .

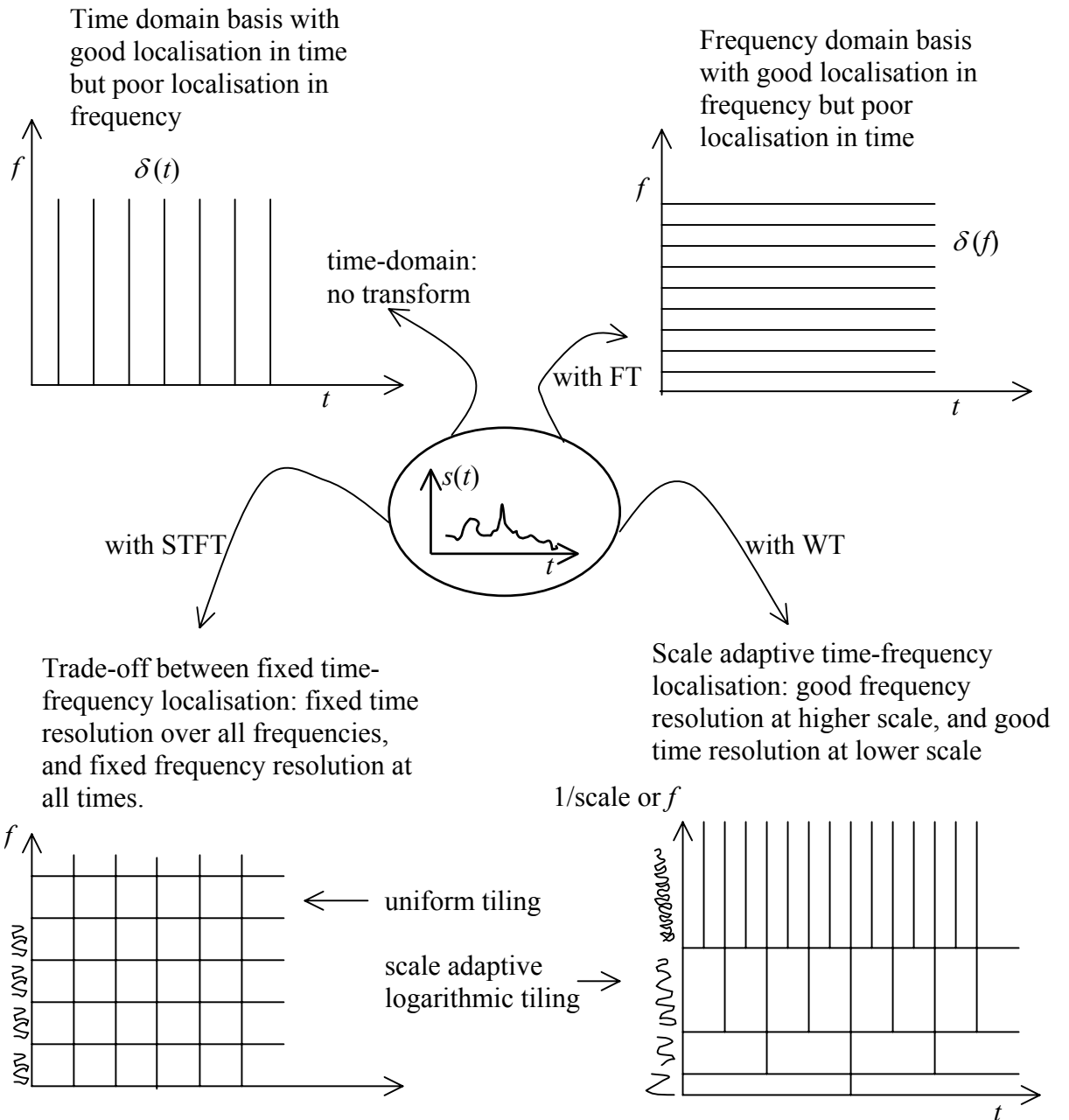
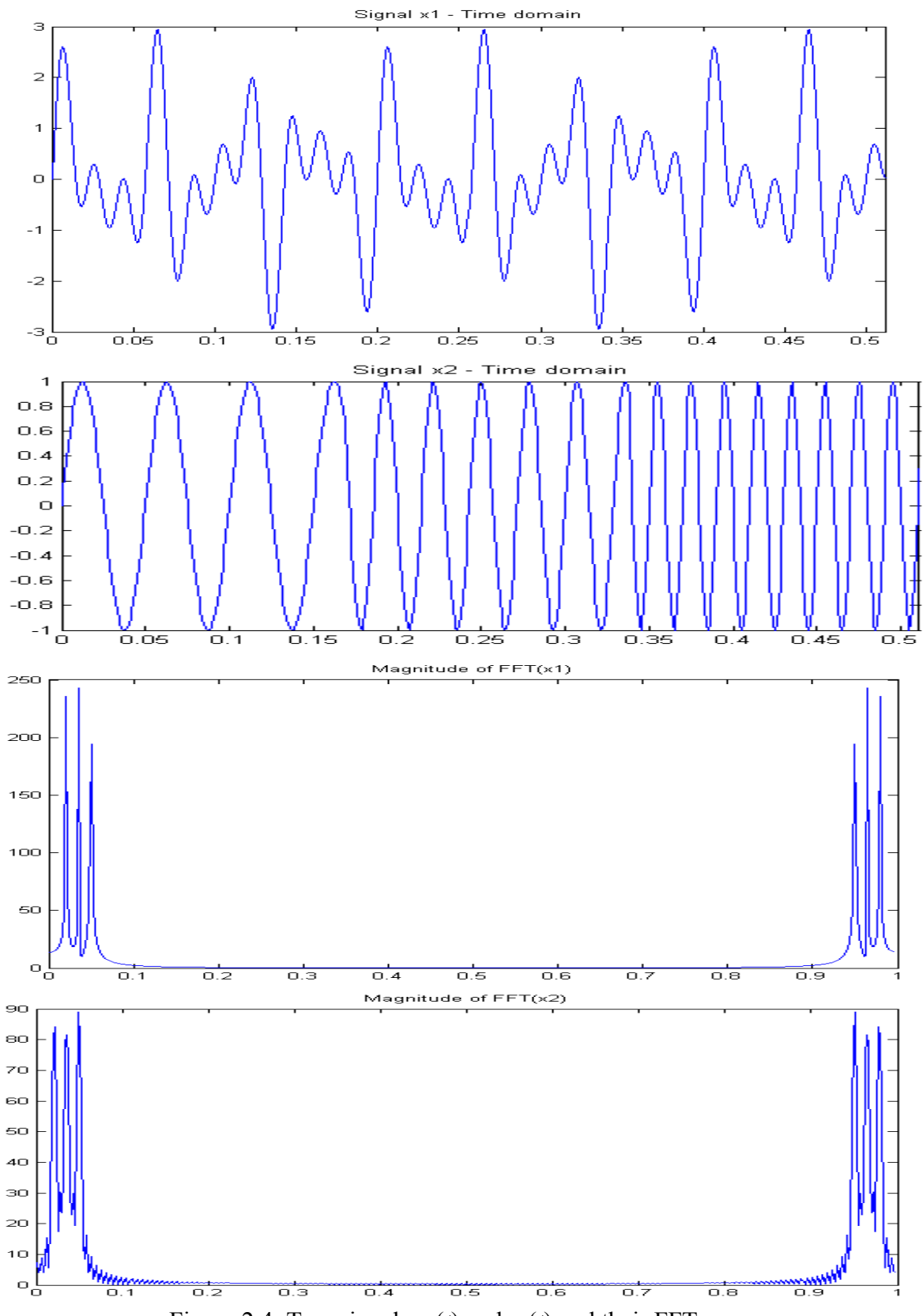
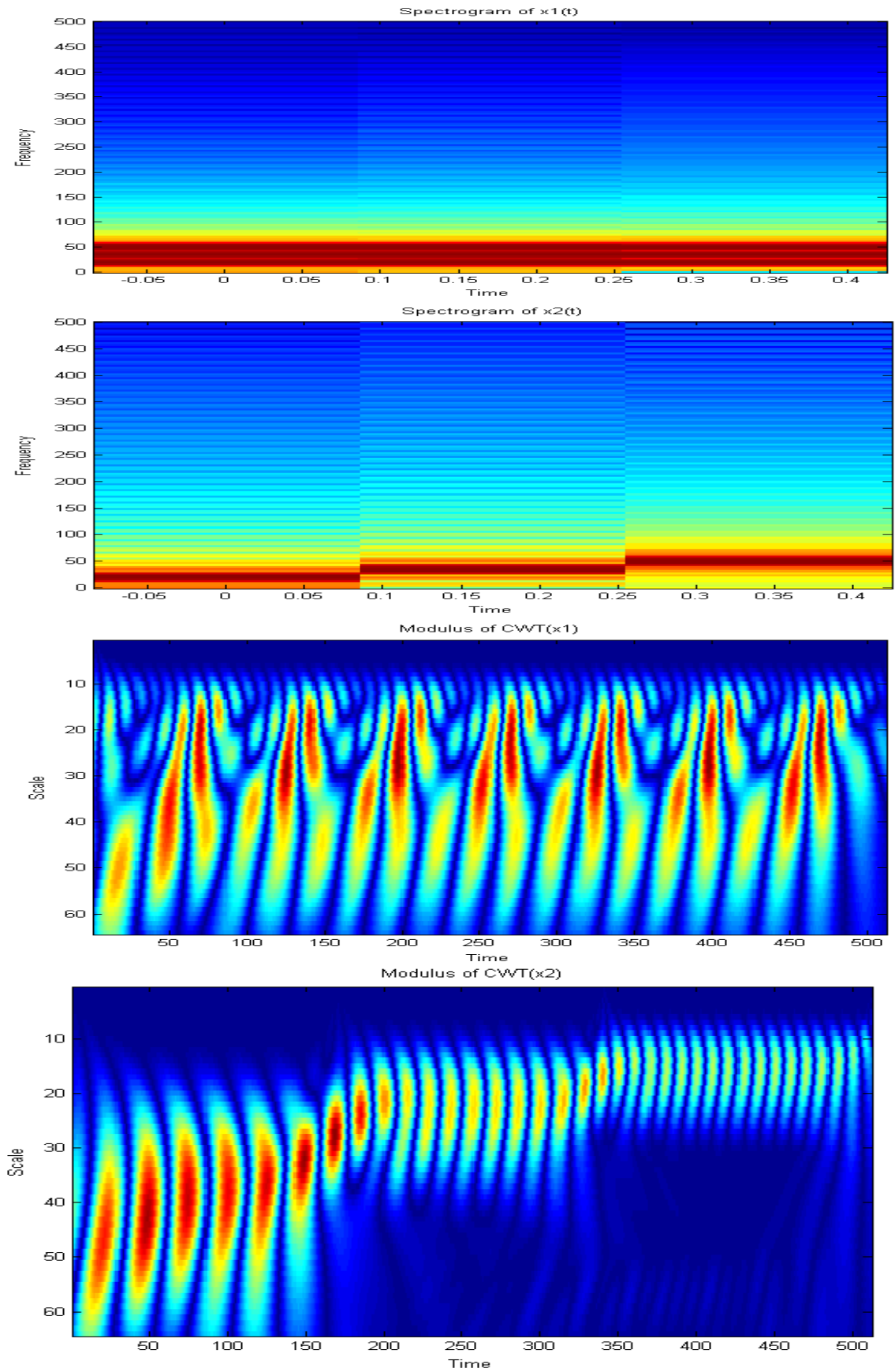


Figure 2.3: Comparative visualisation of time-frequency representation of an arbitrary non-stationary signal in various transform domains

Figure 2.4: Two signals  $x_1(t)$  and  $x_2(t)$  and their FFTs


 Figure 2.5: Spectrograms and scalograms of signals  $x_1(t)$  and  $x_2(t)$

Spectrograms (modulus of STFT) and scalograms (modulus of CoWT) for both signals  $x_1(t)$  and  $x_2(t)$  are shown in figure (2.5), which show the stationarity of  $x_1(t)$  and the time-varying nature of signal  $x_2(t)$ . Spectrogram has fixed resolution for  $x_2(t)$ , where as scalogram gives good frequency-resolution at lower frequency (high scale) and limited frequency-resolution at high frequency (low scale) for the same signal  $x_2(t)$ . But the time localization is good at higher frequency (low scale) compared to low frequency (high scale).

### 2.3 Theoretical Aspects of Wavelet Transform

Wavelet transform can be represented in continuous as well as in discrete domain as follows.

#### 2.3.1 Continuous Wavelet Transform (CoWT)

For a prototype function  $\psi(t) \in L^2(\mathbb{R})$  called the mother wavelet, the family of functions can be obtained by shifting and scaling this  $\psi(t)$  as:

$$\psi_{a,b}(t) = \frac{1}{\sqrt{a}} \psi\left(\frac{t-b}{a}\right), \text{ where } a, b \in \mathbb{R} \quad (a > 0) \quad (2.5)$$

Parameter  $a$  is a scaling factor and  $b$  is shifting factor. Normalization ensures that  $\|\psi_{a,b}(t)\| = \|\psi(t)\|$ . The mother wavelet has to satisfy the following admissibility condition

$$C_\psi = \int_{-\infty}^{\infty} \frac{|\Psi(\omega)|^2}{\omega} d\omega < \infty, \text{ where } \Psi(\omega) \text{ is the Fourier transform of } \psi(t).$$

In practice  $\Psi(\omega)$  will have sufficient decay, so that the admissibility condition reduces to

$$\int_{-\infty}^{\infty} \psi(t) dt = \Psi(0) = 0. \quad (2.6)$$

Thus, the wavelet will have bandpass behaviour.

The ‘continuous wavelet transform’ (CoWT) of a function  $f(t) \in \Re$  is then defined as:

$$\text{CoWT}_f(a,b) = \int_{-\infty}^{\infty} \psi_{a,b}^*(t) f(t) dt = \langle \psi_{a,b}(t), f(t) \rangle \quad (2.7)$$

A basis function  $\psi_{a,b}(t)$ , can also be seen as filterbank impulse response. With the increase in scale ( $a > 1$ ), the function  $\psi_{a,b}(t)$  is dilated in time to focus on long-time behaviour of associated signal  $f(t)$  with it. In general, very large scale means global view of the signal while very small-scale means a detailed view of the signal. A related notion with scale is resolution. The resolution of a signal is limited to its frequency content. The scale change of continuous time signals in CoWT does not alter their resolution, since the scale change can be reversed [11].

Through continuous wavelet transform analysis, a set of wavelet coefficients  $\{\text{CoWT}_f(a,b)\}$  are obtained. These coefficients indicate how close the signal is to a particular basis function. Since, the CoWT behaves like orthonormal basis decomposition, it can be shown that it is isometric [6], i.e. it preserves energy. Hence the function  $f(t)$  can be recovered from its transform by the following reconstruction formula:

$$f(t) = \frac{1}{C_\psi} \int_{-\infty}^{\infty} \int_{-\infty}^{\infty} CWT_f(a,b) \psi_{a,b}(t) \frac{da db}{a^2} \quad (2.8)$$

### 2.3.2 Discrete Wavelet Transform (DWT)

The CoWT has the drawbacks of redundancy and impracticability with digital computers. As parameters  $(a, b)$  take continuous values, the resulting CoWT is a very redundant representation, and impracticability is the result of redundancy. Therefore, the scale and shift parameters are evaluated on a discrete grid of time-scale plane leading to a discrete set of continuous basis functions [38]. The discretization is performed by setting

$$a = a_0^j \text{ and } b = k a_0^j b_0 \quad \text{for } j, k \in \mathbb{Z}. \quad (2.9)$$

where,  $a_0 > 1$  is a dilated step and  $b_0 \neq 0$  is a translation step. The family of wavelets then becomes

$$\psi_{j,k}(t) = a_0^{-j/2} \psi(a_0^{-j} t - k b_0) \quad (2.10)$$

and the wavelet decomposition of a function  $f(t)$  is

$$f(t) = \sum_j \sum_k D_f(j, k) \psi_{j,k}(t) \quad (2.11)$$

where 2-dimensional set of coefficients  $D_f(j, k)$  is called DWT of a given function  $f(t)$ .

The most widely used form of such discretization with  $a_0 = 2$ , and  $b_0 = 1$  on a dyadic time-scale grid is shown in figure (2.6). Such a wavelet transform is described as the standard DWT.

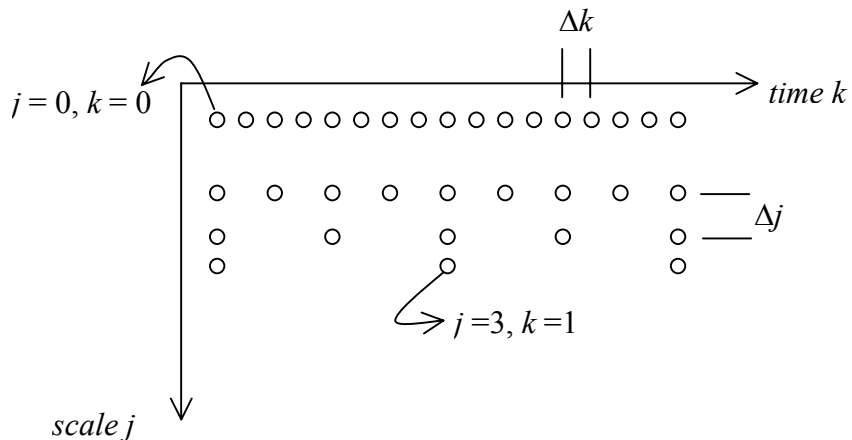


Figure 2.6: Standard DWT on dyadic time-scale grid

The selection of  $\psi(t)$  is made in such a way that basis function set  $\{\psi_{j,k}\}$  constitute an orthonormal basis of  $L^2(\mathbb{R})$  so that

$$D_f(j, k) = \int_{-\infty}^{\infty} \psi_{j,k}^*(t) f(t) dt = \langle \psi_{j,k}(t) f(t) \rangle \quad (2.12)$$

Several such wavelet bases have been reported in literature [45-48] to evaluate  $f(t)$  using the summation of finite basis over index  $j$  and  $k$  with finite DWT coefficients with almost no error. All these wavelets can be derived with an arbitrary resolution and with finite DWT coefficients.

## 2.4 Implementation of DWT

The practical usefulness of DWT comes from its Multi-Resolution Analysis (MRA) ability [48-50], and efficient Perfect Reconstruction (PR) filterbank structures.

### 2.4.1 Multiresolution Analysis (MRA)

Multiresolution analysis (or Multiscale analysis) consists of a sequence of embedded subspaces  $\dots V_2 \subset V_1 \subset V_0 \subset V_{-1} \subset V_{-2} \dots$  of  $L^2(\mathbb{R})$  as shown in figure (2.7).

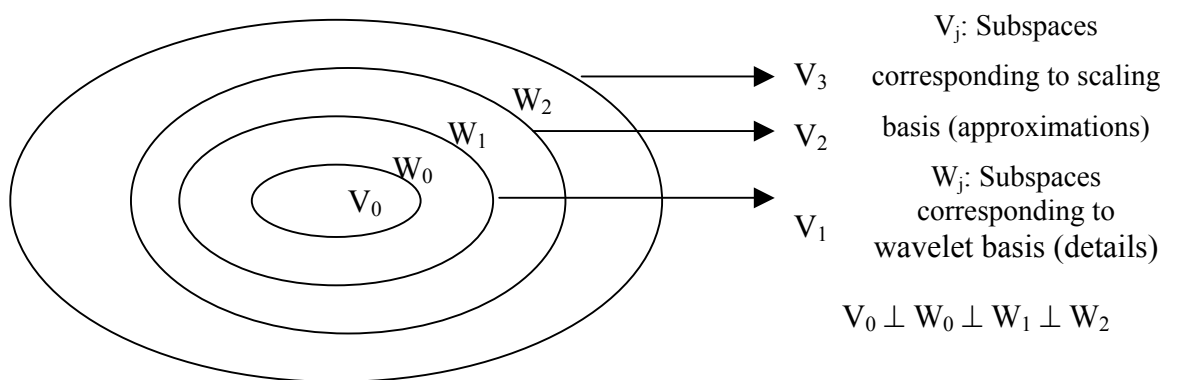


Figure 2.7: Nested vector spaces spanned by scaling and wavelet basis

The MRA follows the following conditions:

1.  $V_j \subset V_{j+1}, \quad j \in \mathbb{Z}$
2.  $V_{-\infty} = \{0\}$  and  $V_{\infty} = L^2$
3.  $f(t) \in V_j \Leftrightarrow f(2t) \in V_{j+1}$

---


$$\begin{aligned}
 4. \quad & V_2 = V_0 + W_0 + W_1 \\
 5. \quad & L^2 = \dots + W_{-2} + W_{-1} + W_0 + W_1 + W_2 + \dots = V_0 + W_1 + W_2 + \dots \\
 6. \quad & W_{-\infty} + \dots + W_{-2} + W_{-1} = V_0
 \end{aligned} \tag{2.13}$$

A scaling function  $\varphi(t)$  (Father wavelet) is introduced such that for each fixed  $j$ , the family

$$\varphi_{j,k} = 2^{-j/2} \varphi(2^{-j/2}t - k), (j, k \in \mathbb{Z}) \text{ and } \int \varphi(t) dt = 1 \tag{2.14}$$

is an orthonormal basis of the subspace  $V_j$ .

If  $W_j$  is orthonormal component of  $V_j$  ( $W_j \perp V_j$ ) in subspace  $V_{j+1}$ , then there exist a function  $\psi(t)$  (Mother wavelet) such that for each fixed  $j$  the family

$$\psi_{j,k} = 2^{-j/2} \psi(2^{-j/2}t - k), (j, k \in \mathbb{Z}) \tag{2.15}$$

is an orthonormal basis of the subspace  $W_j$ .

Because of the nested subspaces and MRA condition (3), the scaling function satisfies the following 2-scale (dilation or refinement) equation,

$$\varphi(t) = \sqrt{2} \sum_{n=-\infty}^{\infty} h_0[n] \varphi(2t - n), n \in \mathbb{Z} \tag{2.16}$$

where it satisfies the admissibility condition  $\sum_n h_0[n] = \sqrt{2}$ .

The wavelet function satisfies similar equation,

$$\psi(t) = \sqrt{2} \sum_{n=-\infty}^{\infty} h_1[n] \varphi(2t - n), n \in \mathbb{Z} \tag{2.17}$$

with the conditions  $\sum_n h_1[n] = 0$  and  $h_1[n] = (-1)^n h_0[-n + 1]$ .

where,  $h_0[n]$  and  $h_1[n]$  can be viewed as the coefficients of lowpass and highpass filters. For a function  $f(t)$ , the wavelet coefficients  $\langle \psi_{j,k}(t), f(t) \rangle$  describes the information loss when going from projection of  $f(t)$  onto the space  $V_{j+1}$ , to the projection onto the lower resolution space  $V_j$ . With MRA, any function  $f(t) \in L^2$  described by equation (2.11) can be modified by using both scaling function and wavelet function as:

$$f(t) = \sum_{j=J_0}^{J_1} \sum_{k=-\infty}^{\infty} C_f(j, k) \varphi_{J_1, k}(t) + \sum_{j=J_0}^{J_1} \sum_{k=-\infty}^{\infty} D_f(j, k) \psi_{j, k}(t) \quad (2.18)$$

where,  $C_f(j, k) = \langle \varphi_{j, k}(t), f(t) \rangle$  are the scaling function coefficients,  $J_0$  is an arbitrary starting scale for coarsest resolution, and  $J_1$  is an arbitrary finite upper limit for highest resolution with  $J_1 > J_0$ .

In practice, the selection of  $J_0$  and  $J_1$  depends on the characteristics of the signal  $f(t)$ , range of resolution required and the sampling rate of the signal as per Ch:9 [1].

#### 2.4.2 Filterbank Implementation

Assuming  $C_f(j, k)$  and  $D_f(j, k)$  are the scaling coefficients (approximations) and wavelet coefficients (details) of the projection of a signal  $f$  onto  $V_j$  and  $W_j$  respectively, the successive lower resolution coefficients are then recursively derived based on equations (2.16) and (2.17) with MRA concept as:

$$\begin{aligned} C_f(j+1, k) &= \sum_n h_0[n - 2k] C_f(j, n) \\ D_f(j+1, k) &= \sum_n h_1[n - 2k] D_f(j, n) \end{aligned} \quad (2.19)$$

These equations can be implemented as a tree-structured filterbank shown in figure (2.8) [27]. Because of the orthonormal wavelet basis, this 3-level analysis filterbank also satisfies the synthesis of high resolution scaling coefficients from the next immediate level lower resolution scaling and wavelet coefficients as:

$$C_f(j, k) = \sum_n h_0[k - 2n] C_f(j+1, n) + \sum_n h_1[k - 2n] D_f(j+1, n) \quad (2.20)$$

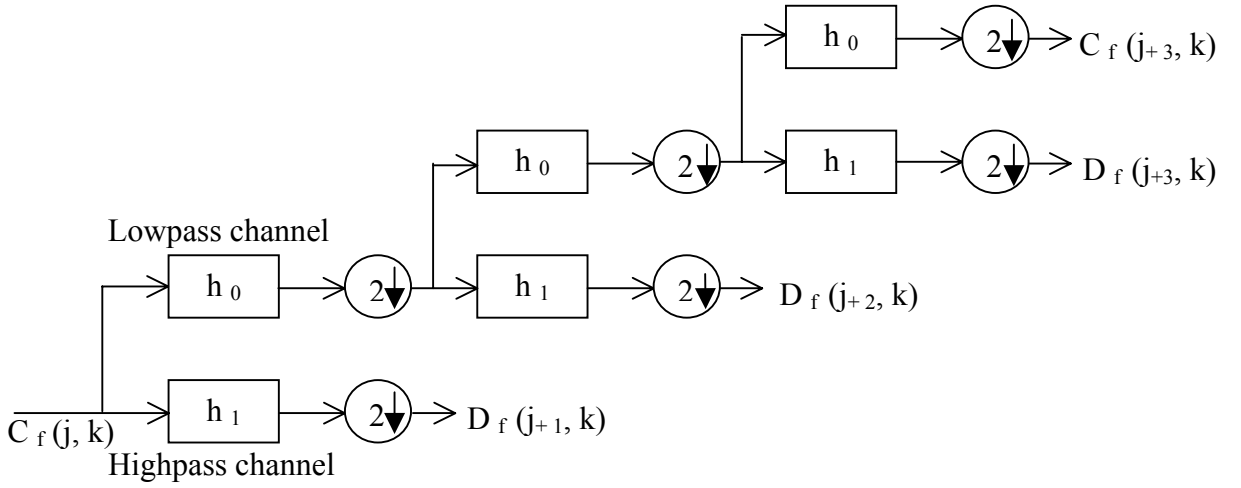


Figure 2.8: Two-channel, three-level analysis filterbank with 1-D DWT

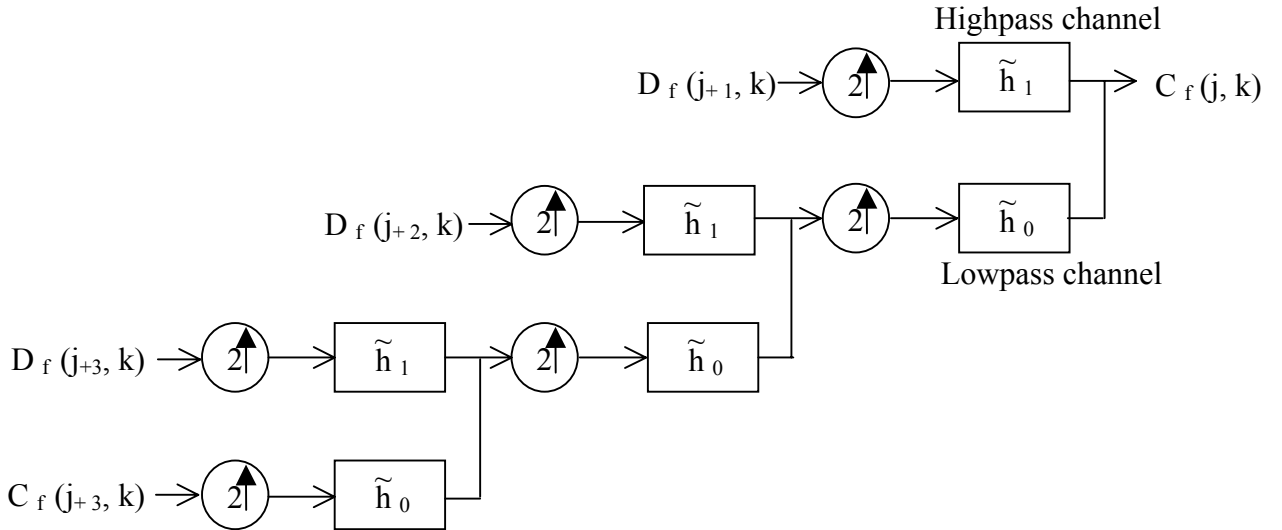


Figure 2.9: Two-channel, three-level synthesis filterbank with 1-D DWT

For a sampled signal, the filterbank tree is also viewed as an implementation of 1-D DWT with initial maximum resolution component  $C_f(j=0, k)$  and its decomposition into number of details  $D_f(j, k)$  at successive lower resolution scales.

For the standard DWT, the size of approximate (scaling) coefficients and detail (wavelet) coefficients decreases by a factor of 2 at each successive decomposition level. Thus the standard DWT is perfectly non-redundant of  $O(n)$  representation of a given signal in multi-resolution, multi-scale environment. The sparse representation with energy compaction makes the standard DWT widely accepted for signal compression.

The reconstruction filterbank structure shown in figure (2.9) follows the recursive synthesis similar to equation (2.20) with reconstruction filters  $\tilde{h}_0$  and  $\tilde{h}_1$ , which are identical to their corresponding decomposition filters  $h_0$  and  $h_1$  but with time reversal.

The most important criterion with filterbank implementation (subband decomposition) of DWT is the proper retrieval of signal, which is commonly termed as perfect reconstruction in literature [14-15, 28, 51-52]. The perfect reconstruction imposes certain constraints on analysis and synthesis filters. The nature of constraints relates these filters to either the orthogonal wavelet bases or to the biorthogonal wavelet basis as discussed in section 2.4.3.

### 2.4.3 Perfect Reconstruction (PR)

As shown in figure (2.10), when reconstructed signal  $\tilde{f}(t)$  is identical to the original signal  $f(t)$  for a simple 2-channel filterbank structure, the associated analysis and synthesis filters satisfy certain conditions.

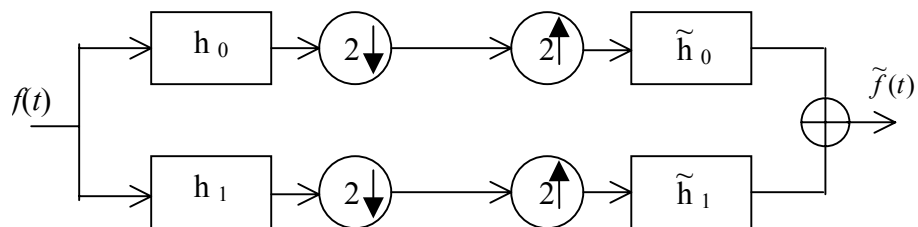


Figure 2.10: A simple 2-channel filterbank model

---

These perfect reconstruction (PR) conditions finally boils down as:

$$\begin{aligned} H_0(z)\tilde{H}_0(z) + H_1(z)\tilde{H}_1(z) &= 2 \\ H_0(z)\tilde{H}_0(-z) + H_1(z)\tilde{H}_1(-z) &= 0 \end{aligned} \quad (2.21)$$

where,  $H_0(z)$  and  $H_1(z)$  are the Z-transforms of  $h_0[n]$  and  $h_1[n]$  respectively.

Most of the orthonormal wavelet basis associated with PR filterbank of figure (2.10) has prototype wavelet  $\psi$  with infinite support (length). Hence all the filters require infinite taps. A design method introduced by [26] generates a finite support orthonormal wavelet  $\psi$ , and the associated filterbank can be realized through finite tap FIR filters.

If the FIR filterbank shown in figure (2.8) is iterated on the lowpass channel, the overall impulse response of the iterated filter-tree takes the form of continuous time function with compact support. With infinite iterations over filter-tree, the impulse response converges to a smooth function (mother wavelet). Filter having this property are called ‘regular’ [51,53-55]. A necessary condition for regularity is for lowpass filter to have at least one zero at the aliasing frequency  $\omega = \pi$ . The number of zeros at  $\omega = \pi$  determines the degree of smoothness or differentiability of the resulting wavelet. Regularity (smoothness) is an important feature of wavelet for its application in detection of discontinuities [56].

For an orthogonal wavelet system, the conditions for analysis and synthesis filters are given as:

$$\begin{aligned} \tilde{h}_0[n] &= h_0[-n] \\ \tilde{h}_1[n] &= h_1[-n] \\ \sum_n h_0[n] \tilde{h}_0[-n+2k] &= \delta(k) \end{aligned} \quad (2.22)$$

In signal processing applications, it is often desirable to use FIR filters with linear phase [33]. It has been shown that there are no nontrivial orthonormal linear

phase FIR filters [53]. By allowing non-orthogonal and dual basis, a biorthogonal wavelet system is formed. Biorthogonal wavelet basis have the advantages of linear phase, and more degrees of freedom in filter design [29,30,32]. If the scaling function set  $\{\varphi_{j,k}(t), \tilde{\varphi}_{j,k}(t)\}$ , and the wavelet function set  $\{\psi_{j,k}(t), \tilde{\psi}_{j,k}(t)\}$  represent the dual basis for analysis and synthesis for biorthogonal system then the 2-scale equations similar to equation (2.16) and (2.17) are given as:

$$\begin{aligned}\varphi(t) &= \sqrt{2} \sum_n h_0[n] \varphi(2t-n), \tilde{\varphi}(t) = \sqrt{2} \sum_n \tilde{h}_0[n] \varphi(2t-n) \\ \psi(t) &= \sqrt{2} \sum_n h_1[n] \psi(2t-n), \tilde{\psi}(t) = \sqrt{2} \sum_n \tilde{h}_1[n] \psi(2t-n)\end{aligned}\quad (2.23)$$

Biorthogonal wavelet basis also satisfy the relation:

$$\langle \psi_{j,k}(t), \tilde{\psi}_{m,n}(t) \rangle = \delta[j-m] \delta[k-n]$$

and reconstruction formula becomes:

$$f(t) = \sum_j \sum_k \langle \psi_{j,k}(t), f(t) \rangle \tilde{\psi}_{j,k}(t) \quad (2.24)$$

For the biorthogonal wavelet system, the constraints for analysis and synthesis filters are given as:

$$\begin{aligned}\tilde{h}_1[n] &= (-1)^n h_0[-n+1] \\ h_1[n] &= (-1)^n \tilde{h}_0[-n+1] \\ \sum_n h_0[n] \tilde{h}_0[-n+2k] &= \delta(k)\end{aligned}\quad (2.25)$$

## 2.5 Extensions of DWT

The DWT is extensively used in its non-redundant form known as standard DWT. The filterbank implementation of standard DWT for images is viewed as 2-D DWT. There are certain applications for which the optimal representation can be achieved

through more redundant extensions of standard DWT such as WP (Wavelet Packet Transform) and SWT (Stationary Wavelet Transform).

### 2.5.1 Two Dimensional Discrete Wavelet Transform (2-D DWT)

Filterbank structure discussed in section 2.4.2 is the simple implementation of 1-D DWT, whereas image-processing applications requires two-dimensional implementation of wavelet transform. Implementation of 2-D DWT is also referred to as ‘multidimensional’ wavelet transform in literature [11,27,57]. The state of the art image coding algorithms such as e.g. the recent JPEG2000 standard [58] make use of the separable dyadic 2-D DWT, which is only an extension of 1-D DWT applied separately on rows and columns of an image.

The implementation of an analysis filterbank for a single level 2-D DWT is shown in figure (2.11). This structure produces three detailed sub-images (HL, HL, HH) corresponding to three different directional-orientations (Horizontal, Vertical and Diagonal) and a lower resolution sub-image LL. The filterbank structure can be iterated in a similar manner on the LL channel to provide multilevel decomposition. Multilevel decomposition hierarchy of an image is illustrated in figure (2.12).

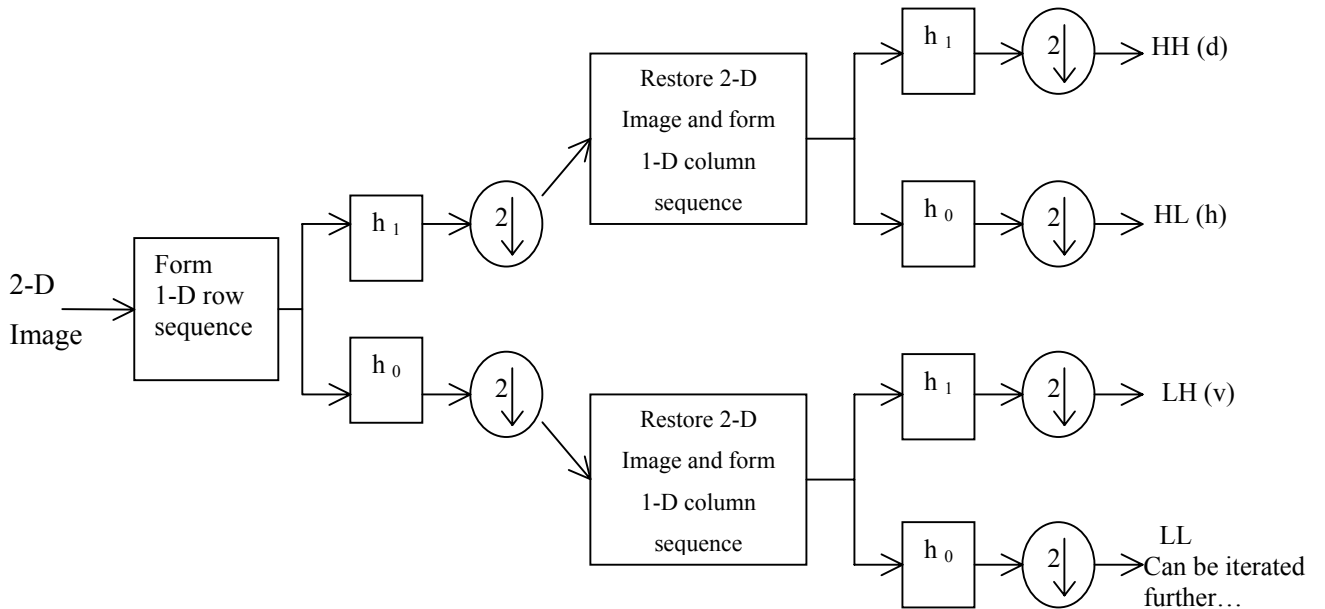


Figure 2.11: Single level analysis filterbank for 2-D DWT

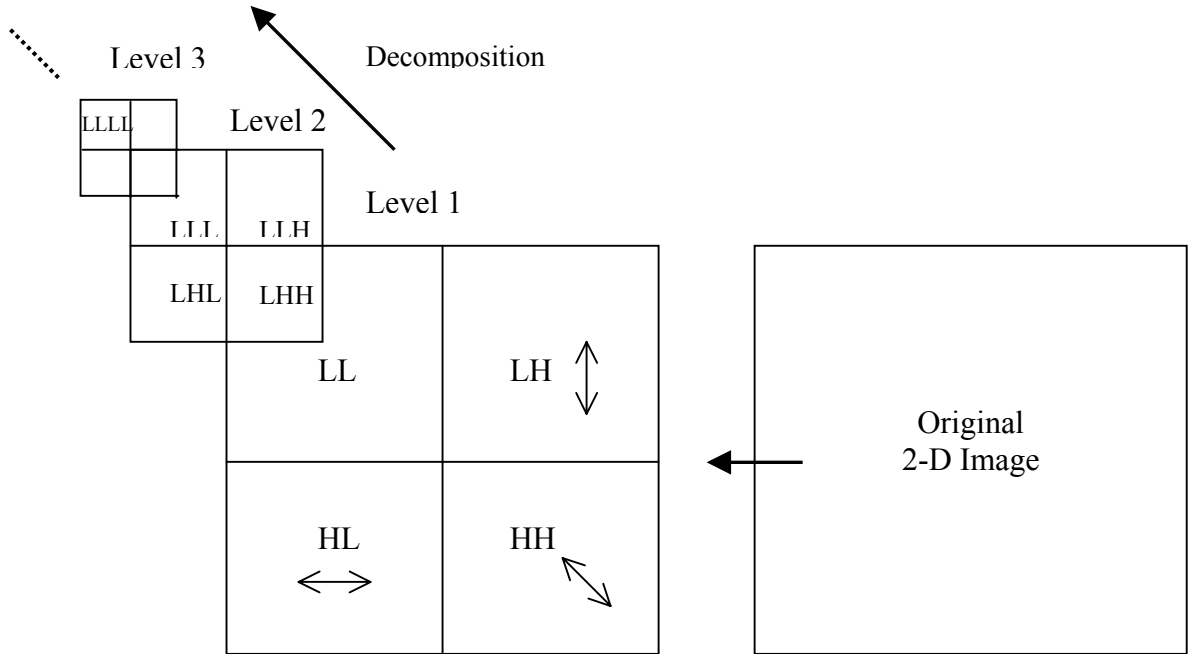


Figure 2.12: Multilevel decomposition hierarchy of an image with 2-D DWT

Each decomposition breaks the parent image into four child images. Each of such sub-images is of one fourth of the size of a parent image. The sub-images are placed according to the position of each subband in the two-dimensional partition of frequency plane as shown in figure (2.13). The structure of synthesis filterbank follows the reverse implementation of analysis filterbank but with the synthesis filters  $\tilde{h}_0$  and  $\tilde{h}_1$ .

The separable wavelets are also viewed as tensor products of one-dimensional wavelets and scaling functions. If  $\psi(x)$  is the one-dimensional wavelet associated with one-dimensional scaling function  $\varphi(x)$ , then three 2-D wavelets associated with three sub-images are given as:

$$\begin{aligned}
 \psi^V(x, y) &= \varphi(x) \psi(y) \rightarrow && \text{LH} \\
 \psi^H(x, y) &= \psi(x) \varphi(y) \rightarrow && \text{HL} \\
 \psi^D(x, y) &= \psi(x) \psi(y) \rightarrow && \text{HH}
 \end{aligned} \tag{2.26}$$

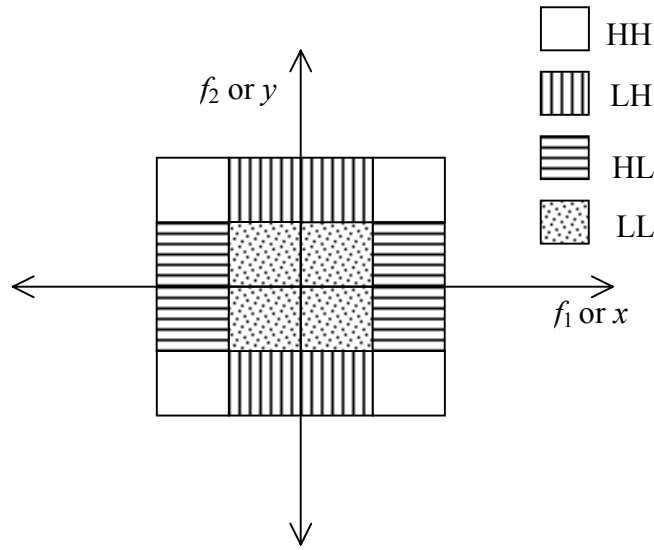


Figure 2.13: Frequency plane partitioning with 2-D DWT

The test image ‘Pattern’ and its 2-D DWT decomposition is shown in figure (2.14). This decomposition is done with the help of ‘wavelet toolbox’ of Matlab [25].

There are also various extensions available for 2-D wavelet transform in non-separable form. Non-separable multidimensional filterbanks and wavelets bases with their applications to image coding can be found from [59-62]. Non-separable methods offer true multidimensional processing, freedom in filter design, non-rectangular sub-sampling (e.g quincunx [63] and hexagonal [64]), and even linear phase. Though the non-separable methods have several advantages, separable filtering is a common choice because of the simplicity of its implementation.

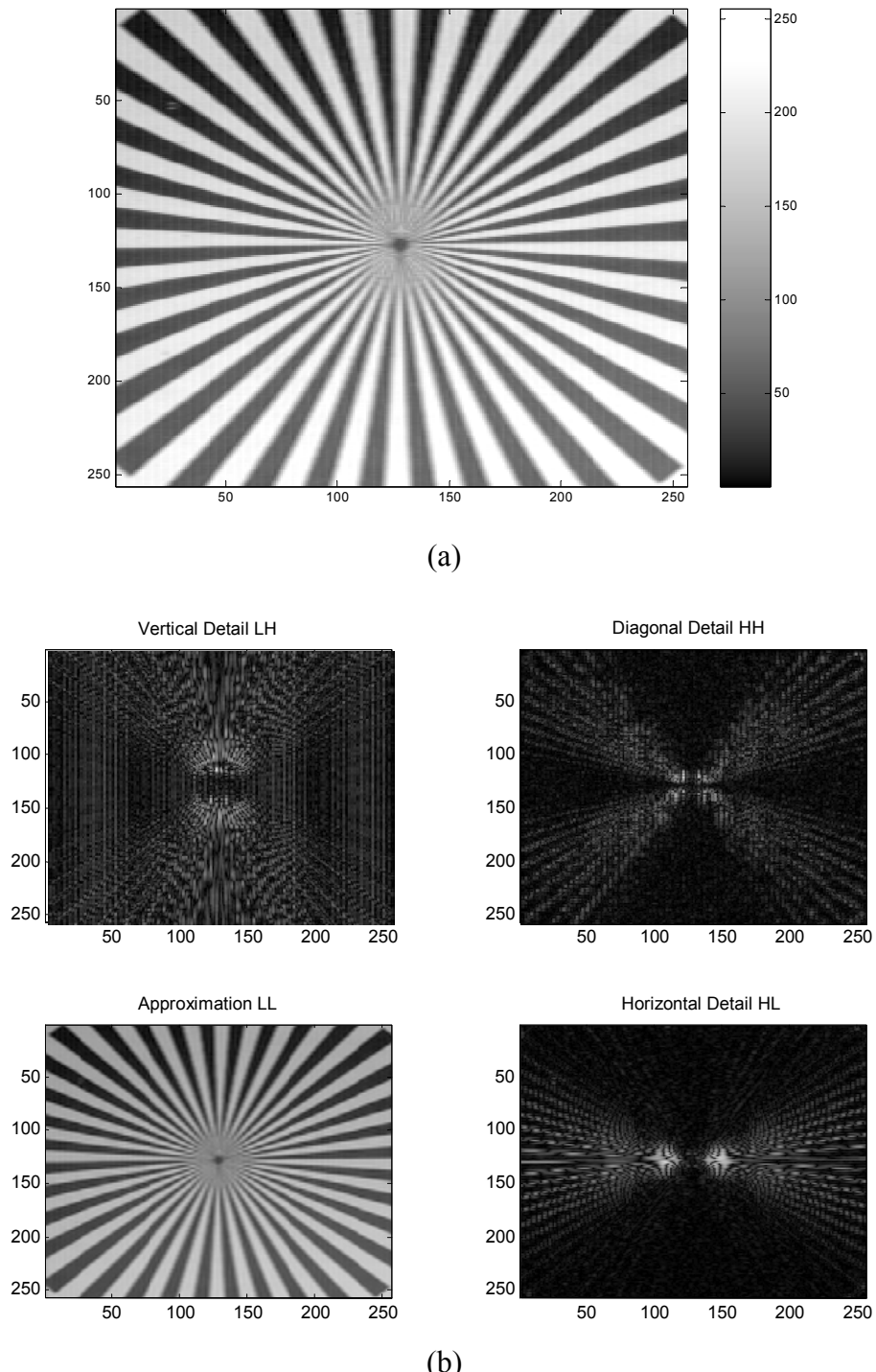


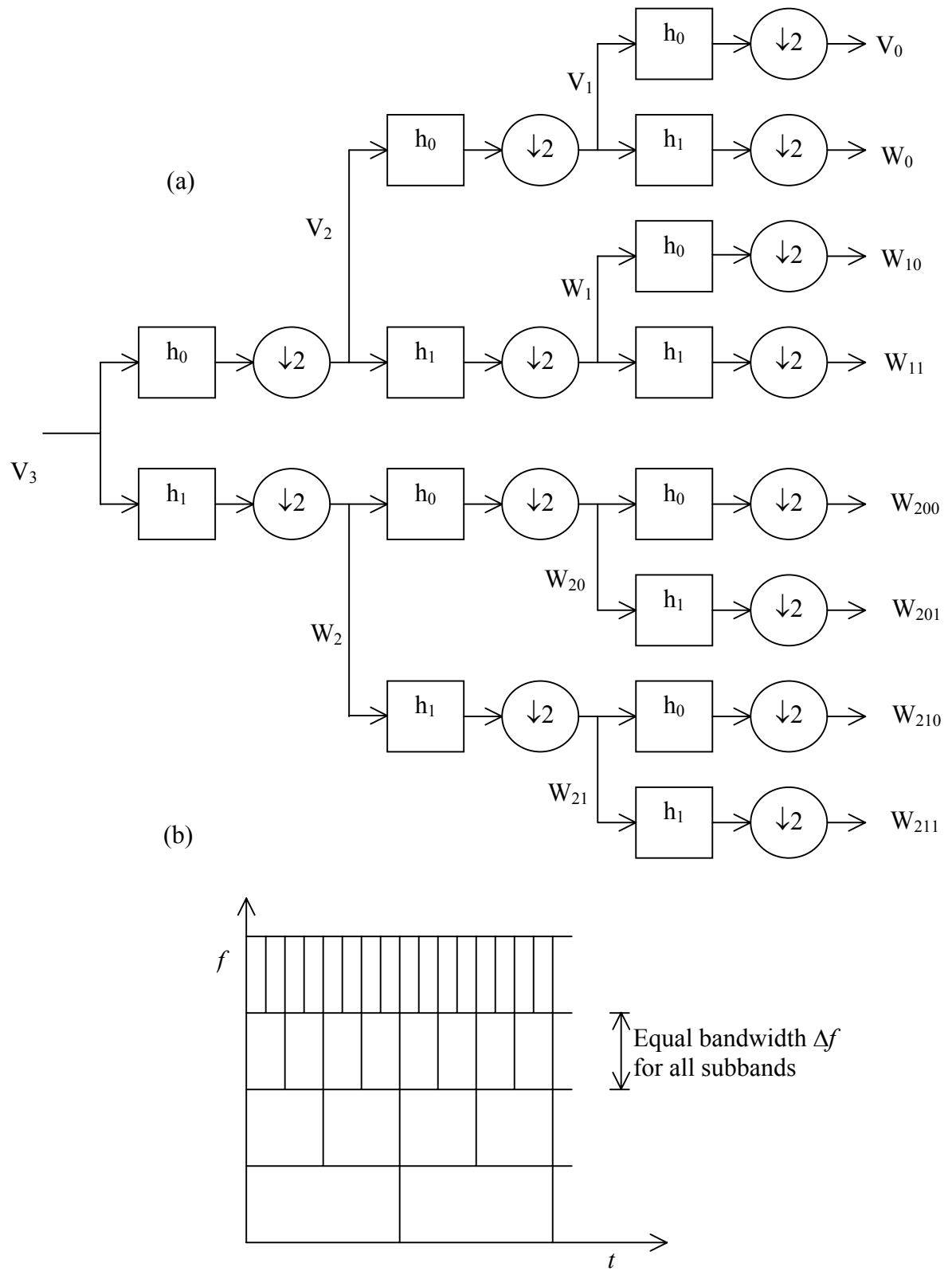
Figure 2.14: (a) Test image ‘Pattern’, (b) single level 2-D DWT decomposition of the same

## 2.5.2 Wavelet Packet Transform (WP)

Octave band filtering with iteration over lowpass channel implements 1-D DWT as discussed in section 2.4.2. The octave band filtering does not provide uniform frequency resolution for all subbands as shown in figure (2.2 b). If the highpass channel of figure (2.8) is also decomposed in similar manner and iterated, then a complete ‘binary-tree’ is achieved. Families of orthonormal basis associated with this binary-tree (WP-tree) are known as ‘wavelet packets’. This extension of standard DWT is denoted as Wavelet Packet Transform (WP).

The binary-tree for WP decomposition, and the time-frequency tiling for wavelet packets basis are shown in figure (2.15). Figure (2.16) shows vector subspaces for WP. Uniform frequency division with equal frequency resolution for all subbands is illustrated in figure (2.17). Two possible ways of WP decomposition (square and round shapes) for the original signal in subspace  $V_3$  is shown in figure (2.18). It demonstrates the flexibility and freedom of WP. In general, WP, a modified form of standard DWT, combines the ideas of the best basis selection and entropy based criteria for accurate representation of the signal. It offers high degree of freedom but with complex data-structure algorithms. The complexity of computation for WP is  $O(n \log n)$ .

Algorithms for choosing the best wavelet packets for a particular image, and more technical descriptions on WP are given in [65-68]. Usefulness of WP in compression and de-noising can be seen through a quick GUI: ‘wavemenu’ and various wavelet packet function using ‘wavelet toolbox’ of Matlab.



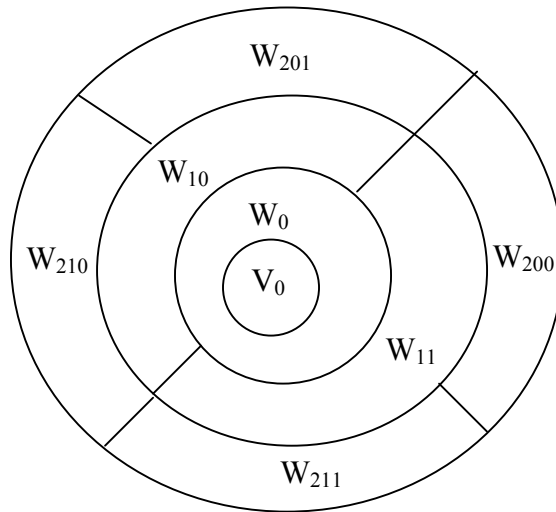


Figure 2.16: Vector subspaces for WP

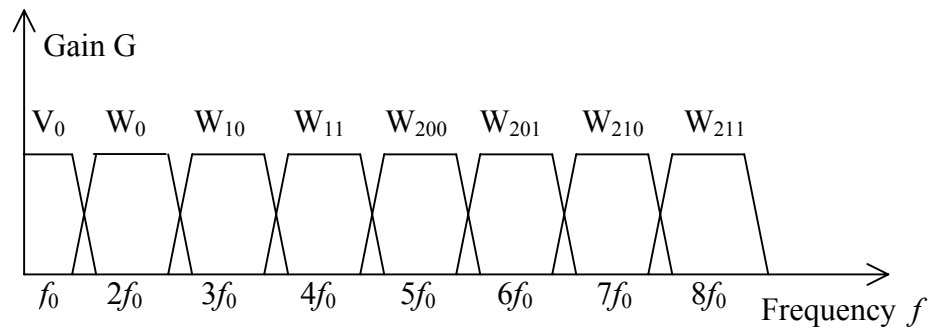


Figure 2.17: Uniform frequency division for WP

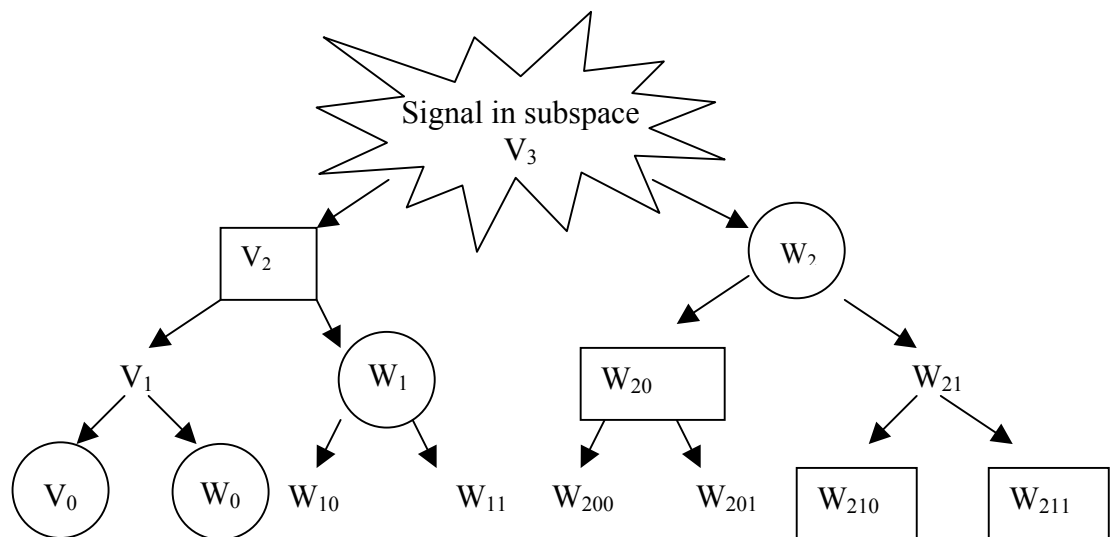


Figure 2.18: Flexible representation with WP: either with boxes or with circles

### 2.5.3 Stationary Wavelet Transform (SWT)

The standard DWT as discussed in section 2.4.2 is a non-redundant and compact representation of signal in transform domain. The decimation step after filtering makes the standard DWT time shift-variant. The stationary wavelet transform (SWT) has a similar tree structured implementation without any decimation (sub-sampling) step. The balance for PR is preserved through level dependent zero-padding interpolation of respective lowpass and high pass filters in the filter bank structures. DWT of such kind is based on the ‘A Trous’ algorithm, which modifies the filters through insertion of holes [69].

In literature, various interpretations of SWT are referred to as redundant, non-decimated, overcomplete or shift-invariant wavelet transform. The implementation structure for SWT is shown in figure (2.19), where  $*$  denotes the discrete time convolution,  $d_i$  are detail (wavelet) coefficients and  $c_i$  are approximate (scaling) coefficients generated through the convolution chain originated from an original signal sequence  $c_0$  and level-adaptive size-varying highpass filter  $h_1$  and lowpass filter  $h_0$  respectively.

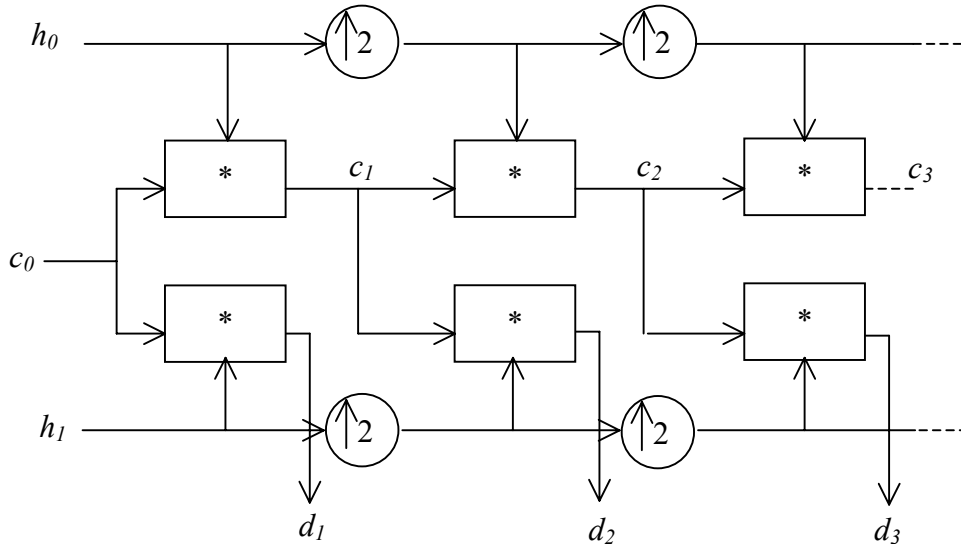


Figure 2.19: Three level decomposition with SWT

SWT has equal length wavelet coefficients at each level. The computational complexity of SWT is  $O(n^2)$ . The redundant representation makes SWT shift-invariant and suitable for applications such as edge detection, denoising and data fusion. The wavelet toolbox function ‘swt’ is the Matlab implementation of the same algorithm.

## 2.6 Applications of Wavelet Transforms

Finally, applications of widely used standard DWT implementations, utilizing its Multiscale and Multiresolution capabilities with fast filterbank algorithms are numerous to describe. Depending upon the application, extensions of standard DWT namely WP and SWT are also employed for improved performance at the cost of higher redundancy and computational complexity.

A few of such applications in Data compression, Denoising, Source and channel coding, Biomedical, Non-destructive evaluation, Numerical solutions of PDE, Study of distant universe, Zero-crossings, Fractals, Turbulence, and Finance etc. are comprehensively covered in [13]. Wavelet applications in many diverse fields such as Physics, Medicine and biology, Computer Graphics, Communications and multimedia etc. can be found in various books on wavelets [70-74].

## 2.7 Limitations of Wavelet Transforms

Although the standard DWT is a powerful tool, it has three major disadvantages that undermines its application for certain signal and image processing tasks [75]. These disadvantages are described as below.

### *1. Shift Sensitivity:*

A transform is shift sensitive, if the shifting in time, for input-signal causes an unpredictable change in transform coefficients. It has been observed that the standard DWT is seriously disadvantaged by the shift sensitivity that arises from down samplers in the DWT implementation [14,76]. Shift sensitivity is an undesirable property because it implies that DWT coefficients fail to distinguish between input-

signal shifts. The shift variant nature of DWT is demonstrated with three shifted step-inputs in figure (2.20). In figure (2.20) input shifted signals are decomposed up to  $J= 4$  levels using ‘db5’. It shows the unpredictable variations in the reconstructed detail signal at various levels and in final approximation. Wavelet packets have also been investigated for shift sensitivity. WP gives better results than standard DWT implementation at the cost of complexity. The selection of best bases and cycle spinning reduces shift sensitivity, but a general representation of WP is not shift invariant [31,77]. Though SWT is shift invariant, it has a very large redundancy and increased computational complexity.

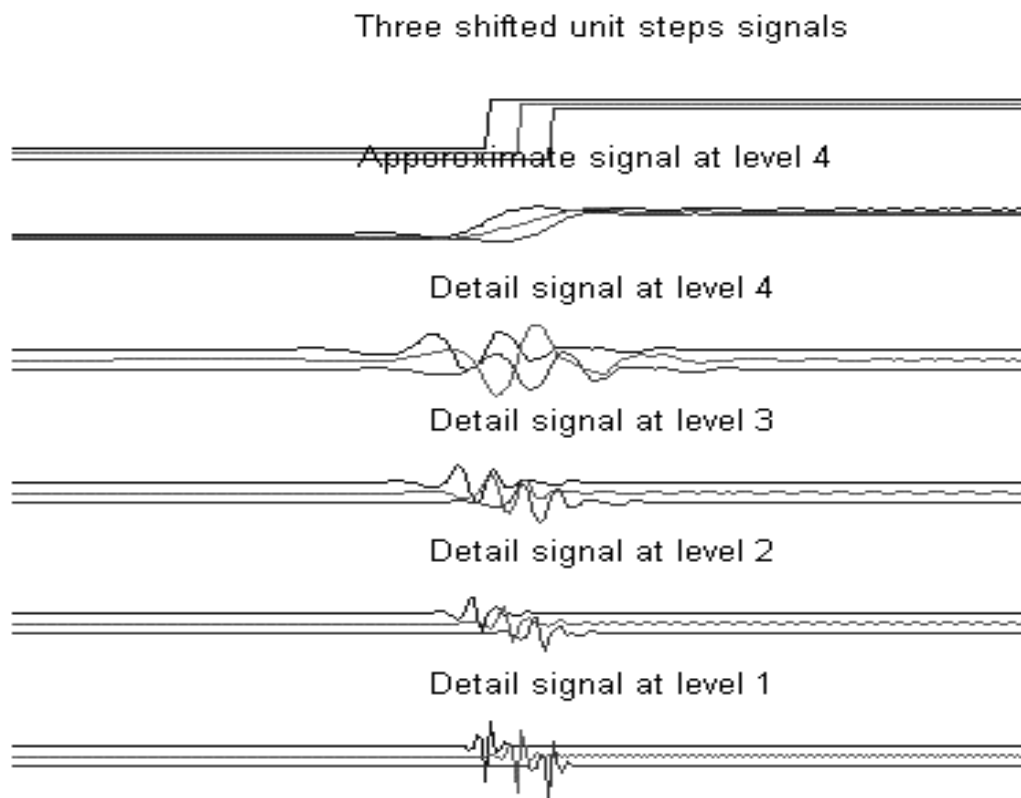


Figure 2.20: Shift-sensitivity of standard 1-D DWT

## 2. Poor Directionality:

An  $m$ - Dimensional transform ( $m > 1$ ) suffers poor directionality when the transform coefficients reveal only a few feature orientations in the spatial domain. As discussed in section 2.5.1, the separable 2-D DWT partitions the frequency domain into three directional subbands.

As shown in figures (2.14 b) and (2.21), 2-D DWT can resolve only three spatial-domain feature orientations: horizontal (HL), vertical (LH) and diagonal (HH). Natural images contain number of smooth regions and edges with random orientations; hence poor directionality affects the optimal representation of natural images with of the separable standard 2-D DWT.

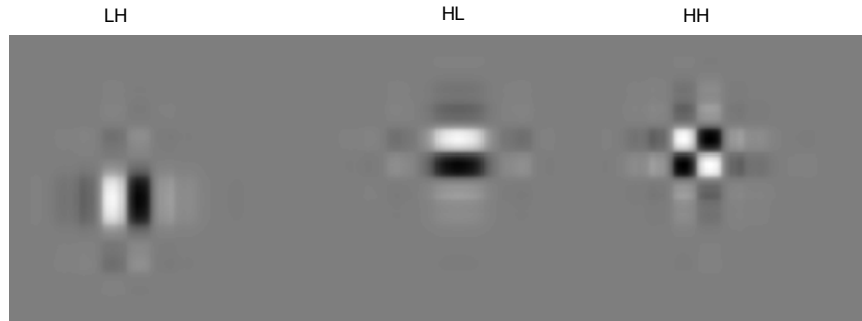


Figure 2.21: Directionality of standard 2D DWT

Implementations of 2-D WP explore all frequency bands, and it can be tailored for the selection of the best pattern (basis). However, the Multiscale structure of wavelet decomposition and the concept of ‘spatial orientation tree’ [78] are lost. 2-D form of WP is investigated for directionality in texture analysis applications [79,80]. When compared with the standard 2-D DWT, because of its richer set of basis, WP perform better in terms of fidelity of direction but not in terms of improved directionality. The SWT is based on a filterbank structure, identical to standard DWT as far as directionality is concerned, and hence SWT has poor directionality. But SWT has improved fidelity in available direction because of large redundancy.

### **3. *Absence of Phase Information:***

For a complex valued signal or vector, its phase can be computed by its real and imaginary projections. Digital image is a data matrix with a finite support in 2-D. Filtering the image with 2-D DWT increases its size and adds phase distortion. Human visual system is sensitive to phase distortion [81]. Further more, ‘Linear phase’ filtering can use symmetric extension methods to avoid the problem of

increased data size in image processing [81]. Phase information is valuable in many signal processing applications [83] such as e.g. in image compression and power measurement [84,85].

Most DWT implementations (including standard DWT, WP and SWT) use separable filtering with real coefficient filters associated with real wavelets resulting in real-valued approximations and details. Such DWT implementations cannot provide the local phase information. All natural signal are basically real-valued, hence to avail the local phase information, complex-valued filtering is required [86,87]. The difference between ‘real’ and ‘analytic’ wavelets is shown in figure (2.22).

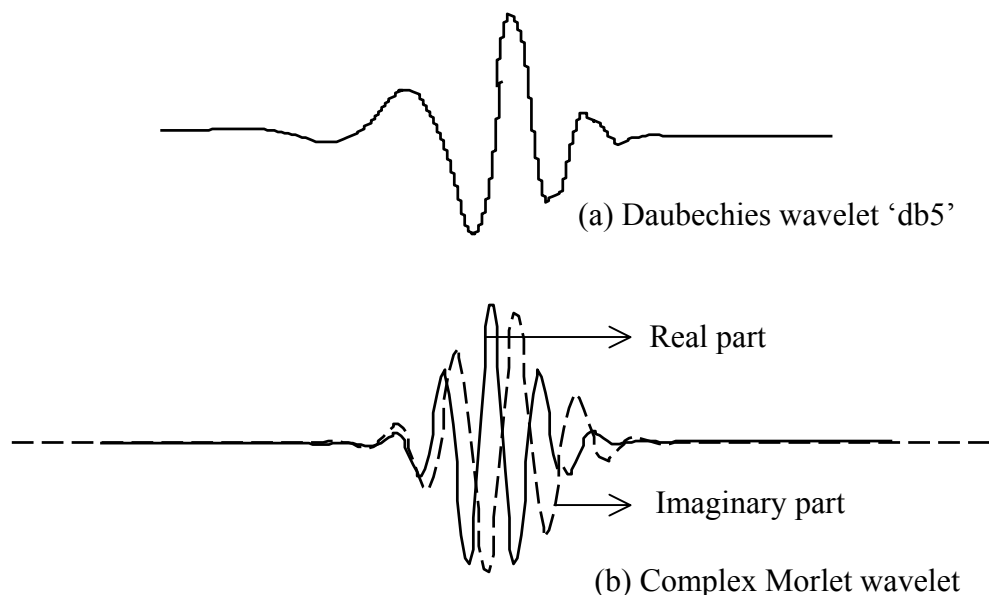


Figure 2.22: Presentation of (a) real, and (b) analytic wavelets

## 2.8 Summary

It is perceived that the wavelet transform is an important tool for analysis and processing of non-stationary signals. The wavelet transform in its continuous form can accurately represent minor variations in signal characteristics, but it is data intensive. Critically sampled version of continuous wavelet transform, known as

standard DWT, is very popular for denoising and compression in a number of applications by the virtue of its computational simplicity through fast filterbank algorithms, and non-redundancy. Though there are certain signal processing applications (e.g. Edge detection, Time-division multiplexing in Telecommunication), where more optimal representation is achieved through redundant and computationally intensive extensions of standard DWT such as WP and SWT.

All these forms of DWTs result in real valued transform coefficients with two or more limitations as discussed in section 2.7. There is an alternate way of reducing these limitations with a limited redundant representation in complex domain. Formulation of complex-valued ‘analytic\* filters’ or ‘analytic wavelets’ helps to get the required phase information, more orientations, and reduced shift-sensitivity. Various approaches of filterbank implementation employing analytic filters associated with analytic wavelets are commonly referred to as ‘Complex Wavelet Transforms’ (CWT). The formulations of analytic filter and associated complex wavelet transforms are discussed in chapter 3.

---

\* An ‘Analytic function’ is a complex valued function, constructed from a given real-valued function by its projections on real and imaginary subspaces (Hilbert space). These projections are termed as ‘Hardy space’ projections. The important property of an analytic signal is that its FT has single-sided spectral components [2,88,89].

# Chapter 3:

## Complex Wavelet Transforms (CWT)

### 3.1 Introduction

It is discussed in section 2.7 that standard DWT and its extensions suffer from two or more serious limitations. The initial motivation behind the earlier development of complex-valued DWT was the third limitation that is the ‘absence of phase information’ [86]. Complex Wavelets Transforms (CWT) use complex-valued filtering (analytic filter) that decomposes the real/complex signals into real and imaginary parts in transform domain. The real and imaginary coefficients are used to compute amplitude and phase information, just the type of information needed to accurately describe the energy localisation of oscillating functions (wavelet basis).

Edges and other singularities in signal processing applications manifest themselves as oscillating coefficients in the wavelet domain. The amplitude of these coefficients describes the strength of the singularity while the phase indicates the location of singularity. In order to determine the correct value of localised envelope and phase of an oscillating function, ‘analytic’ or ‘quadrature’ representation of the signal is used. This representation can be obtained from the Hilbert transform of the signal as described in section 3.4 [88,89]. It is shown in [90] that for radar and sonar applications, the complex I/Q orthogonal signals can be efficiently processed with complex filterbanks rather than processing the I and Q channel separately. Thus, the

complex orthogonal wavelet may prove to be a good choice, since it will allow processing of both magnitude and phase simultaneously.

Chapter 3 is organised into eight sections. An introduction to complex wavelet transforms is given in section 3.1. A review of earlier work and the recent developments in the field of complex wavelet transforms are given in section 3.2 and in section 3.3 respectively. Formal definition and mathematical formulation of ‘analytic filter’ is described in section 3.4, which is central to the design of all recent complex wavelet transforms (CWT). In section 3.5, Dual-Tree DWT (DT-DWT) forms of Redundant Complex Wavelet Transforms (RCWT) are discussed. The filterbank structure, design methods and typical properties of DT-DWTs are also described in section 3.5. Section 3.6 describes the basic design concept of complex projection (mapping) based Non-Redundant CWT (NRCWT) and their properties. All forms of CWTs are comprehensively compared in section 3.7, their advantages and applications over standard DWT are also presented. Section 3.8 is a summary of the investigations on CWTs.

## 3.2 Earlier Work

There is no one unique extension of the standard DWT into the complex plane. *Lawton* [86], and *Lina* [91], showed that complex solutions of Daubechies wavelets are possible. The complex valued Symmetric Daubechies Wavelets (SDW) has been used for applications such as image enhancement, restoration and coding [86,87,91,92]. The filterbank design to generate complex wavelets with useful properties of orthogonality, symmetry and linear phase is described by *Zang et. al.* [90].

The orthogonality is necessary to preserve the energy in transform domain. The symmetry property of filter makes it easy to handle the boundary problem for finite length signals [14]. Linear phase response of the filter is necessary, to reduce the visually objectionable artifacts caused by nonlinear phase distortion, for the quality of image [32]. All these complex solutions [86,87,90] result in orthogonal,

symmetric, linear phase filter pairs, resulting in a combination of beneficial properties that cannot be obtained with real-valued filter bank.

However, the impulse responses of the filters of all such complex solutions lack the quadrature (Hilbert pair) between their real and imaginary parts, a desirable property for the correct interpretation of local phase of the signal. As the Hilbert transform is global in nature (infinitely extended in both time/frequency domain), it is not directly applicable to localised wavelets with compact support. This observation points to the need for the design of local filters with properties similar to the Hilbert transform. The recent research in the field of CWT is directed towards the design of complex valued filter bank structure such that the resulting wavelets (real and imaginary parts) after high pass filtering form the (approximately) Hilbert transform pairs at each successive level in the framework of standard DWT decomposition structure (as described in section 2.4.2) [93-100].

### 3.3 Recent Developments

Recent research in the development of CWTs can be broadly classified in two groups; RCWT (Redundant CWTs) and NRCWT (Non-redundant CWTs) as shown in table (3.1). Standard DWT is critically decimated and gives N samples in transform domain for the same N samples of a given signal. While the redundant transform gives M samples in transform domain for N samples of given input signal (where  $M > N$ ) and hence it is expensive by the factor  $M/N$ . The NRCWT follows the design aim to approach towards N samples in transform domain for a given N input samples [101-105].

The RCWT include two almost similar CWTs. They are denoted as DT-DWT (Dual-Tree DWT based CWT) with two almost similar versions namely *Kingsbury's* DT-DWT(K), and *Selesnick's* DT-DWT(S) as classified in table (3.1). These redundant transforms consist of two conventional DWT filterbank trees working in parallel with respective filters of both the trees in approximate quadrature. The filterbank structure of both DT-DWTs (as described in section 3.5.2) is same but the

design methods to generate the filter coefficients are different. Both DT-DWTs provide phase information; they are shift-invariant with improved directionality [94,98-99]. *Selesnick* [98,99] proposed an alternative filter design methods for DT-DWT(K) and designed DT-DWT(S), almost equivalent to DT-DWT(K) such that in the limit the scaling and wavelet functions form Hilbert transform pairs. DT-DWT(S) is designed with simple methods to obtain filter coefficients.

*Selesnick's* DDTWT (Double Density Dual-Tree DWT) [108] is the initial and more redundant version of DT-DWT(S). DDTWT can be viewed as the combination of DDWT (Double Density DWT) [107] and DT-DWT(K). DDTWT again consists of two DDWT (Double Density DWT) trees working in parallel with respective filters in both trees are in approximate quadrature. Though the dual-tree DWT based CWT reduce all three disadvantages of standard DWT, the redundancy (though limited) of the transform is a drawback for applications like compression.

To remove this disadvantage, *Spaendonck et. al.* [104] created a set of projection-based non-redundant complex wavelet transforms (NRCWT). The projection (mapping) means converting a real signal to analytic (complex) form through digital filtering. NRCWT is the DWT of that complex valued projection. While these transforms are restricted to IIR filters, *Fernandes et. al.* [105] showed that they produce orthogonal solutions. *Fernandes*'s projection based CWT (PCWT) use flexible design techniques to trade-off between redundancy and shift-invariance.

*Spaendonck's* OHCWT (Orthogonal Hilbert transform filterbank based CWT) [103] is a three-band orthonormal complex wavelet transform with no-redundancy for both real- and complex- valued signals. The class of projection based NRCWT suggest their potential benefit in compression. Various design approaches to reduce one or more disadvantages of standard DWT are summarized in [75].

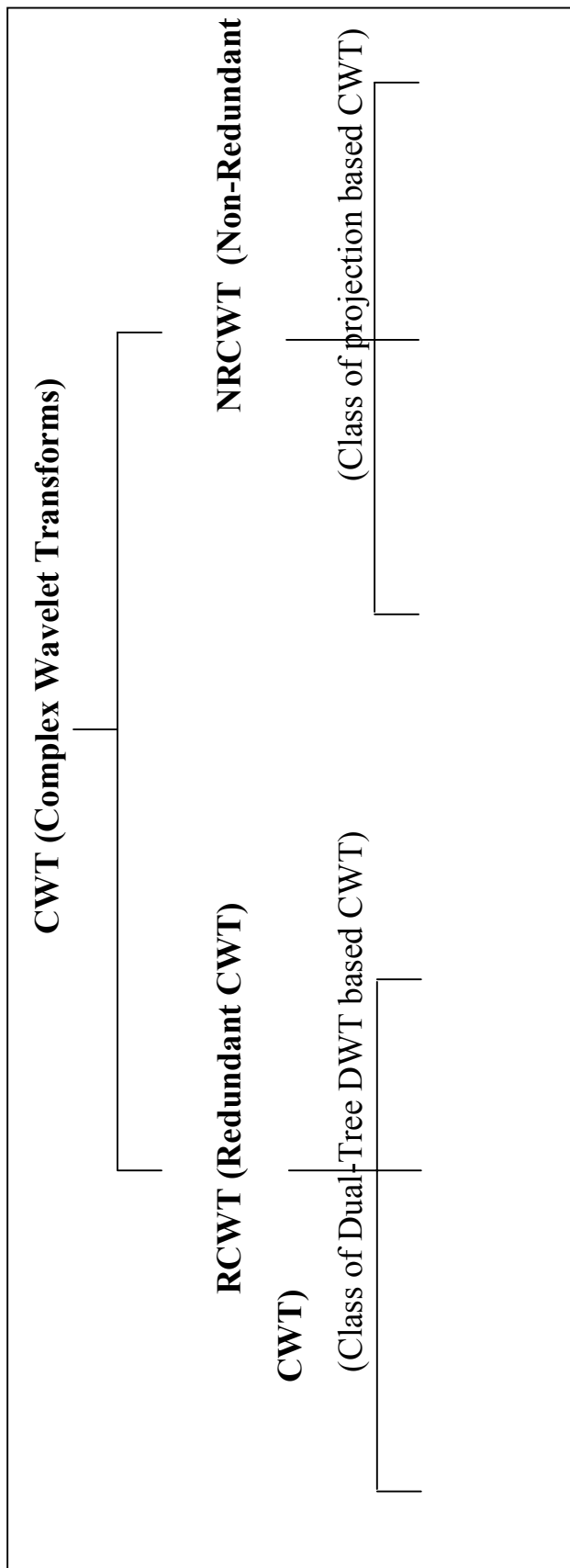


Table 3.1: Classification of complex wavelet transforms

### 3.4 Analytic Filter

*Gabor* introduced the Hilbert transform into signal theory in [40], by defining a complex extension of a real signal  $f(t)$  as:

$$x(t) = f(t) + j g(t) \quad (3.1)$$

where,  $g(t)$  is the Hilbert transform of  $f(t)$  and denoted as  $H\{f(t)\}$  and  $j = (-1)^{1/2}$ .

The signal  $g(t)$  is the  $90^\circ$  shifted version of  $f(t)$  as shown in figure (3.1 a). The real part  $f(t)$  and imaginary part  $g(t)$  of the analytic signal  $x(t)$  are also termed as the ‘Hardy Space’ projections of original real signal  $f(t)$  in Hilbert space. Signal  $g(t)$  is orthogonal to  $f(t)$ . In the time domain,  $g(t)$  can be represented as [106]:

$$g(t) = H\{f(t)\} = \frac{1}{\pi} \int_{-\infty}^{\infty} \frac{f(\tau)}{t - \tau} d\tau = f(t) * \frac{1}{\pi t} \quad (3.2)$$

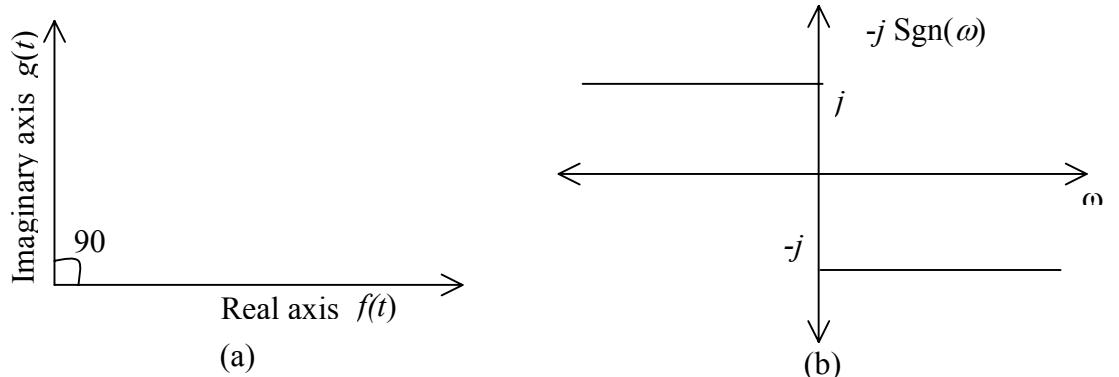


Figure 3.1: Hilbert Transform in (a) polar form, (b) frequency domain

If  $F(\omega)$  is the Fourier transform of signal  $f(t)$  and  $G(\omega)$  is the Fourier transform of signal  $g(t)$ , then the Hilbert transform relation between  $f(t)$  and  $g(t)$  in the frequency domain is given by

$$G(\omega) = F\{H\{f(t)\}\} = -j \text{Sgn}(\omega) F(\omega) \quad (3.3)$$

where,  $-j \text{Sgn}(\omega)$  is a modified ‘signum’ function as shown in figure (3.1 b).

This analytic extension provides the estimate of instantaneous frequency and amplitude of the given signal  $x(t)$  as:

$$\begin{aligned}\text{Magnitude of } x(t) &= \sqrt{(f(t)^2 + g(t)^2)} \\ \text{Angle of } x(t) &= \tan^{-1}[g(t)/f(t)]\end{aligned}\quad (3.4)$$

The other unique benefit of this quadrature representation is the non-negative spectral representation in Fourier domain [89,106], which leads toward half the bandwidth utilisation. The reduced bandwidth consumption is helpful to avoid aliasing of filter bands especially in multirate signal processing applications. The reduced aliasing of filter bands is the key for shift-invariant property of CWT. The single-sided spectral representation of an analytic signal is illustrated in figure (3.2).

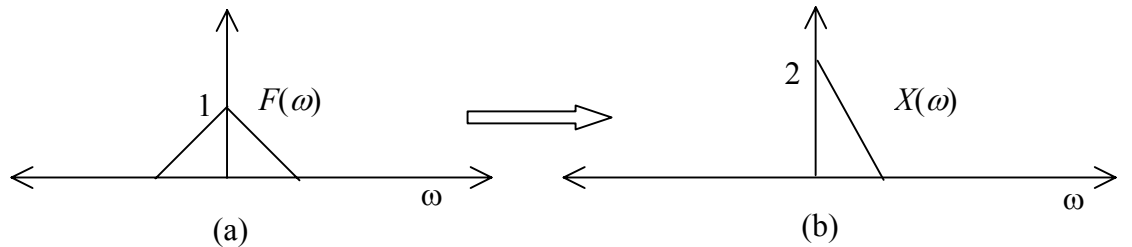


Figure 3.2: Spectral representation of (a) original signal  $f(t)$ , (b) analytic signal  $x(t)$

The same concept of analytic or quadrature formulation is applied to the filterbank structure of standard DWT to produce complex solutions and in turn the CWT. The real-valued filter coefficients are replaced by complex-valued coefficients by proper design methodology that satisfies the required conditions for convergence. Then the complex filter can again be decomposed into two real-valued filters. Thus, two real-valued filters that give their respective impulse responses in quadrature will form the Hilbert transform pair. The combined pair of two such filters is termed as an analytic filter. The formulation and interpretation of the analytic filter is shown in figure (3.3).

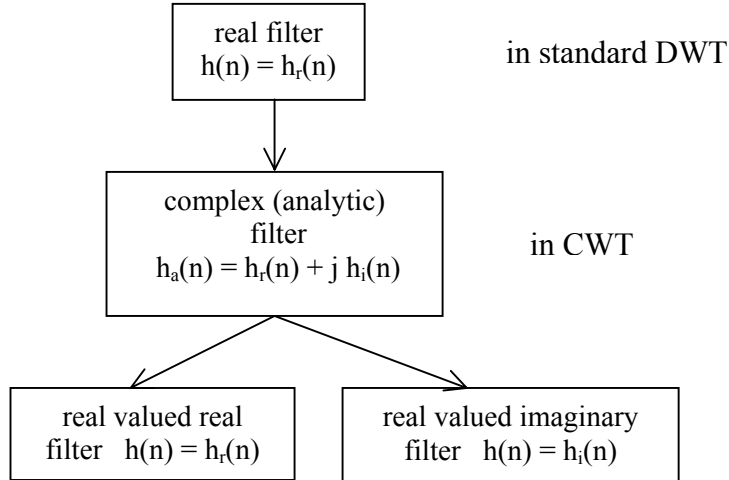


Figure 3.3: Interpretation of an analytic filter by 2-real filters

## 3.5 Redundant Complex Wavelet Transforms (RCWT)

### 3.5.1 Introduction

RCWT comprise two types of DT-DWT (Dual-Tree DWT based complex wavelet transforms as introduced in 3.3); one is *Kingsbury's* DT-DWT(K) [93-97] and the other is *Selesnick's* DT-DWT(S) [98-100]. These DT-DWT based transforms are redundant because of two conventional DWT filterbank trees working in parallel and are interpreted as complex because of the respective filters of both the trees are in approximate quadrature. In other words, respective scaling and the wavelet functions at all decomposition levels of both the trees form the (approximate) Hilbert transform pairs. Both versions of DT-DWT use 2-band PR filter sets.

The DT-DWT(S) is the less redundant version of its primitive 3-band PR Double-Density Dual-Tree DWT (DDTWT) structure that can be found in [108]. The DDTWT is derived by combining two parallel Double-Density DWT (DDWT) trees, preserving the quadrature properties of their respective wavelet filters. Thus, DDTWT has two important benefits: first is the shift-invariance due to redundant DDWT and second is Hilbert pair of wavelets because of two parallel trees in

quadrature. It is important to note that DDWT is a shift invariant 3-band redundant DWT but not a CWT [107].

Both DT-DWTs have same filterbank structure, which is described in 3.5.2. The DT-DWTs use the analysis and synthesis filterbank structures (figure (3.4)) that seem identical to those used for standard DWT as shown in figures (2.8) and (2.9). The key difference is that all the real filters are replaced with analytic filters formulated in figure (3.3) to have complex solutions. The replacement of real filters with analytic filters makes the new structure equivalent to two standard DWT filterbank structures operating in parallel. Because of two parallel trees for analysis as well as synthesis, these CWT are described as Dual-Tree DWT based CWT. The insertion of the parallel structure eliminates the disadvantages of standard DWT but makes it redundant (limited) and expensive for applications like signal compression.

### 3.5.2 Filterbank Structure of Dual-Tree DWT based CWT

The filterbank structures for both DT-DWTs are identical. Figure (3.4) shows 1-D analysis and synthesis filterbanks spanned over three levels. It is evident from the filterbank structure of DT-DWT that it resembles the filterbank structure of standard DWT with twice the complexity. It can be seen as two standard DWT trees operating in parallel. One tree is called as a real tree and other is called as an imaginary tree. Sometimes in future discussions the real tree will be referred to as *tree-a* and the imaginary tree as *tree-b*.

The form of conjugate filters used in 1-D DT-DWT is given as:

$$(h_x + j g_x)$$

where,  $h_x$  is the set of filters  $\{h_0, h_1\}$ , and  $g_x$  is the set of filters  $\{g_0, g_1\}$  both sets in only  $x$ -direction (1-D).

The filters  $h_0$  and  $h_1$  are the real-valued lowpass and highpass filters respectively for real tree. The same is true for  $g_0$  and  $g_1$  for imaginary tree.

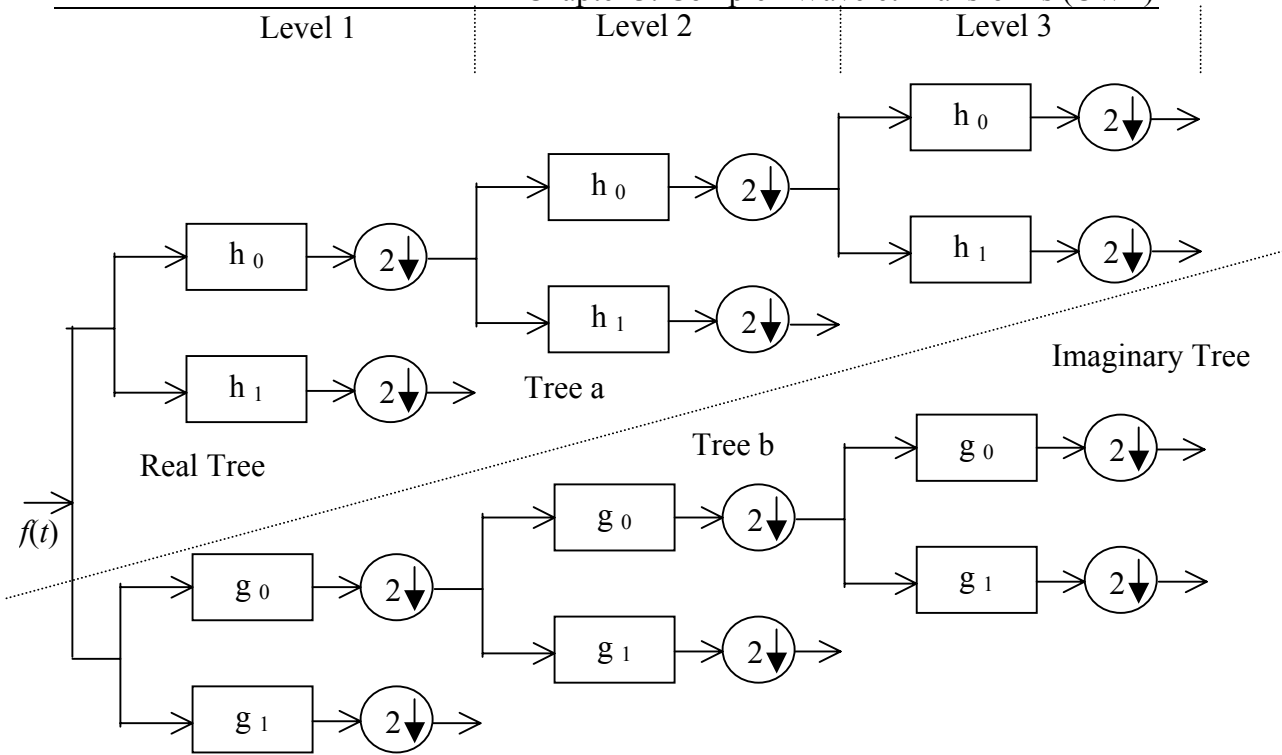


Figure 3.4: (a) Analysis filterbank for 1-D DT-DWT

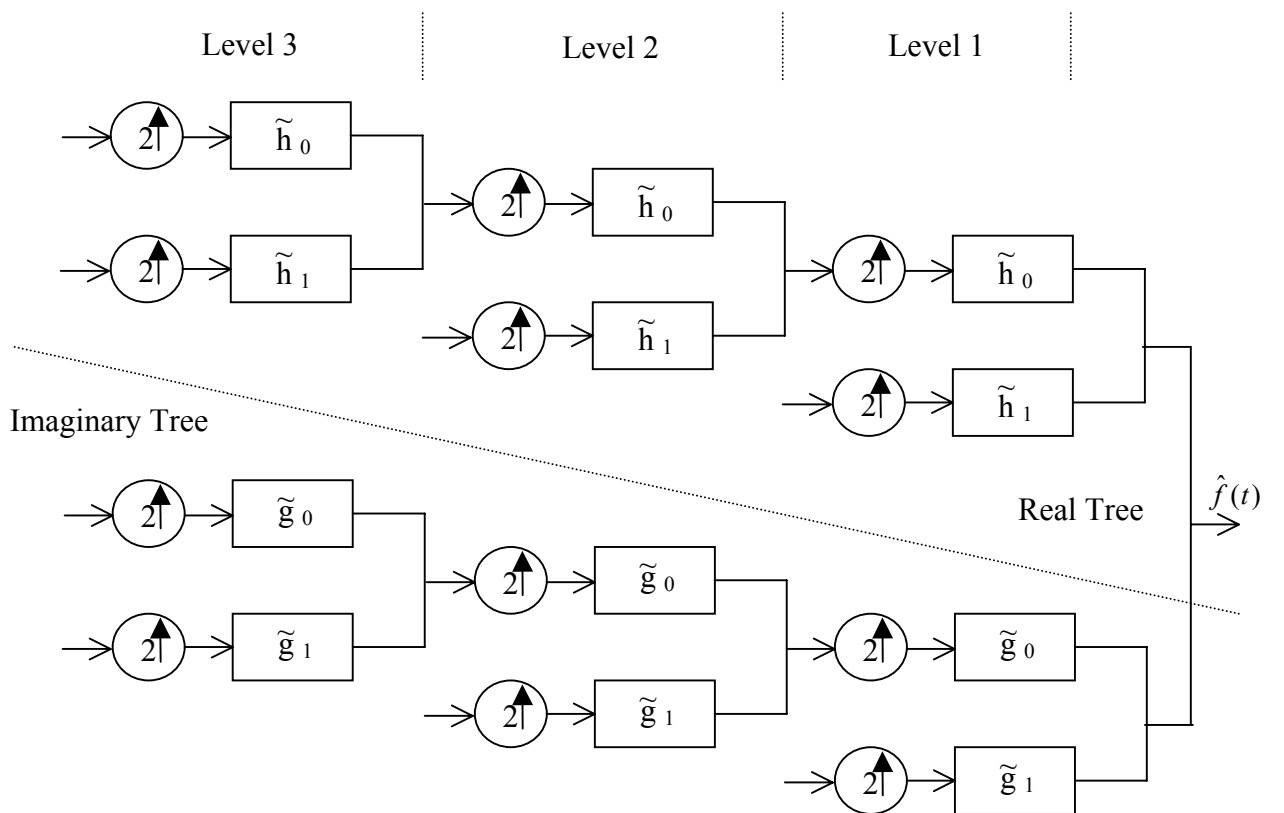


Figure 3.4: (b) Synthesis filterbank for 1-D DT-DWT

Though the notation of  $h_0$  and  $h_1$  are used for all levels in the real part of analysis tree,  $h_0$  and  $h_1$  of first level are numerically different than the respective filters at all other levels above level-1. The reason for such difference will be discussed later in the filter designs for both the DT-DWTs separately. The same notion is applied for imaginary tree filters  $g_0$  and  $g_1$ . The synthesis filter pairs  $\tilde{h}_0, \tilde{h}_1$ , and  $\tilde{g}_0, \tilde{g}_1$  as shown in figure (3.4 b) form orthogonal or biorthogonal pairs with their respective counterpart filters of analysis tree as shown in figure (3.4 a).

The 2-D DT-DWT structure has an extension of conjugate filtering in 2-D case. The filterbank structure of 2-D dual-tree is shown in figure (3.5). 2-D structure needs four trees for analysis as well as for synthesis. The pairs of conjugate filters are applied to two dimensions ( $x$  and  $y$ ), which can be expressed as:

$$(h_x + j g_x)(h_y + j g_y) = (h_x h_y - g_x g_y) + j(h_x g_y + g_x h_y) \quad (3.5)$$

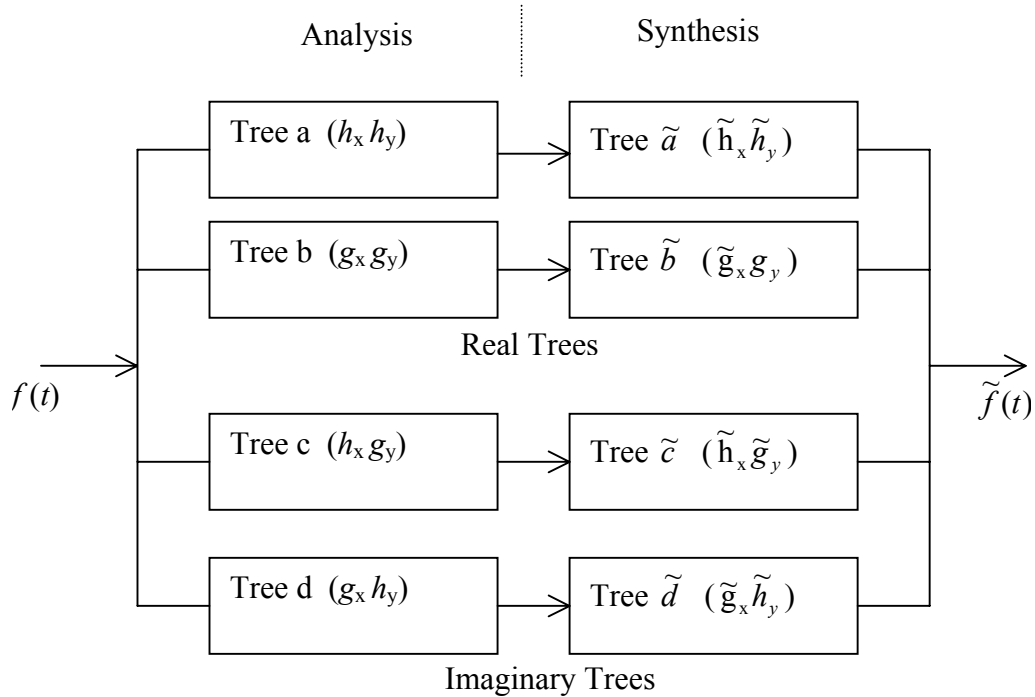


Figure 3.5: Filterbank structure for 2-D DT-DWT

The filterbank structure of *tree-a*, similar to standard 2-D DWT spanned over 3-level, is shown in figure (3.6). All other *trees-(b,c,d)* have similar structures with the appropriate combinations of filters for row- and column- filtering. The overall 2-D dual-tree structure is 4-times redundant (expensive) than the standard 2-D DWT. The *tree-a* and *tree-b* form the real pair, while the *tree-c* and *tree-d* form the imaginary pair of the analysis filterbank. *Trees-( $\tilde{a}, \tilde{b}$ )* and *trees-( $\tilde{c}, \tilde{d}$ )* are the real and imaginary pairs respectively in the synthesis filterbank similar to their corresponding analysis pairs.

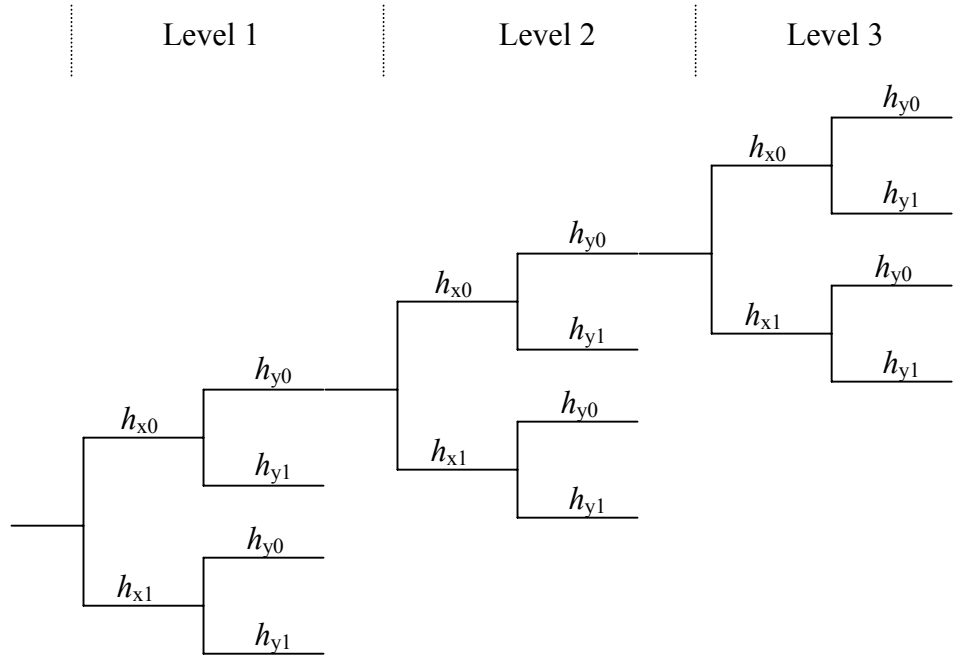


Figure 3.6: Filterbank structure of *tree-a* of figure 3.5

### 3.5.3 Kingsbury's Dual-Tree DWT (DT-DWT(K))

It is observed that approximate shift invariance is possible with standard DWT (i.e. *tree-a*) by doubling the sampling rate at each level of the tree [95]. For this to work, the samples must be evenly spaced and down samplers must be eliminated after the level-1 filters. This is equivalent to having two parallel fully decimated trees, real (*tree-a*) and imaginary (*tree-b*) as in figure (3.4) if the delays of first level filters of *tree-b* are one sample offset by their corresponding filter in *tree-a*.

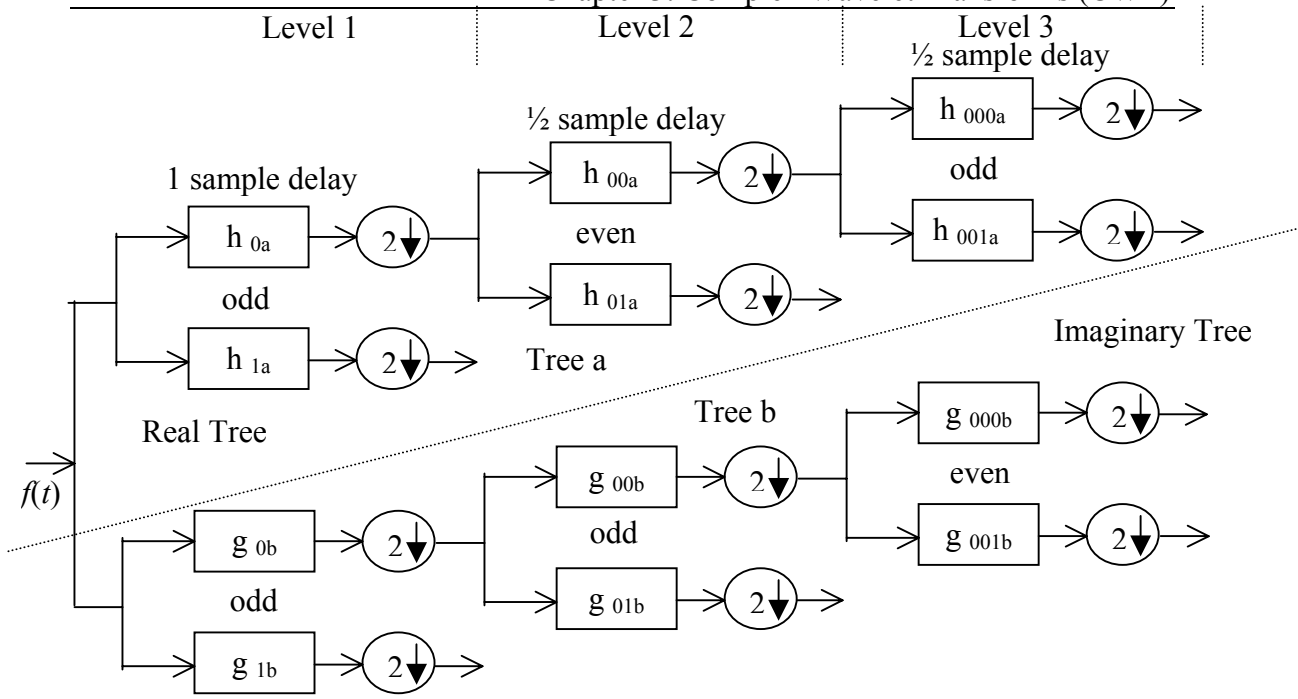
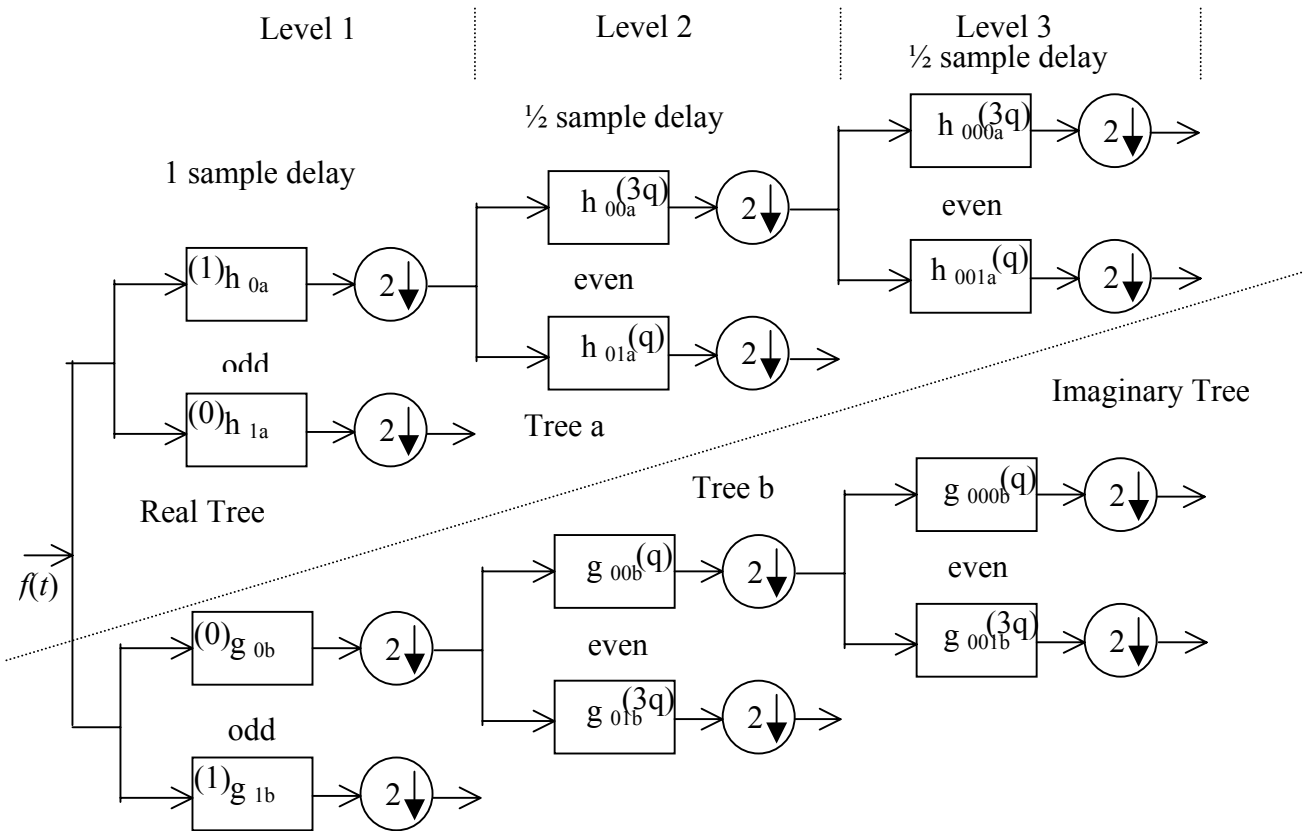


Figure 3.7: Analysis tree using odd-even filters


 Figure 3.8: Analysis tree using Q-shift filters. Figure in brackets inside a filter block indicates the delay for each filter, where  $q = \frac{1}{4}$  samples

This offset ensures the pickup of opposite samples in both trees. To get uniform interval between the samples of both trees after level-1, filters in one tree must provide delays that are half a sample different from those in opposite tree.

The DT-DWT(K) can be designed in two ways to have required delays. The first is based on odd-even length filters and the second employs Q-shift (quarter shift) filter design. The filterbank structures of analysis tree with odd-even filters and Q-shift filters are shown in figures (3.7) and (3.8) respectively. The key issue in the design of DT-DWT(K) is to obtain (approximate) shift invariance using any of the filter forms.

#### **Constraints for Shift Invariance:**

To check the shift invariance, only one type of coefficients (either scaling or wavelet) of both the trees at any one level is retained and all other coefficients at all other levels are set to zero. If the reconstructed signal  $\tilde{f}(t)$  from these coefficients is free of aliasing and follows the PR then the transform is said to be shift-invariant at that level.

DT-DWT(K) structure (same as shown in figure 3.4) can be modelled as shown in figure (3.9) using either odd-even (figure 3.7), or Q-shift (figure 3.8) filter types.

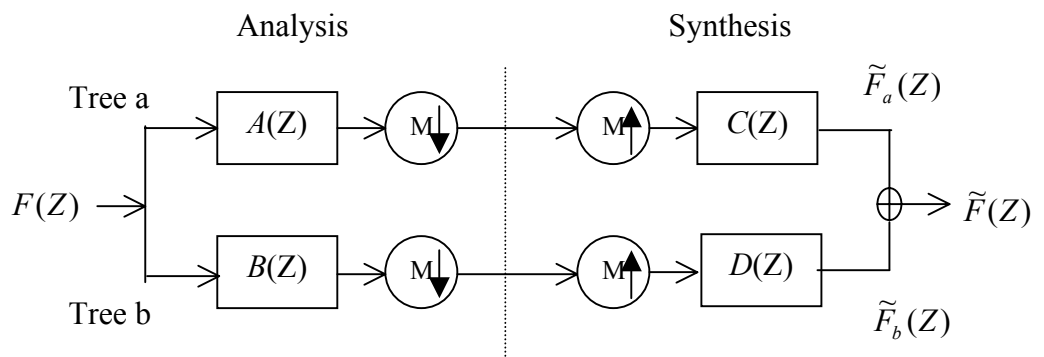


Figure 3.9: Modelling of DT-DWT(K) filter structure for deriving the shift-invariance constraints

The PR condition for DT-DWT(K) model (shown in figure (3.9)), using standard multirate identities of [14] is given as:

$$\begin{aligned}\tilde{F}(Z) &= \tilde{F}_a(Z) + \tilde{F}_b(Z) = F(Z) \\ &= \frac{1}{M} \sum_{k=0}^{M-1} X(W^k Z) [A(W^k Z)C(Z) + B(W^k Z)D(Z)]\end{aligned}\quad (3.6)$$

where,  $M = 2^m$  is the total up/down sampling factor determined by the number of levels ( $m$ ) of the dual-tree. The factor  $W = e^{\frac{j2\pi}{M}}$ . Letters A, B represent transfer functions of the analysis dual-tree and C, D represent the corresponding transfer functions for the synthesis dual-tree.

For the sake of simplicity (by taking  $m = 3$ ), and only the wavelet coefficients of level-3 are chosen to derive the constraints of shift invariance of DT-DWT(K). In this case the transfer function  $A(Z)$  ( $h_{0a}$  to  $h_{001a}$ ) and  $B(Z)$  ( $g_{0b}$  to  $g_{001b}$ ) as shown in figure (3.7) are modelled as:

$$\begin{aligned}A(Z) &= H_{0a}(Z)H_{00a}(Z^2)H_{001a}(Z^4) \\ B(Z) &= G_{0b}(Z)G_{00b}(Z^2)G_{001b}(Z^4)\end{aligned}\quad (3.7)$$

Similarly,  $C(Z)$  and  $D(Z)$  can be derived for synthesis tree.

The DT-DWT(K) can be shift-invariant if the aliasing terms  $A(W^k Z)C(Z)$  and  $B(W^k Z)D(Z)$  of equation (3.6) are either very small or cancel each other for  $k \neq 0$ . The designing strategies, to reduce these aliasing terms for approximate shift-invariance, are different for scaling (lowpass) and wavelet (highpass) coefficients [95].

For lowpass case aliasing can be reduced by letting:

$B(Z) = z^{\frac{\pm M}{2}} A(Z)$  and  $D(Z) = z^{\mp \frac{M}{2}} C(Z)$  so that

$$B(W^k Z) D(Z) = (-1)^k A(W^k Z) C(Z), \text{ for odd values of } k. \quad (3.8)$$

For highpass (bandpass) case, aliasing is generated by overlap of opposite frequency pass bands in a single wavelet tree, where as wanted terms ( $k = 0$ ) are produced by overlap of same frequency pass bands. The solution is to give B and D the upper and lower passbands of opposite polarity while A and C have the passbands of the same polarity (or vice versa). The need to discriminate in this way suggests the use of complex filters. Suppose  $P(Z)$  and  $Q(Z)$  are the prototype complex filters, each with just a single sided passband, and let

$$\begin{aligned} A(Z) &= 2\Re[P(Z)] = P(Z) + P^*(Z) \\ B(Z) &= 2\Im[P(Z)] = -j[P(Z) - P^*(Z)] \\ C(Z) &= 2\Re[Q(Z)] = Q(Z) + Q^*(Z) \\ D(Z) &= -2\Im[Q(Z)] = j[Q(Z) - Q^*(Z)] \end{aligned} \quad (3.9)$$

where  $\Re[]$  and  $\Im[]$  take real and imaginary parts, and conjugation of  $P(Z)$  is given by  $P^*(Z)$ .

Hence  $P$  and  $Q$  are filters corresponding to the upper passbands of  $A$  and  $C$  while  $P^*$  and  $Q^*$  correspond to their lower passbands. This also applies to filters  $B$  and  $D$ , except that their lower passbands are negated. The (real) impulse responses of  $B$  and  $D$  are the Hilbert transforms of those of  $A$  and  $C$ . The portion of equation (3.6) can be written as:

$$A(W^k Z) C(Z) + B(W^k Z) D(Z) = 2P(W^k Z) Q(Z) + 2P^*(W^k Z) Q^*(Z) \quad (3.10)$$

The task of designing the filters such that the positive frequency complex filter  $Q(Z)$  does not overlap with shifted versions of the similar filter  $P(Z)$  becomes easy due to their single sided spectral representation. The formulations in equation

(3.9) show that the bandpass filter responses for *trees-(a, b)* (*A, B* for analysis; *C, D* for reconstruction) should be regarded as the ‘real’ and ‘imaginary’ parts of complex responses (*P* for analysis; *Q* for synthesis) that have passbands only on one side of zero frequency. It is also possible to relate the pairs of scaling function coefficients of both trees as real and imaginary parts.

The design of DT-DWT(K) is based on viewing the scaling coefficients from *tree-b* as interpolating mid-way between the corresponding ones from *tree-a*. In practice, the filters with compact support will not have zero gain in their stop bands and the aliasing terms in equation (3.6) will not be zero. Furthermore, odd-length filters cannot have precisely the same frequency responses as the even-length ones. So a typical DT-DWT(K) will only be ‘approximately’ shift-invariant.

#### ***Odd-even length filters:***

To have linear phase filters with required delay offset between filters beyond level-1 of both trees, it is necessary to have odd-length filters in one tree and even-length filters in the other tree (figure 3.7). Greater symmetry between two trees can be achieved if each tree uses odd and even filters alternately from level to level. The filters at level-1 in both trees are odd length, and the corresponding lowpass and highpass filter pairs are apart by one sample. The filters in synthesis tree may be biorthogonal for PR or near-orthogonal for energy preservation (in transform domain) to the filters of analysis tree. The odd-even filter design is based on minimum mean squared error in the approximation. The coefficients of (13-19) tap odd length and (12-16) even length filters can be found in [94,95].

#### ***Q-shift filters:***

There are certain problems with odd-even length filter approach. First is that the sub-sampling structure is not very symmetrical (wavelet and scaling functions at a given scale are not well aligned). Second, the two trees have slightly different frequency responses and the third problem is that filter sets must be biorthogonal, rather than orthogonal, because they are linear phase.

To overcome all above problems, Q-shift filter are used for DT-DWT(K) (figure 3.8), in which all filters beyond level-1 are even length [95]. However, the Q-shift filters are no longer strictly linear phase. The filters are designed to have a group delay of approximately  $\frac{1}{4}$  samples (q). The required delay difference ( $\frac{1}{2}$  sample (2q)) between the corresponding filters of both the trees is achieved by using the time reverse of the *tree-a* filters in *tree-b* so that the delay of *tree-b* filters become 3q. As the filter coefficients are no longer symmetric, the perfect reconstruction filter sets are orthonormal and the synthesis filters are just the time reverse of equivalent analysis filters in both trees.

The key to the designing of filters for the Q-shift version of the DT-DWT(K) is based on the selection of a good even length lowpass filter  $H_L(Z)$  with the delay of  $\frac{1}{4}$  sample which also satisfies the standard orthonormal PR condition of 2-band filterbank [109]. The lowpass filter  $H_L(Z)$  of length  $2n$  with a delay that approximates  $\frac{1}{4}$  sample is designed with linear phase lowpass FIR filter  $H_{L2}(Z)$  of length  $4n$  as:

$$H_{L2}(Z) = H_L(Z^2) + Z^1 H_L(Z^2) \quad (3.11)$$

where,  $H_{L2}$  has half the desired bandwidth and twice the desired delay. The alternate coefficients of  $H_{L2}$  are taken to obtain  $H_L$ .

The filters after first level of DT-DWT(K) are derived as:

$$\begin{aligned} H_{00a}(Z) &= z^{-1} H_L(Z^1), & H_{01a}(Z) &= H_L(-Z) \\ H_{00b}(Z) &= H_L(Z), & H_{01b}(Z) &= z^{-1} H_L(-Z^1) \end{aligned} \quad (3.12)$$

The same filters are used for further levels in analysis tree. The time-reversed versions of these filters are used in synthesis tree. The recent design methods for Q-shift filters in frequency domain with filter coefficients can be found in [96].

### 3.5.4 Selesnick's Dual-Tree DWT (DT-DWT(S))

The DT-DWT(S) is again a DT-DWT form of redundant complex wavelet transform having the 1-D filterbank structure shown in figure (3.4). DT-DWT(S), proposed by *Selesnick* [98] is an alternate design approach to *Kingsbury*'s DT-DWT(K) discussed in section 3.5.3.

In [98,99], the alternate way to design the quadrature wavelet pair with specified length and vanishing moment multiplicity is shown. The DT-DWT(S) employs either ‘Grobner bases’ or general ‘spectral factorization’ methods for the design of analytic filters to have quadrature pair of wavelets in a dual-tree structure. The design of Hilbert transform pairs of wavelet basis with general spectral factorization using flat-delay allpass filters is simpler than the Grobner bases based solutions. The design of DT-DWT(S) also proves that for two orthogonal wavelets to form a Hilbert transform pair, the scaling filters of both trees should be offset by a half sample. The design is based on the limit function defined by infinite product formula rather than the concept of midway interpolation of two lowpass filters for approximate shift invariance (as in the case of DT-DWT(K)). The underlying constraints for the design of DT-DWT(S) are discussed here with key equations from [99].

For the filterbank structure, shown in figure (3.4), let  $h_0$  and  $h_1$  represent CQF (Conjugate Quadrature Filter) pair [53]. That is,

$$h_1(n) = (-1)^{(1-n)} h_0(1-n) \quad (3.13)$$

and, in Z-transform domain

$$\begin{aligned} H_0(Z)H_0\left(\frac{1}{Z}\right) + H_0(-Z)H_0\left(-\frac{1}{Z}\right) &= 2 \\ H_1(Z) &= \frac{1}{z}H_0\left(-\frac{1}{Z}\right) \end{aligned} \quad (3.14)$$

The filters  $g_0$  and  $g_1$  represent a second CQF pair.

For all these real-valued filters  $h_i$  and  $g_i$  of DT-DWT(S), the dilation and wavelet equations give the scaling and wavelet functions for the real tree as:

$$\begin{aligned}\varphi_h(t) &= \sqrt{2} \sum_n h_0(n) \varphi_h(2t-n) \\ \psi_h(t) &= \sqrt{2} \sum_n h_1(n) \psi_h(2t-n).\end{aligned}\tag{3.15}$$

The scaling function  $\varphi_g(t)$  and wavelet  $\psi_g(t)$  are defined similarly for the imaginary tree.

As discussed in section 3.4,  $\psi_g(t)$  is the Hilbert transform of  $\psi_h(t)$ ,  $\psi_g(t) = H\{\psi_h(t)\}$ , if

$$\begin{aligned}\psi_g(\omega) &= -j\psi_h(\omega), \quad \omega > 0 \\ &= j\psi_h(\omega), \quad \omega < 0\end{aligned}\tag{3.16}$$

where,  $\psi_h(\omega)$  and  $\psi_g(\omega)$  are the Fourier transforms of the wavelets associated with the highpass filters of real and imaginary parts of DT-DWT(S). Similarly,  $H_0(\omega) = \text{DTFT}\{h_0(n)\}$ ,  $G_0(\omega) = \text{DTFT}\{g_0(n)\}$  are the Fourier transforms of scaling filters  $h_0$  and  $g_0$  respectively.

If  $\psi_h(t)$  and  $\psi_g(t)$  form Hilbert transform pair, then

$$|\psi_h(\omega)| = |\psi_g(\omega)| \text{ and therefore } |H_0(\omega)| = |G_0(\omega)|\tag{3.17}$$

That is, the two lowpass filters are related as:

$$G_0(\omega) = H_0(\omega) e^{-j\theta(\omega)}\tag{3.18}$$

It is derived using infinite-product formula in [98] that it is possible only when

$$\theta(\omega) = \frac{\omega}{2}, \quad |\omega| < \pi \quad (3.19)$$

Equivalently, the digital filter  $g_0(n)$  is a half-sample delayed version of  $h_0(n)$ ,

$$g_0(n) = h_0(n-1/2) \quad (3.20)$$

As a half-sample delay can not be implemented with FIR filter, the approximate design of FIR filters  $h_0(n)$  and  $g_0(n)$  is employed with Grobner bases or spectral factorization [98,99]. The filter coefficients for DT-DWT(S) can be found from [110]. Orthogonal filter sets are used for DT-DWT(S). First level of analysis filterbank of DT-DWT(S) employs a unique lowpass filter pair to produce one pair of Hilbert wavelets at that level, and after first level, a second distinct pair of lowpass filters is repeated for the rest of the structure to produce the pairs of Hilbert wavelets at all subsequent levels of the DT-DWT(S). All the synthesis filters are the time-reversed version of their corresponding analysis filters.

### 3.5.5 Properties of DT-DWT

Both DT-DWTs (Dual-Tree DWT based CWTs) have similar properties because of their identical filterbank structures. The important properties for the comparison with standard DWT are Shift-sensitivity, Directionality and Phase-information. The key properties of DT-DWT(K) and DT-DWT(S) are [95,99]:

#### 1. *Shift Invariance:*

DT-DWT has approximate shift-invariance, or in other words, improved time-shift sensitivity in comparison with standard DWT. The reconstructed details at various levels and approximation at the last level have almost uniform shifts for the time-shifted unit step functions. This property is very clear from figure (3.10) compared to figure (2.20). The property of shift invariance makes the DT-DWT well suited for applications such as Motion estimation [111], and Image fusion [112] at various resolution levels.

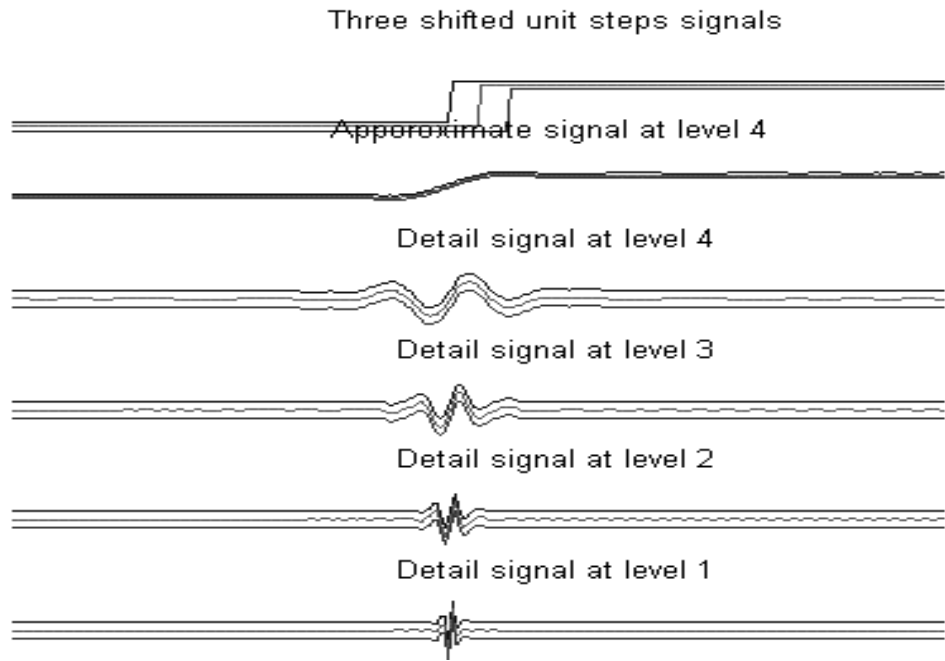


Figure 3.10: Shift-invariance property of 1-D DT-DWT

## 2. *Directionality:*

DT-DWT gives better directional selectivity in 2-D with Gabour like filters (also true for higher dimensionality  $m$ -D). Standard DWT offers the feature selectivity in only 3 directions with poor selectivity for diagonal features (figures (2.14) and (2.21)), where as DT-DWT has 12 directional wavelets (6 for each of real and imaginary trees) oriented at angles of  $\pm 15, \pm 45, \pm 75$  in 2-D as shown in figure (3.11). Three-dimensional view of all 12 wavelets is given as figure (3.12). The improved directionality with more orientations suggests the advantage of DT-DWT in a wide range of directional image processing applications, e.g. texture analysis [113].

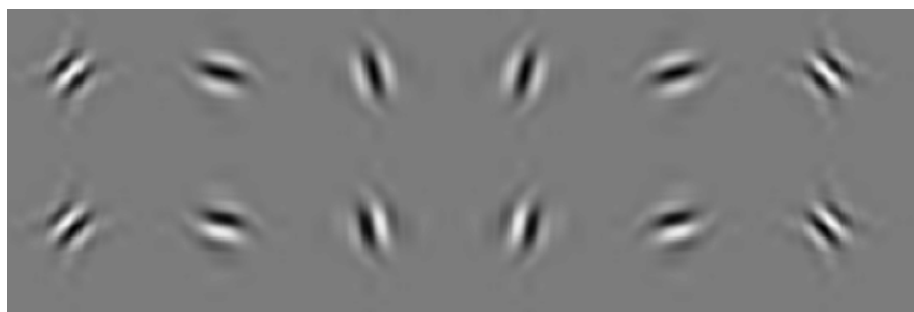


Figure 3.11: Directionality of 2-D DT-DWT

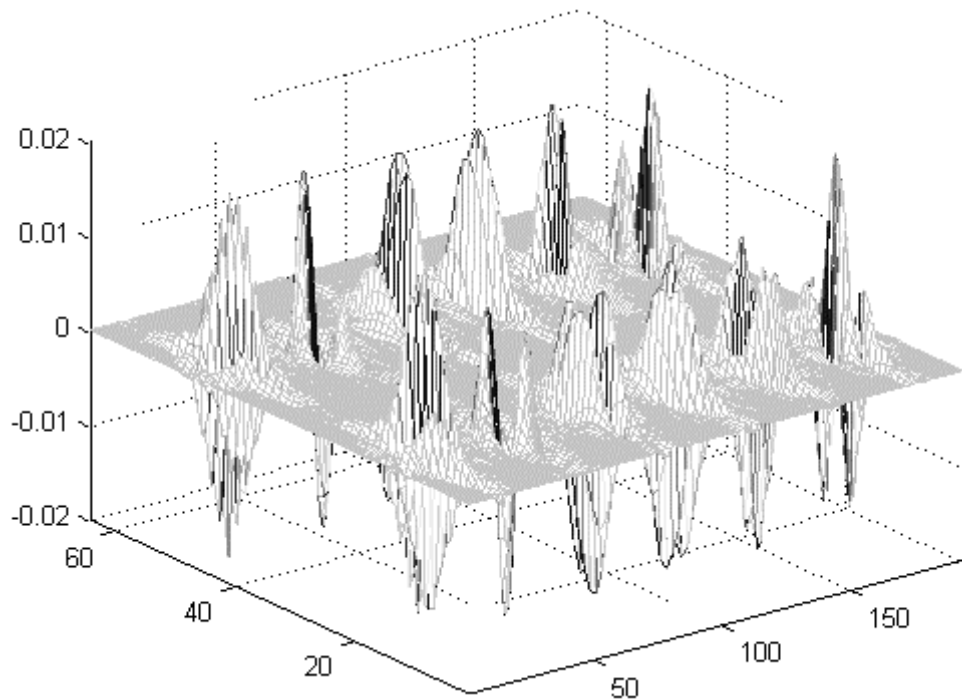


Figure 3.12: 3-D representation of 12 wavelets of DT-DWT

### 3. ***Phase Information:***

Local phase extraction is possible through analytic interpretation of two parallel trees of DT-DWT. The phase of any given subband at a given level can be computed with its corresponding real and imaginary coefficients based on equation (3.4). A 1-D complex wavelet is an envelope of real and imaginary wavelets in quadrature (Hilbert pair) as shown in figure (3.13).

### 4. ***Perfect Reconstruction:***

The DT-DWT structure follows PR conditions; hence, the original signal can be reconstructed from the transform domain complex wavelet coefficients.

### 5. ***Limited Redundancy:***

DT-DWT has redundancy of 2:1 ( $2^m:1$ ) for 1-D ( $m$ -D) independent of scales (levels) of iteration. Though DT-DWT structure is expensive than standard DWT, it is significantly less expensive than WP, or non-decimated DWT (SWT) for the same advantage of reduced shift-sensitivity. Moreover, DT-

DWT has other advantages such as improved directionality and phase information to compensate for its limited redundancy over standard DWT.

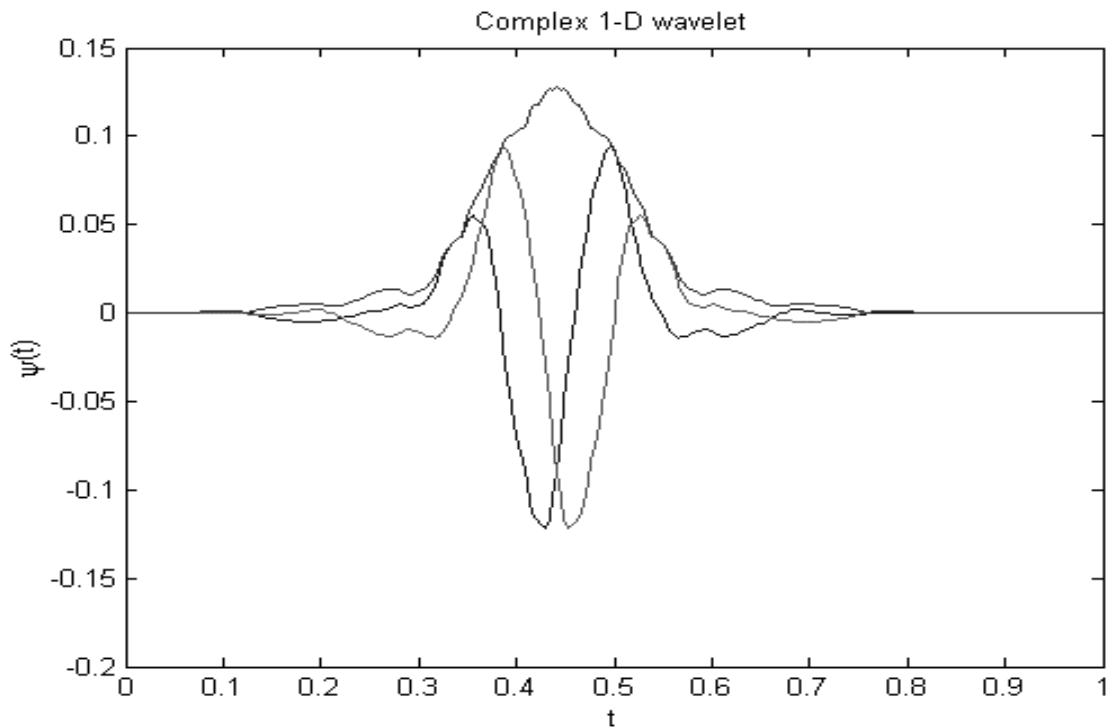


Figure 3.13: A complex wavelet as a quadrature combination of real and imaginary wavelets for 1-D DT-DWT

## 3.6 Non-Redundant Complex Wavelet Transforms (NRCWT)

### 3.6.1 Introduction

NRCWT is the class of complex projection (mapping) based DWT introduced in section 3.3. NRCWT has two-stage implementation (figure 3.14); first is the complex projection of a given signal and second is the implementation of any type of DWT on that complex valued projection. The independence of two stages allows them to be performed separately and alternatively leading towards a greater flexibility of implementation.

In true sense, all of the class of NRCWT are not exactly non-redundant CWT, which are designed to mitigate all three disadvantages of standard DWT. These complex wavelet transforms are categorized under NRCWT because of their two broad design aims. First is to offer controllable redundancy that is equal or less than the redundancy of DT-DWT (Dual-Tree based CWT or RCWT) while preserving all the benefits similar to DT-DWT. Second aim is to offer improved directionality and phase information with perfect non-redundancy at the cost of shift-invariant property targeting mainly the signal compression applications.

Three types of NRCWT are listed in table (3.1). *Fernandes*'s PCWT-CR (Projection based CWT with Controllable Redundancy) are the arbitrary DWT implemented on redundant complex projection of the original signal to preserve all potential benefits of DT-DWT. The PCWT-NR (Projection based CWT with No-Redundancy) can be designed with perfectly no-redundancy using non-redundant complex projection (mapping). PCWT-NR is directional but not shift-invariant. In the same way *Spaendonck*'s OHCWT (Orthogonal Hilbert transform filterbank based CWT) is a 3-band perfectly non-redundant and directional transform but is not shift-invariant.

### 3.6.2 Projection based CWT (PCWT)

*Fernandes et al.* [75,105,114] introduced 2-stage projection (mapping) based CWT that consist of mapping of a given real-world signal onto complex function space through some digital filtering technique (will be discussed later) followed by any type of DWT on the complex mapping.

#### 3.6.2.1 Generic Structure

A generic implementation of projection based complex wavelet transform (PCWT) is shown in figure (3.14). The forward CWT consists of an arbitrary DWT filterbank preceded by a mapping stage (or vice versa). The reverse CWT has inverse mapping stage after a synthesis DWT filterbank (or vice versa).

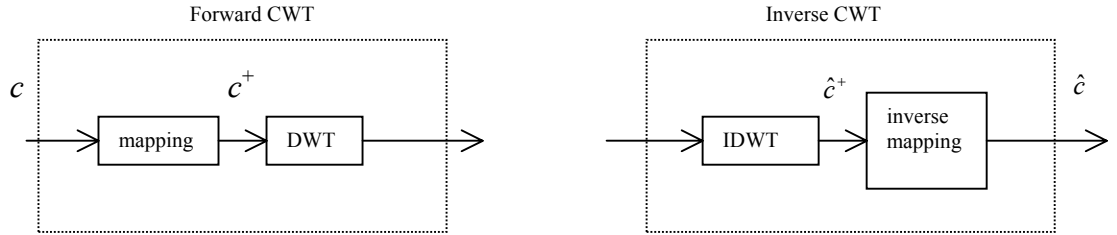


Figure 3.14: Generic implementation of PCWT

Unlike other redundant complex wavelet transforms such as DT-DWT and DDTWT that also mitigate DWT shortcomings, the decoupled implementation of PCWT (from a class of NRCWT) as shown in figure (3.14) has two important advantages. First, the controllable redundancy of the mapping stage offers a balance between degree of shift sensitivity and transform redundancy. This in turn allows creating directional, non-redundant complex wavelet transform with potential benefits for image coding systems. Second advantage of PCWT is the flexibility to use any DWT in the transform implementation.

In [101,102,114] this flexibility is exploited to create Complex Double Density DWT (CDDWT): a shift-invariant, directional CWT with a low redundancy of  $\frac{3^m - 1}{2^m - 1}$  in  $m$  direction (2.67 in 2-D) using non-redundant mapping preceded by DDWT (Double-Density DWT). Depending on the type of mapping and selection of DWT type, the PCWT may be controllable redundant (PCWT-CR) or non-redundant (PCWT-NR). Thus, PCWT can either be controllable redundant with shift-invariance, or non-redundant and directional without shift-invariance

### 3.6.2.2 Theory of Complex Projection

The ‘mapping’ block shown figure (3.14) shows the complex projection of the real sequence  $c$ . The other similar term to identify complex projection is the Hardy space projection. The Hardy space projection  $c^+$  of a real sequence  $c$  is nothing but the formulation of an analytic sequence. The Hardy space  $H^2(\mathbb{R} \rightarrow \mathbb{C})$  of a real valued  $L^2(\mathbb{R} \rightarrow \mathbb{R})$  function  $f$  is given as:

$$H^2(\mathbb{R} \rightarrow \mathbb{C}) \equiv \{f \in L^2(\mathbb{R} \rightarrow \mathbb{R}) : F(\omega) = 0 \text{ for all } \omega < 0\} \quad (3.21)$$

or in frequency domain,

$$F^H(\omega) = F(\omega)\chi_{[0,\infty)}(\omega) \quad (3.22)$$

where,  $H$  denotes hardy space mapping and  $\chi$  is an indicator function (same as unit step) on positive frequency axis.  $F^H$  gives single sided spectral representation.

The other important term related to this complex mapping is ‘unitary map’. The unitary map is a linear, bijective, inner-product preserving map. The function spaces that are related through unitary map are called isomorphic to each other. The unitary map or isomorphism is realisable if it can be implemented through digital filter. Thus, complex or Hardy space projection of a real signal is said to be realisable if it is possible to use some form of digital filtering for the mapping.

Let  $f$  be the projection of an  $L^2(\mathbb{R} \rightarrow \mathbb{R})$  function onto the arbitrary scaling space  $V_1$  so that  $f(x) = \sum_n c(n) \varphi(x - n)$  or equivalently  $F(\omega) = C(\omega)\Phi(\omega)$ . Hence,

Hardy space image is given by:

$$F^H(\omega) = \chi_{[0,\infty)} C(\omega)\Phi(\omega) \quad (3.23)$$

Unfortunately  $\chi_{[0,\infty)}$  is not  $2\pi$  periodic, it can not be applied to the scaling coefficient sequence  $c$  using a digital filter. Since Hardy space images of  $L^2(\mathbb{R} \rightarrow \mathbb{R})$  function are unrealisable, *Fernandes* [75] defined the ‘Softy-space  $S^+$ ’, a practical approximation to Hardy-space, which employs  $2\pi$  periodic indicator function  $\chi^{2\pi}_{[0,\infty)}$ .

### 3.6.2.3 Realisation of Complex Projection

Let  $h_0$  and  $g_0$  be the arbitrary lowpass analysis and synthesis filters of any 2-band, real coefficient, PR filterbank.

The mapping and inverse mapping filters  $h^+$  and  $g^+$  respectively are created by shifting  $H_0(\omega)$  and  $G_0(\omega)$  by  $\pi/2$  so that,

$$H^+(Z) = H_0(-jZ), \quad G^+(Z) = G_0(-jZ) \quad (3.24)$$

Let the real scaling-coefficient sequence  $c$  be associated with function  $f$  in some arbitrary MRA subspace  $V_1$ . The mapping filter  $h^+$  in figure (3.15) illustrates the forward map to the scaling-coefficient sequence  $c^+$  associated with  $f^+ \in V_1^+$ , the image of  $f$  where,

$$\begin{aligned} V_1^+ \equiv \{f^+ : \forall f \in V_1, \text{ where } F(\omega) = C(\omega)\Phi(\omega), \\ \text{define } C^+(\omega) = H^+(\omega) C(\omega), \\ F^+(\omega) = C^+(\omega)\Phi(\omega)\}. \end{aligned} \quad (3.25)$$

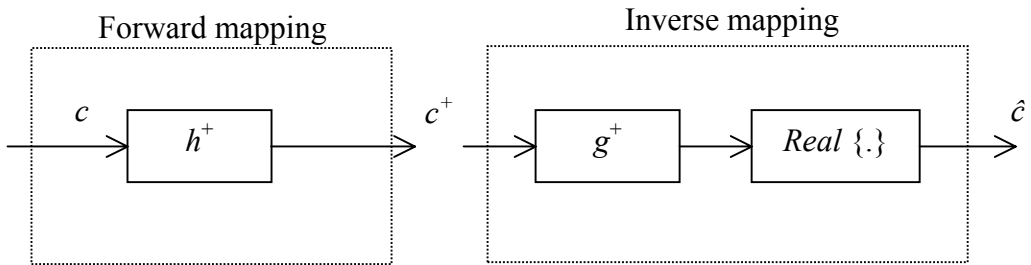


Figure 3.15: Realisable complex projection in softy-space

Figure (3.15) demonstrates that unitary map between  $V_1$  and  $V_1^+$  is realisable as it is implemented with digital filters  $h^+$  and  $g^+$ . The same concept can be extended to multilevel representation i.e.  $V_k$  to  $V_k^+$ ,  $\forall k \in \mathbb{Z}$ . All representation of  $V_k$  to  $V_k^+$  also follows the unitary map.

A filter  $h^+$  is a complex-coefficient forward mapping filter. It enables mapping of function  $f$  from  $V_k$  to  $V_k^+$ . Since  $h^+$  is a complex valued, it introduces redundancy by a factor of two when applied to real valued scaling-coefficient sequence. Filter  $g^+$  is an inverse mapping from  $V_k^+$  to  $V_k$ . Typical frequency response of the forward mapping filter  $H^+(\omega)$  is given in figure (3.16).

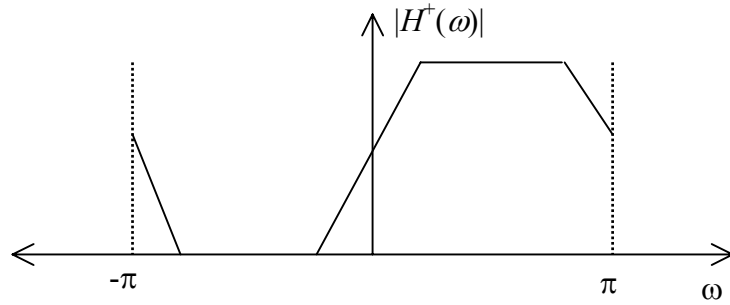


Figure 3.16:  $|H^+(\omega)|$ , the magnitude response of complex projection filter  $h^+$

The projection filter  $h^+$  significantly suppresses negative frequency. Hence the projection filter  $h^+$  maps original sequence  $c$  of  $L^2(\mathbb{R} \rightarrow \mathbb{R})$  to  $c^+$  of Softy-space  $S^+$ , which is equivalent to the analytic or Hardy space projection  $c^H (f^H)$  in  $H^2(\mathbb{R} \rightarrow \mathbb{C})$  of the sequence  $c$  associated with function  $f$ . For a lowpass filter  $h_0$  of length  $M$  and a mapping filter  $h^+$  of length  $N$ , the Softy-space associated with  $h_0$  and  $h^+$  is given as  $S_{MN}^+ \equiv \overline{U_{k \in Z} V_k^+}$ , where  $S^+$  is the family of function space spanned by multiresolution representation of function  $f$  in the Softy-space.

The relation between  $L^2(\mathbb{R} \rightarrow \mathbb{R})$ , Hardy-space  $H^2(\mathbb{R} \rightarrow \mathbb{C})$  and Softy-space  $S^+$  can be depicted as figure (3.17).

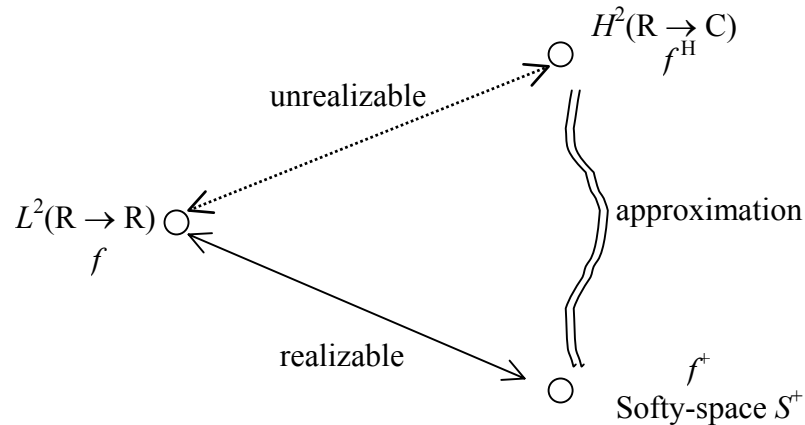


Figure 3.17: Relation between function spaces

### 3.6.2.4 Non-Redundant Complex Projection

The non-redundant complex projection is defined as the concatenation of a projection filter  $h^+$  and a down sampler as shown in figure (3.18). The down sampler eliminates odd-indexed scaling coefficients and removes the redundancy created by the complex valued projection filter  $h^+$ . It is important to note that the scaling coefficient sequence  $c$  and  $\tilde{c}^+$  can both be represented by  $N$  real numbers within a digital computer; therefore, there is no data redundancy in sequence  $\tilde{c}^+$ .

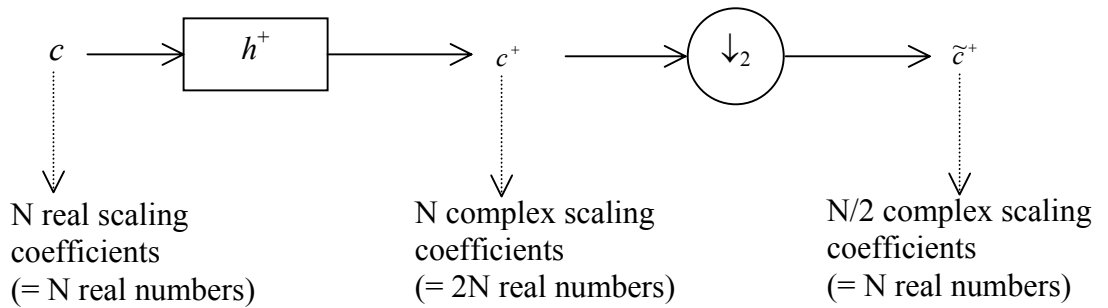


Figure 3.18: Non-redundant complex projection

Let the non-redundant complex projection be defined as  $\tilde{H}^+$  such that the scaling coefficient sequence  $c$  of function  $f$  in scaling space  $V_1$  is mapped to a sequence  $\tilde{c}^+$  of  $\tilde{f}^+$  in the function space  $\tilde{V}_0^+$  as:

$$\begin{aligned}
 \tilde{V}_0^+ \equiv & \left\{ \tilde{f}^+ : \tilde{F}^+(\omega) = \tilde{C}^+(2\omega)\Phi(2\omega), \text{ where } \tilde{c}^+ = \downarrow_2 c^+, \right. \\
 & \text{and } C^+(\omega) = H^+(\omega)C(\omega), \\
 & \left. \text{with } F(\omega) = C(\omega)\Phi(\omega), \forall f \in V_1 \right\}
 \end{aligned} \tag{3.26}$$

The equivalent relationship between the Non-redundant complex projection and Softy-space projection is given in figure (3.19). Let  $V_1^L$  denote the subset of lowpass functions in  $V_1$ . Where,  $f_1$  is the function associated with the original scaling coefficient sequence  $c_1$ , and  $f_0$  is the lowpass function in lower resolution space  $V_0$  after 1-level DWT decomposition through MRA. The function  $f_0^+$  associated with sequence  $c^+$  is a Softy-space projection in  $V_0^{L+}$  of a given lowpass function  $f_0$

associated with the  $c_0$  (decimation of sequence  $c_1$ ) through a complex projection filter  $h^+$ .

The  $\tilde{H}^+$  is a direct non-redundant complex projection of function  $f_1$  of  $V_1$  to  $\tilde{f}_0^+$  of  $\tilde{V}_0^+$  through the decimation of complex coefficients of Softy-space projections. It is proved in [114], that the non-redundant complex projection of a real signal approximates its Softy-space projection, if the signal has a lowpass characteristic. It is shown as  $\tilde{f}_0^+ \approx f_0^+$  in figure (3.19).

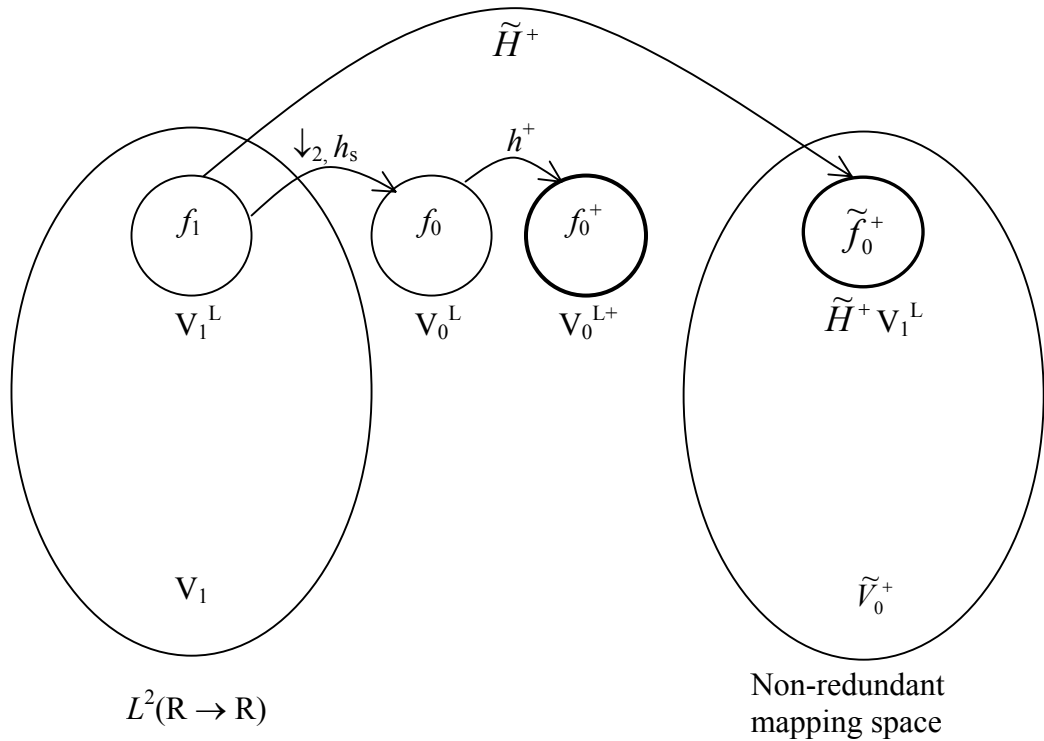


Figure 3.19: The relationship between non-redundant mapping  $\tilde{H}^+$  and softy-space mapping  $h^+$  shows that for all lowpass functions  $f_1$ , the associated functions  $\tilde{f}_0^+$  and  $f_0^+$  are approximately equal.

### 3.6.3 PCWT with Controllable Redundancy (PCWT-CR)

Softy-space  $S^+$  projection as discussed in section 3.6.2.3 is way of practical realisation of complex projection  $f^+$  of  $f$  which is equivalent to the Hardy space projection  $f^H$  of  $f$  (figure 3.17). Such a complex projection without any decimation step is redundant by nature. The projection based CWT (PCWT) of figure (3.14) with realisable redundant complex projection through Softy-space  $S^+$  can be viewed as figure (3.20).

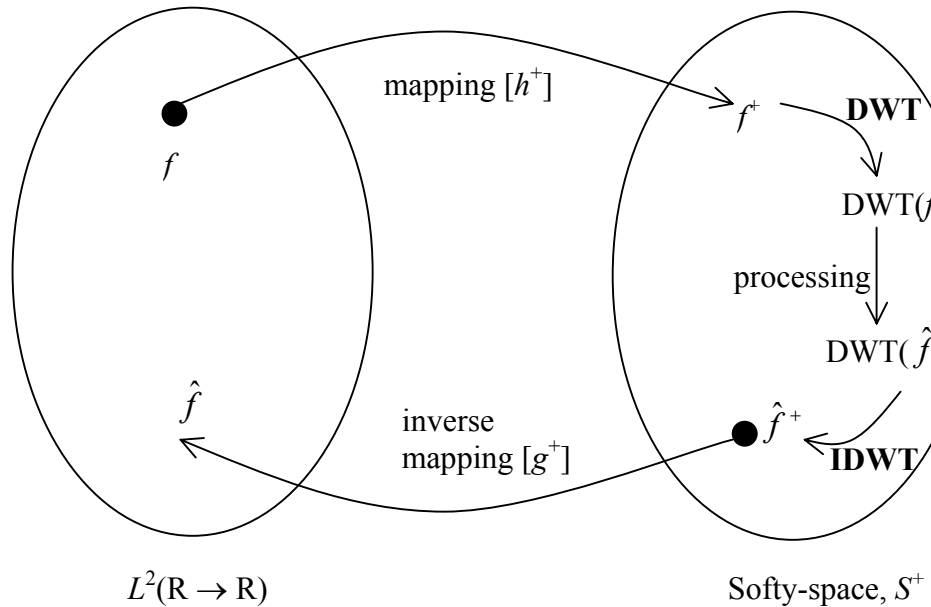


Figure 3.20: Implementation of realisable PCWT: PCWT-CR

The complex projection of real valued data introduces the redundancy by a factor of two. Hence, PCWT shown in figure (3.20) is denoted as ‘projection based CWT with controllable redundancy’ (PCWT-CR).

Due to the redundant projection and flexible arbitrary DWT implementation, PCWT can be controllable redundant with the minimum redundancy equal to that of DT-DWT. Since  $f^+ \approx f^H$ , the PCWT-CR has approximate shiftability: the subband energy in  $DWT(f^+)$  will remain approximately constant under shifts of  $f$ . The PCWT-CR has also improved directionality. It also exhibits explicit phase information using complex valued DWT implementation of a complex projection  $f^+$ .

### 3.6.4 PCWT with No-Redundancy (PCWT-NR)

As discussed in section 3.6.3, a PCWT-CR has all the advantages that are possible with DT-DWT (a class of RCWT) with the same controllable redundancy. Still the main disadvantage with PCWT-CR is the redundant projection (mapping). The softy space projection of a function  $f$  is redundant by a factor of two because of its complex valued nature. This redundancy is unacceptable in application such as data compression.

Thus, the technique of non-redundant projection is developed as discussed in section 3.6.3.4. PCWT based on non-redundant mapping incurs no data redundancy while mapping  $L^2(\mathbb{R} \rightarrow \mathbb{R})$  function onto the function space that approximates Softy space as shown in figures (3.18) and (3.19). The arbitrary DWT of the non-redundant complex projection of an  $L^2(\mathbb{R} \rightarrow \mathbb{R})$  function is defined as PCWT-NR. The implementation scheme for PCWT-NR is same as generic PCWT but with non-redundant projects is shown in figure (3.18).

The reversible implementation (realisable bijection or PR) of non-redundant complex projection through digital filter ensures its potential applicability in signal processing applications. The realisation of non-redundant mapping through real-valued allpass filters is shown in figure (3.21).

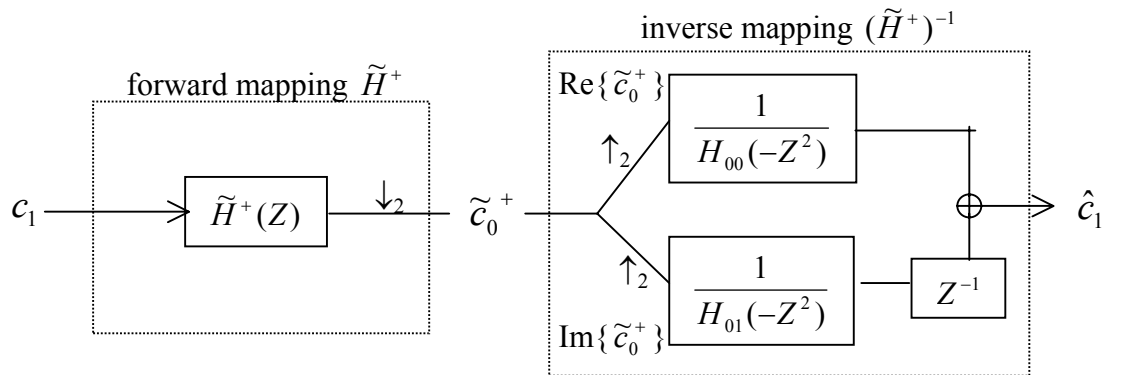


Figure 3.21: Realisation of non-redundant mapping

Let  $h_{00}$  and  $h_{01}$  are the even and odd polyphase components of a kernel lowpass filter  $h_0$  then

$$H_0(Z) = H_{00}(Z^2) + Z^{-1} H_{01}(Z^2) \quad (3.27)$$

The projection filter  $h^+$  is such that  $H_1^+(Z) = H_0(-jZ)$ . If  $H_{+0}(Z)$  and  $H_{+1}(Z)$  are the even and odd polyphase component of the projection filter  $h^+$ , and  $c_{10}$  and  $c_{11}$  are of original sequence  $c_1$  then the sequence  $\tilde{C}_0^+(Z)$  can be represented as:

$$\begin{aligned} \tilde{C}_0^+(Z) &= H_{+0}(Z) C_{10}(Z) + Z^{-1} H_{+1}(Z) C_{11}(Z) \\ &= H_{00}(-Z) C_{10}(Z) + jZ^{-1} H_{01}(-Z) C_{11}(Z) \end{aligned} \quad (3.28)$$

where  $H_{+0}(Z) = H_{00}(-Z)$  and  $H_{+1}(Z) = jH_{01}(-Z)$

For the reversible implementation of figure (3.21), it is derived in [114] that  $\hat{c}_1 = c_1$  can be realised through inverse map  $(\tilde{H}^+)^{-1}$  since

$$\frac{1}{H_{00}(-Z)} = H_{00}(-Z^{-1}), \text{ and} \quad \frac{1}{H_{01}(-Z)} = H_{01}(-Z^{-1}) \quad (3.29)$$

because  $H_{00}(-Z)$  and  $H_{01}(-Z)$  are allpass filters.

The DWT implementation with PCWT-CR or with PCWT-NR is flexible and arbitrary depending on the application to tradeoff between redundancy and shift-invariance. Thus by using Selesnick's [107] Double Density DWT (DDWT) after non-redundant complex mapping yields Complex Double Density DWT (CDDWT) [75,101] that has redundancy of 2.67 in 2-D. In other words, CDDWT is a kind of PCWT-NR, which is not perfectly non-redundant.

The non-redundant projection preserves the advantages such as phase information and improved directionality of Softy-space mapping. But due to the insertion of decimator block in non-redundant projection, it is not shift-invariant.

The advantage of PCWT-NR is the reduced and controllable redundancy in comparison with DT-DWT based redundant CWT (with redundancy of 4 in 2-D).

### 3.6.5 Orthogonal Hilbert Transform Filterbanks based CWT (OHCWT)

The Orthogonal Hilbert Transform Filterbanks based CWT (OHCWT) proposed by *Spaendonck et al.* [103] is a kind of non-redundant CWT. It uses the basic concept of complex projection in a modified form.

The 3-band filterbank structure of OHCWT is shown in figure (3.22). This structure is derived with the design specification such as preservation of polynomial trend, Hilbert transform pairs of wavelets, orthogonality and realisation with FIR filters. The design aim of OHCWT is to offers no redundancy for both real and complex valued signals. The filterbank features one real lowpass filter and two complex highpass filters. All filters are critically sampled. The formulation of complex wavelets is achieved through two complex highpass filters.

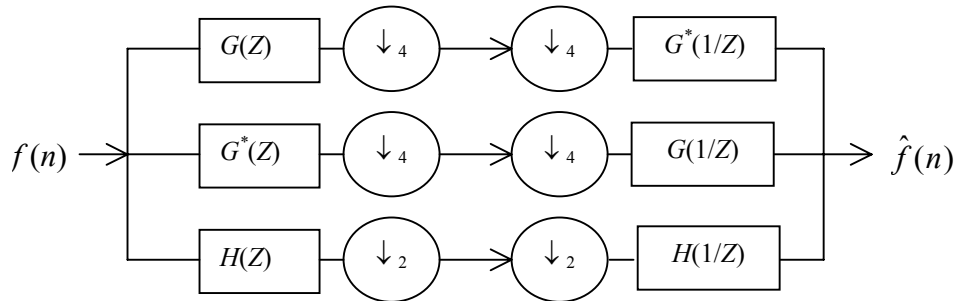


Figure 3.22: 3-band filterbank structure for 1-D OHCWT

The foundation filterbank structure shown in figure (3.22) has unbalanced down/up sampling. The lowpass branch consist of a conventional real-valued lowpass filter  $H(Z)$  whose output is down sampled by two. The two highpass branches consist of two complex highpass filters  $G(Z)$  and  $G^*(Z)$  whose outputs are down sampled by four. The suitability of OHCWT for processing real valued signal demands special symmetry between two complex highpass filters such that one can be removed in case of real signal.

It is also shown in [103] that for real signals, a single highpass filter with down sampling by four can be decomposed as a two stage filterbank, in which the first stage consists of a real valued highpass filter and subsampler, and the second stage contains a complex projection filter (Hilbert transform). This equivalent decomposed structure is shown in figure (3.23).

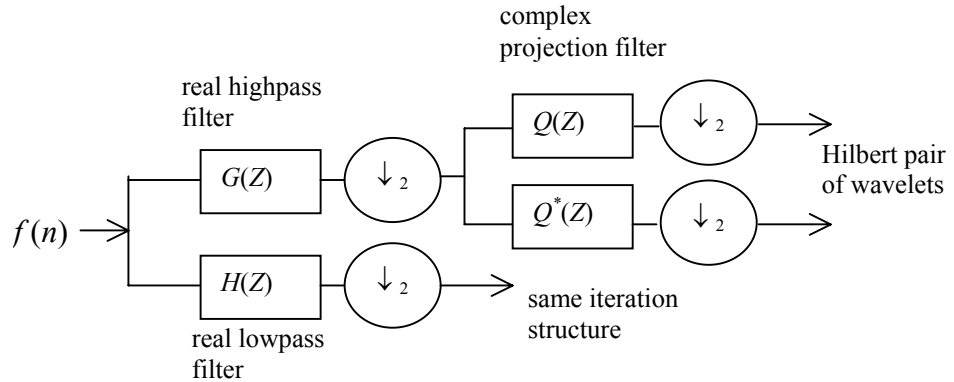


Figure 3.23: Single level analysis filterbank equivalence of 1-D OHCWT for real signal as shown in figure (3.22). One highpass filter is removed and other highpass filter is decomposed in two-stage filterbank.

The complex projection filter and its complex conjugate form a separable filterbank that can be designed in isolation. Thus, OHCWT can be implemented with standard DWT followed by the complex projection of highpass branch output. The transform can be computed up to desired level by iterating the modified filterbank structure of figure (3.23) on the real lowpass branch.

The crucial problem of designing a complex highpass filter  $G(Z)$  for OHCWT is simplified to the design of a conventional real orthonormal filterbank structure  $G(Z)$ , and the orthogonal conjugate symmetric complex filterbank structure  $Q(Z)$  and  $Q^*(Z)$ . The filter  $G(Z)$  in figure (3.23) is the complementary to the lowpass filter  $H(Z)$ . The orthoconjugate complex projection FIR filter can be obtained from an orthonormal filter  $U(Z)$  which satisfies half sample symmetry condition as:

$$U(Z) = zU(Z^1) \quad (3.30)$$

Through a simple shift of  $\pi/2$  in frequency so that the projection filter  $Q(Z)$  is

$$Q(Z) = U(-jZ) \quad (3.31)$$

Coefficients of such projection filters can be availed through the complex Daubechies solutions of *Lawton, and Lina* [85, 86]. These are the shortest FIR solutions with required half-sample symmetry.

The OHCWT proposed by *Spaendonck et al.* [103] with orthonormal bases has a simple filterbank structure. This structure permits the design of two types of FIR filterbanks; a general (standard) multiresolution DWT and a complex conjugate symmetric filterbank with Hilbert transform properties. Separable and isolated implementation of both filterbank makes this transform very flexible. Due to its non-redundancy for real- and complex- valued signals, the transform is promising for application such as compression and related problems where both amplitude and phase play pivotal role. The approximate Hilbert transform imposition between real and imaginary parts of the conjugate filters show substantial aliasing energy in negative frequency range, which may affect the reliability of amplitude and phase information.

### 3.7 Advantages and Applications of CWT

The initial versions of complex wavelet transforms by *Lina*, and *Lawton* [86,87] proved their potential for signal/image denoising and enhancement in comparison with standard real wavelet transform. As classified in section 3.3, the recent developments in CWT can be broadly categorised in two groups; first is RCWT (redundant complex wavelet transforms) with the important DT-DWT forms as discussed in section 3.5, and the second is NRCWT (non redundant complex wavelet transforms) with PCWT variants as discussed in section 3.6.

The DT-DWT versions of RCWT have limited redundancy with very good properties of shift-invariance, improved directionality and availability of phase information, which are not present in standard DWT. RCWT has a huge potential in signal/image Denoising, Enhancement, Segmentation, Edge detection and Motion

estimation. The investigations in [112,115] also suggest the potential of RCWT in Image fusion and Digital watermarking, but RCWT is not suitable for applications like image compression, where no-redundancy is of primary concern. The suitable class of CWTs for compression is NRCWT (non-redundant complex wavelet transforms).

All forms of NRCWT discussed in section 3.6 are based on complex projection filters. The PCWT (projection based CWT) and OHCWT (orthogonal Hilbert transform filterbank based CWT) are designed with the aim to have non-redundancy for improved image compression applications where the directionality and phase information play an important role. Though the class of NRCWT with non-redundant mapping achieves the non-redundancy, the approximate and tight design of Hilbert transform pairs of wavelets does not give approximate shift-invariance. The filterbank design for CWT to achieve all the benefits with non-redundancy is still an active and challenging area. The comparative summary of all CWT (as classified in table 3.1) is given in the table (3.2).

The possible advantages of the recent CWTs, either RCWT or NRCWT have yet not been investigated in many signal/image processing applications. It has been suggested in [93], that DT-DWT based RCWT can yield better results in signal/image Denoising and Enhancement. Because of the additional advantages of RCWT, there are ample potential applications for investigation such as Motion estimation for video signal processing, Remote sensing, Bio-medical image analysis/registration, and Texture analysis/classification. The PCWT (from the class of NRCWT) has potential for improved image compression especially for the transmission and storage of information. NRCWT has also some of the available benefits of RCWT in terms of directionality and phase information.

DT-DWT can be investigated for many 1-D signal (e.g. ECG, Speech) and 2-D imaging (e.g. MRI, SAR) for analysis, denoising and enhancement. Due to the properties of shift-invariance, better directionality, and explicit phase information, it is proposed that RCWT may yield improved analysis/denoising of various signals

which in turn be very useful in applications such as Automated Diagnostics for medical professional for bio-medical signals, Target Recognition/Tracking and Remote sensing for SAR signals.

NRCWT can be investigated for signal compression as they are non-redundant and have improved properties than the standard DWT. The combination of RCWT and NRCWT may also yield significant improvements in many signal/image applications. Use of RCWT can extract crucial information with flexible timings and storage for processing, while NRCWT can be useful for compressed transmission or storage when instant retrieval of signals is of prime importance.

Three possible ways of implementing CWT for natural signals are illustrated in figure (3.24). The hybrid mode of operation as shown in figure (3.24 c) is the application specific time-variant combination of RCWT and NRCWT. The NRCWT can be used at the first instance to select the region of interest (ROI), and then RCWT can be applied onto the region of interest (ROI) for improved feature detection, enhancement or analysis. The implementation of RCWT on a small sized ROI avails all the benefits of RCWT with only a limited increase in redundancy for a small part of an entire signal/image.

### 3.8 Summary

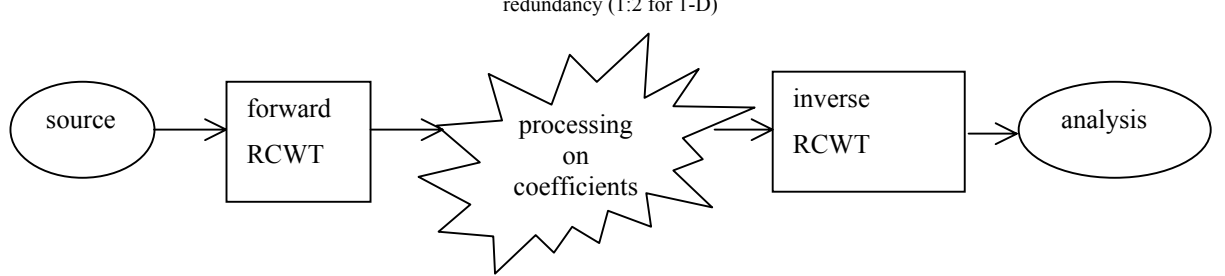
In this chapter, a thorough investigation on CWT is presented. Earlier work and recent developments on CWT are discussed. The motivation to avail phase information was the key objective of the earlier work on CWT. Recent developments explored the complex extensions to widely used standard DWT, and presented the recent forms of CWTs such as RCWT and NRCWT. These newer forms of CWT, with improved properties in terms of shift-sensitivity, directionality, and phase information, has the potential to replace the standard DWT in many signal processing applications (e.g video coding). DT-DWT is an important form of RCWT with the potential for Motion estimation, whereas PCWT-NR is an important form of NRCWT with the potential for Compression.

Type	Standard DWT	RCWT		NRCWT		
		DT-DWT(K)	DT-DWT(S)	PCWT-CR	PCWT-NR (CDDWT)	OHCWT
Features						
Proposed by	Mallat [27]	Kingsbury [93]	Selesnick [98]	Fernandes [101, 114]	Fernandes [101,114]	Spaendonck et al [103]
Key identification feature	Multilevel Resolution	Two parallel standard DWT trees in quadrature	Two parallel standard DWT trees in quadrature	Redundant complex mapping followed by any DWT or vice versa	Non-redundant complex mapping followed by any DWT or vice versa	3-band structure with two conjugate high pass filters decimated by 4
Shift-invariance	No Poor	Yes Very good	Yes Very good	Yes Good	No Poor	No Poor
Directionality (for 2-D)	Poor 3 at each level	Very good 6 at each level for each tree	Very good 6 at each level for each tree	Good 6 at each level	Fair 6 at each level with distortion in image shape in LH and HL subbands	Fair 6 at each level
Phase Information	No	Yes Very good	Yes Very good	Yes Good	Yes Fair	Yes Fair
Redundancy (for 2-D)	No 1:1	Fixed 4:1	Fixed 4:1	Flexible but $\geq 4:1$	Flexible 1:1 with standard DWT, and 2.67 with DDWT	No 1:1

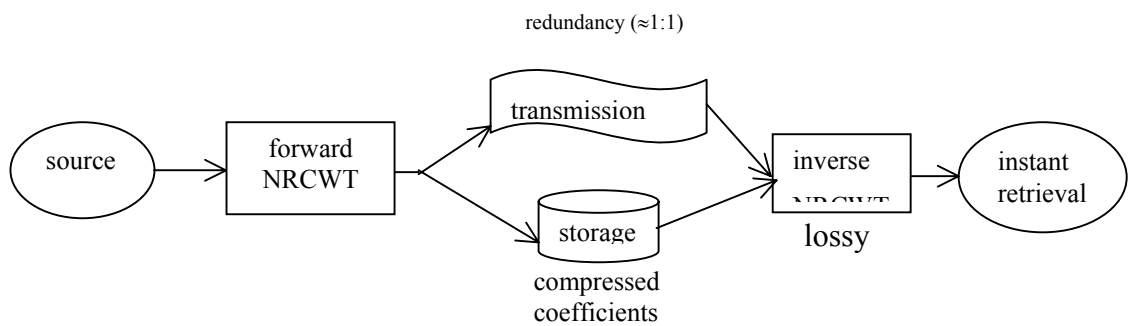
Table 3.2: Comparative summary of complex wavelet transforms (Contd.)

Type	Standard DWT	RCWT		NRCWT		
		DT-DWT(K)	DT-DWT(S)	PCWT-CR	PCWT-NR (CDDWT) OHCWT	
PR	Yes	Yes	Yes	Yes	Yes	Yes
Decomposition Filter band structure	Fixed 2-band	Fixed 2-band	Fixed 2-band	Flexible; Depends on type of DWT	Flexible; Depends on type of DWT	Flexible 3-band for (complex) 2-band for (real)
Strong application area for improved performance compared to standard DWT	-	Denoising, Enhancement, Segmentation, Motion- estimation, Image fusion, Digital watermarking , Texture Analysis [93, 100, 111,112,113, 115]	Denoising, Enhancement, Segmentation, Motion- estimation, Image fusion, Digital watermarking , Texture Analysis [93, 100, 111,112,113, 115]	Denoising, Enhancement, Segmentation, Motion- estimation, Image fusion, Digital watermarking , Texture Analysis [93, 100, 111,112,113, 115]	Directional and Phase based Compression [114]	Directional and Phase based Compression [114,103]

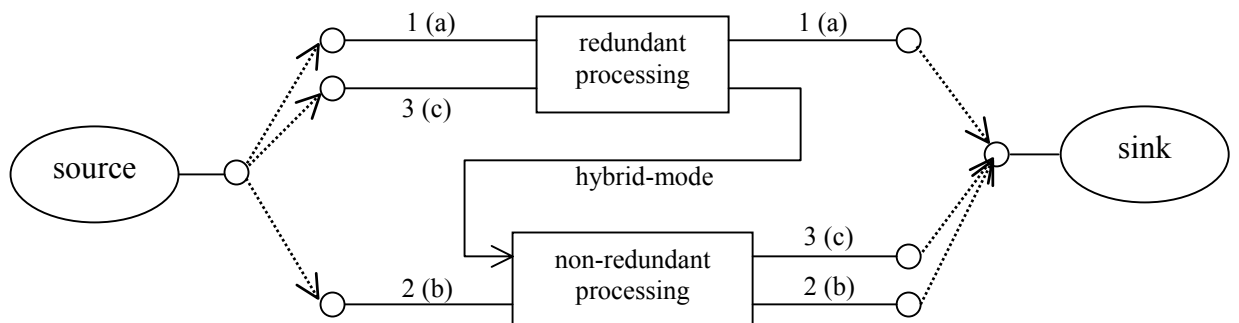
Table 3.2: Comparative summary of complex wavelet transforms



- a. *Redundant processing*: when redundancy is allowed for analysis, improved processing (denoising, enhancement, estimation) or for feature detection.



- b. *Non-redundant processing*: when non-redundancy is of prime importance for high-resolution compression in transmission or storage at the cost of shift-invariance.



- c. *Hybrid processing*: 1(a) for denoising, enhancement or motion estimation 2(b) for compression: transmission and storage, 3(c) for time-context variant applications based on ROI

Figure 3.24: Three possible ways of implementing CWT for natural signals

# Chapter 4:

## Application I- Denoising

### 4.1 Introduction

Many scientific experiments result in datasets corrupted with noise, either because of the data acquisition process, or because of environmental effects. A first pre-processing step in analyzing such datasets is denoising, that is, estimating the unknown signal of interest from the available noisy data. There are several different approaches to denoise signals and images. Despite similar visual effects, there are subtle differences between denoising, de-blurring, smoothing and restoration.

Generally smoothing removes high frequency and retains low frequency (with blurring), de-blurring increases the sharpness signal features by boosting the high frequencies, whereas denoising tries to remove whatever noise is present regardless of the spectral content of a noisy signal [116]. Restoration is kind of denoising that tries to retrieve the original signal with optimal balancing of de-blurring and smoothing. Traditional smoothing filters such as Mean, Median and Gaussian filters are liner operators normally employed in spatial domain, which smooth the signals with blurring effects [117-119].

A frequency domain approach (high pass) of ‘Inverse’ filtering for de-blurring [120] is sensitive to noise, and is not alone suitable for denoising. The Wiener filtering executes an optimal tradeoff (in MSE sense) between inverse

filtering and noise smoothing. It is useful in restoration by removing the additive noise and inverting the blurring simultaneously [120-122]. Wavelet based denoising schemes, widely popular since last decade, are non-linear thresholding of wavelet coefficients in time-scale transform domain.

Recent advances in wavelet based denoising combine variants of wavelet transforms with computationally involved Hidden Markov models, spatially adaptive methods and interscale dependency [125, 137-139] for improved performance. Newer generations of basis functions such as Ridgelets, Curvelets and Contourlets [140-142] have shown noticeable effectiveness over wavelets for images and higher dimensional data processing employing complicated mathematical models.

The fundamental concepts and classifications of Wavelet Transforms (WTs) and Complex Wavelet Transforms (CWTs) are discussed in Chapter 2 and Chapter 3 respectively. Some of the numerous applications of WTs and CWTs in many diverse fields are enlisted in sections 2.6 and 3.7 respectively. The basic purpose of this chapter is to describe the implementation of CWTs for Denoising. For critical evaluation, the performance of redundant CWTs (DT-DWT(K) and DT-DWT(S)) is compared with suitable type(s) of WTs and other conventional approaches.

Chapter 4 is organised into six sections. Section 4.1 is an introduction. Section 4.2 describes the concept of signal and image denoising in wavelet domain. Section 4.3 discusses generalised 1-D denoising, and section 4.4 is about a special case of 1-D denoising for audio signals. Section 4.5 presents 2-D denoising for various images. Section 4.6 is the conclusion for denoising application.

## 4.2 Wavelet Shrinkage Denoising

### 4.2.1 Basic Concept

Wavelet Thresholding, Wavelet Shrinkage, and Non-linear Shrinkage are widely used terms for wavelet domain denoising. Denoising by thresholding in wavelet

domain has been developed principally by *Donoho et al.* [123,124]. In wavelet domain, large coefficients correspond to the signal, and small ones represent mostly noise. The denoised data is obtained by inverse-transforming the suitably thresholded, or shrunk, coefficients.

#### 4.2.2 Shrinkage Strategies

The standard thresholding of wavelet coefficients is governed mainly by either ‘hard’ or ‘soft’ thresholding function as shown in figure (4.1). The first function in figure (4.1 a) is a ‘linear’ function, which is not useful for denoising, as it does not alter the coefficients. The ‘linear’ characteristic is presented in the figure just for comparing the non-linearity of other two functions.

The hard thresholding function is given as:

$$\begin{aligned} z = \text{hard}(w) &= w, |w| > \lambda, \text{ and} \\ z = \text{hard}(w) &= 0, |w| \leq \lambda \end{aligned} \quad (4.1)$$

where,  $w$  and  $z$  are the input and output wavelet coefficients respectively.  $\lambda$  is a threshold value selected.

Similarly, soft thresholding function is given as:

$$\begin{aligned} z = \text{soft}(w) &= \text{sgn}(w) \cdot \max(|w| - \lambda, 0), |w| > \lambda \text{ and} \\ z = \text{soft}(w) &= 0, |w| \leq \lambda \end{aligned} \quad (4.2)$$

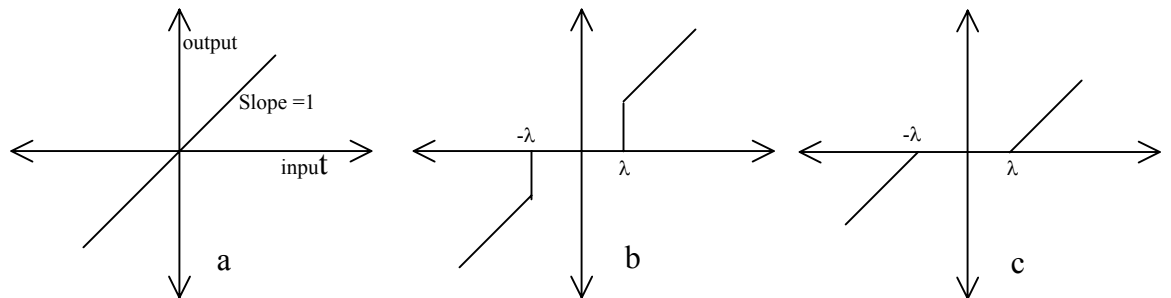


Figure 4.1: Thresholding functions; (a) linear, (b) hard, (c) soft

---

In hard thresholding, the wavelet coefficients (at each level) below threshold  $\lambda$  are made zero and coefficients above threshold are not changed whereas in soft thresholding, the wavelet coefficients are shrunk towards zero by an offset  $\lambda$ . Generally soft thresholding gives fewer artifacts and preserves the smoothness. The choice of threshold value is very crucial for a given signal for denoising.

*Donoho et al.* [123,124] introduced various shrinkage rules based on different threshold values and thresholding functions such as ‘visushrink’ with fixed universal threshold  $\lambda = \sigma\sqrt{2 \log_2 n}$  and ‘sureshrink’ based on Stein’s Unbiased Risk Estimator (SURE), where  $\lambda$  is not fixed but statistically related to the associated transform domain data sets.

There are other variants of thresholds and thresholding functions optimised for specific applications (e.g. MRI, Ultrasonic and SAR signal processing) that shrink the wavelet coefficients in between hard and soft thresholding under varying noise distributions [125-132]. Typically, wavelet based denoising is performed with fast and space saving decimated wavelet transforms. It is observed that the use of non-decimated transforms minimizes the artifacts in the denoised data [133-135]. In [136], it is demonstrated that the complex wavelet transforms (CWTs), being more directional, posses a good potential to tradeoff the denoising performance with its limited redundancy.

### 4.3 1-D Denoising

In section 4.3, level adaptive thresholding (hard and soft) is applied separately for each subband of 1-D signal using standard DWT, WP, SWT and redundant CWTs (DT-DWT(K) and DT-DWT(S)) for a comparative investigation.

#### 4.3.1 Signal and Noise Model

Signal and noise model for 1-D denoising simulations is given as:

$$x(n) = s(n) + \sigma g(n), \quad n = 1 \text{ to } N \quad (4.3)$$

where,  $s(n)$  is an  $N$  point original signal,  $x(n)$  is a noisy signal corrupted by (0,1) additive white Gaussian noise  $g(n)$  with a spread of  $\sigma$  as standard deviation. For experiment, a number of signals with varying degree of smoothness (blocks, bumps, heavy sine etc) and of various SNR are generated using Matlab function ‘wnoise’.

### 4.3.2 Shrinkage Strategy

Level adaptive threshold values are selected in transform domain based on various strategies (rigrsure, heursure etc) using Matlab function ‘thselect’ and actual hard or soft thresholding is performed using Matlab function ‘wthresh’

### 4.3.3 Algorithm

The wavelet shrinkage denoising of 1-D noisy signal  $x(n)$ , in order to recover  $y(n)$  as an estimate of original signal  $s(n)$  is represented as a 4-step algorithm [116] with  $j$  as decomposition levels,  $W$  as forward WT and  $W^{-1}$  as inverse WT.

1.  $\omega_j = W(x), j = 1 \text{ to } J$
2.  $\lambda_j = \text{Level adaptive threshold selection}(\omega_j)$
3.  $z_j = \text{Thresholding}(\omega_j, \lambda_j)$
4.  $y = W^{-1}(z_j)$

The standard DWT is performed with Matlab (wavelet toolbox) functions ‘wavedec’ and ‘waverec’, wavelet packet (WP) algorithm is implemented with functions ‘wpdec’, ‘bestree’, ‘wprec’ and with various tree management utilities available. The SWT is implemented with functions ‘swt’ and ‘iswt’. The DT-DWT algorithms employing DT-DWT(K) and DT-DWT(S) are implemented with Matlab following the discussion given in section 3.5.

#### 4.3.4 Performance Measure

The performance of various denoising algorithms is quantitatively compared using MSE (mean square error) and SNR (signal to noise ratio) as:

$$\text{MSE} = \frac{1}{N} \sum_{n=1}^N |s(n) - y(n)|^2$$

$$\text{SNR} = 10 \log_{10} \left( \frac{\sum_{n=1}^N |s(n)|^2}{\sum_{n=1}^N |s(n) - y(n)|^2} \right) \quad (4.4)$$

where,  $s(n)$  is an original signal and  $y(n)$  is an estimate of  $s(n)$  after denoising.

The qualitative performance is compared by plotting the original and recovered signals based on human visual perspective.

#### 4.3.5 Results and Discussion

Some sample results of experiment to compare performance measures for various signals under different SNR conditions are shown in tables (4.1) to (4.5). Figures (4.2 a) and (4.2 b) show the qualitative comparisons of denoising of 1-D ‘blocks’ signal using various WTs for ‘rigrsure’ case of table (4.1). Where  $\text{MSE}_i$  = initial MSE of noisy signal,  $\text{SNR}_i$  = initial SNR of noisy signal.  $\text{MSE}_h$ ,  $\text{MSE}_s$  = MSE after hard and soft thresholding respectively.

After observing and analysing the statistics of large number of experiments, the conclusions are as follows:

1. The ‘rigrsure’ and ‘minimax’ are optimum for soft and hard thresholding respectively. The threshold value selection based on ‘rigrsure’ is based on SURE criteria and is suitable for level adaptive thresholding with various amounts of noise and for large range of decomposition levels.

- 
- 2. Though threshold value with ‘sqtwolog’ gives the best performance with hard thresholding in case of ‘blocks’, it is not suitable for all types of signals with varying degree of noise and decomposition levels.
  - 3. Denoising performance varies with type of signal under consideration.
  - 4. Redundant CWT namely DT-DWT(K) and DT-DWT(S) perform better than standard DWT and WP but slightly poorer than SWT.
  - 5. Standard DWT has improved performance than the entropy based WP. In case of very high SNR, standard DWT and entropy based WP have the same results because under this condition the best tree is same as standard DWT tree.
  - 6. Denoising with DT-DWT(K) is slightly superior than DT-DWT(S). In poor SNR conditions, DT-DWT(K) performs equally well with either hard or soft thresholding.
  - 7. DT-DWT(K) gives better performance with hard thresholding whereas DT-DWT(S) gives improved performance with soft thresholding.
  - 8. Increasing the filter tap length improves the denoising performance with hard thresholding but degrades the SNR and MSE with soft thresholding. There is no change in performance of DT-DWT algorithms, as the filter lengths are kept fixed for both DT-DWT.
  - 9. Increase in decomposition levels ( $J=8$ ) degrades the performance of standard DWT, and SWT with soft thresholding. It also degrades the performance of WP, DT-DWT(K) and DT-DWT(S) for both hard and soft thresholding.

<b>Performance Measure</b>	<b>DWT</b>	<b>WP</b>	<b>SWT</b>	<b>DT-DWT(K)</b>	<b>DT-DWT(S)</b>
	Threshold criteria: 'rigrsure'				
<b>MSEh</b>	0.63	0.76	0.54	0.24	0.52
<b>MSEs</b>	0.24	0.31	0.19	0.29	0.23
<b>SNRh (dB)</b>	17.53	16.73	18.23	21.81	18.36
<b>SNRs (dB)</b>	21.69	20.64	22.68	20.86	21.90
	Threshold criteria: 'heursure'				
<b>MSEh</b>	0.37	0.47	0.24	0.32	0.27
<b>MSEs</b>	0.37	0.40	0.31	0.57	0.31
<b>SNRh (dB)</b>	19.84	18.85	21.84	20.53	21.21
<b>SNRs (dB)</b>	19.86	19.52	20.65	17.98	20.59
	Threshold criteria: 'sqtwolog'				
<b>MSEh</b>	0.27	0.37	0.14	0.34	0.19
<b>MSEs</b>	0.55	0.58	0.52	0.37	0.49
<b>SNRh (dB)</b>	21.17	19.87	24.07	20.30	22.82
<b>SNRs (dB)</b>	18.17	17.93	18.40	16.93	18.63
	Threshold criteria: 'minimaxi'				
<b>MSEh</b>	0.43	0.61	0.22	0.20	0.37
<b>MSEs</b>	0.27	0.32	0.26	0.37	0.25
<b>SNRh (dB)</b>	19.18	17.70	22.16	22.64	19.85
<b>SNRs (dB)</b>	21.21	20.44	21.43	19.86	21.50

Table 4.1: *Effect of thresholding criteria for 1-D denoising* on a signal ‘blocks’ with  $N=1024$  points, initial  $\text{SNR}_i = 15.36$  dB,  $\text{MSE}_i = 1.05$ , level of WT decomposition  $J=4$ , wavelet type for DWT, WP and SWT is ‘db2’, filters for DT-DWT(K) are ‘near\_sym\_b’ and ‘qshift\_b’ as given in appendix A, filters for DT-DWT(S) are as given in appendix B.

<b>Performance Measure</b>	<b>DWT</b>	<b>WP</b>	<b>SWT</b>	<b>DT-DWT(K)</b>	<b>DT-DWT(S)</b>
Signal: ‘bumps’ with SNR <sub>i</sub> = 7.18, MSE <sub>i</sub> =1.05					
<b>MSEh</b>	0.34	0.59	0.20	0.10	0.20
<b>MSEs</b>	0.16	0.21	0.11	0.12	0.11
<b>SNRh (dB)</b>	12.11	9.70	14.37	17.18	14.36
<b>SNRs (dB)</b>	15.26	14.18	17.15	16.45	17.13
Signal: ‘heavy sine’ with SNR <sub>i</sub> = 20.13, MSE <sub>i</sub> = 1.05					
<b>MSEh</b>	0.28	0.56	0.14	0.12	0.21
<b>MSEs</b>	0.13	0.19	0.09	0.11	0.10
<b>SNRh (dB)</b>	25.81	22.87	28.94	29.65	26.99
<b>SNRs (dB)</b>	29.17	27.64	30.94	29.80	30.50
Signal: ‘doppler’ with SNR <sub>i</sub> = 5.94, MSE <sub>i</sub> = 1.05					
<b>MSEh</b>	0.28	0.50	0.20	0.12	0.15
<b>MSEs</b>	0.15	0.19	0.10	0.11	0.11
<b>SNRh (dB)</b>	11.72	9.17	13.10	15.31	12.14
<b>SNRs (dB)</b>	14.51	13.43	16.02	15.74	15.84
Signal: ‘quad chirp’ with SNR <sub>i</sub> = 11.86, MSE <sub>i</sub> = 1.06					
<b>MSEh</b>	1.05	0.98	1.02	0.82	1.00
<b>MSEs</b>	0.87	0.70	0.78	0.74	0.72
<b>SNRh (dB)</b>	11.84	12.11	11.97	12.91	12.03
<b>SNRs (dB)</b>	12.68	13.59	13.12	13.34	13.43

Table 4.2: *Effect of different SNR<sub>i</sub> and MSE<sub>i</sub> for 1-D denoising* with ‘rigrsure’ thresholding on various signals with  $N=1024$  points, level of WT decomposition  $J=4$ , wavelet type for DWT, WP and SWT is ‘db2’, filters for DT-DWT(K) (‘near\_sym\_b’ and ‘qshift\_b’) and filters for DT-DWT(S) are as given in appendix A and B respectively.

<b>Performance Measure</b>	<b>DWT</b>	<b>WP</b>	<b>SWT</b>	<b>DT-DWT(K)</b>	<b>DT-DWT(S)</b>
<b>MSEh</b>	0.21	0.48	0.14	0.11	0.22
<b>MSEs</b>	0.14	0.18	0.10	0.11	0.11
<b>SNRh (dB)</b>	10.25	6.73	12.06	12.96	10.00
<b>SNRs (dB)</b>	12.11	10.91	13.44	12.97	12.97

Table 4.3: *Effect of low SNR<sub>i</sub> for 1-D denoising* on ‘blocks’ signal with  $N=1024$  points, threshold criteria is ‘rigrsure’,  $\text{SNR}_i = 3.32$ ,  $\text{MSE}_i = 1.05$ , level of WT decomposition  $J= 4$ , wavelet type for DWT, WP and SWT is ‘db2’.

<b>Performance Measure</b>	<b>DWT</b>	<b>WP</b>	<b>SWT</b>	<b>DT-DWT(K)</b>	<b>DT-DWT(S)</b>
<b>MSEh</b>	0.61	0.72	0.53	0.24	0.52
<b>MSEs</b>	0.28	0.36	0.25	0.29	0.23
<b>SNRh (dB)</b>	17.69	17.01	18.30	21.81	18.36
<b>SNRs (dB)</b>	21.09	19.94	21.59	20.86	21.90

Table 4.4: *Effect of long tap filters for 1-D denoising* on ‘blocks’ signals with  $N=1024$  points, threshold criteria = ‘rigrsure’,  $\text{SNR}_i = 15.36$ ,  $\text{MSE}_i = 1.05$ , level of WT decomposition  $J=4$ , wavelet type for DWT, WP and SWT = ‘db6’.

<b>Performance Measure</b>	<b>DWT</b>	<b>WP</b>	<b>SWT</b>	<b>DT-DWT(K)</b>	<b>DT-DWT(S)</b>
<b>MSEh</b>	0.64	0.95	0.54	0.58	0.59
<b>MSEs</b>	0.27	0.75	0.19	0.32	0.44
<b>SNRh (dB)</b>	17.53	15.76	18.24	20.51	17.36
<b>SNRs (dB)</b>	21.30	16.78	22.67	17.92	19.13

Table 4.5: *Effect of more number of decomposition levels for 1-D denoising* on ‘blocks’ signal with  $N=1024$  points, threshold criteria = ‘rigrsure’,  $\text{SNR}_i = 15.36$ ,  $\text{MSE}_i = 1.05$ , level of WT decomposition  $J= 8$ , wavelet type for DWT, WP and SWT = ‘db2’.

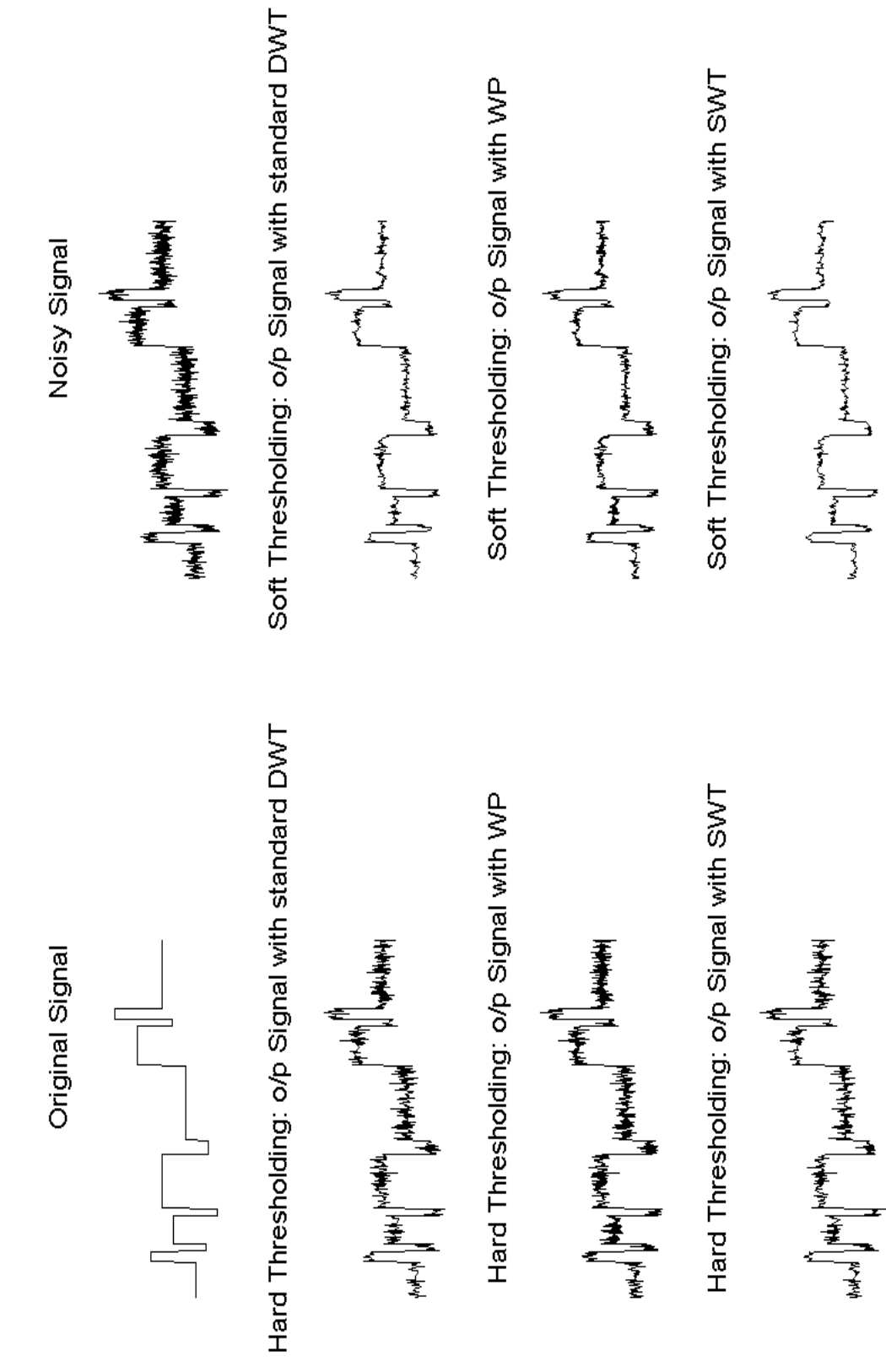


Figure 4.2: (a) Denoising of signal ‘blocks’ with standard DWT, WP and SWT

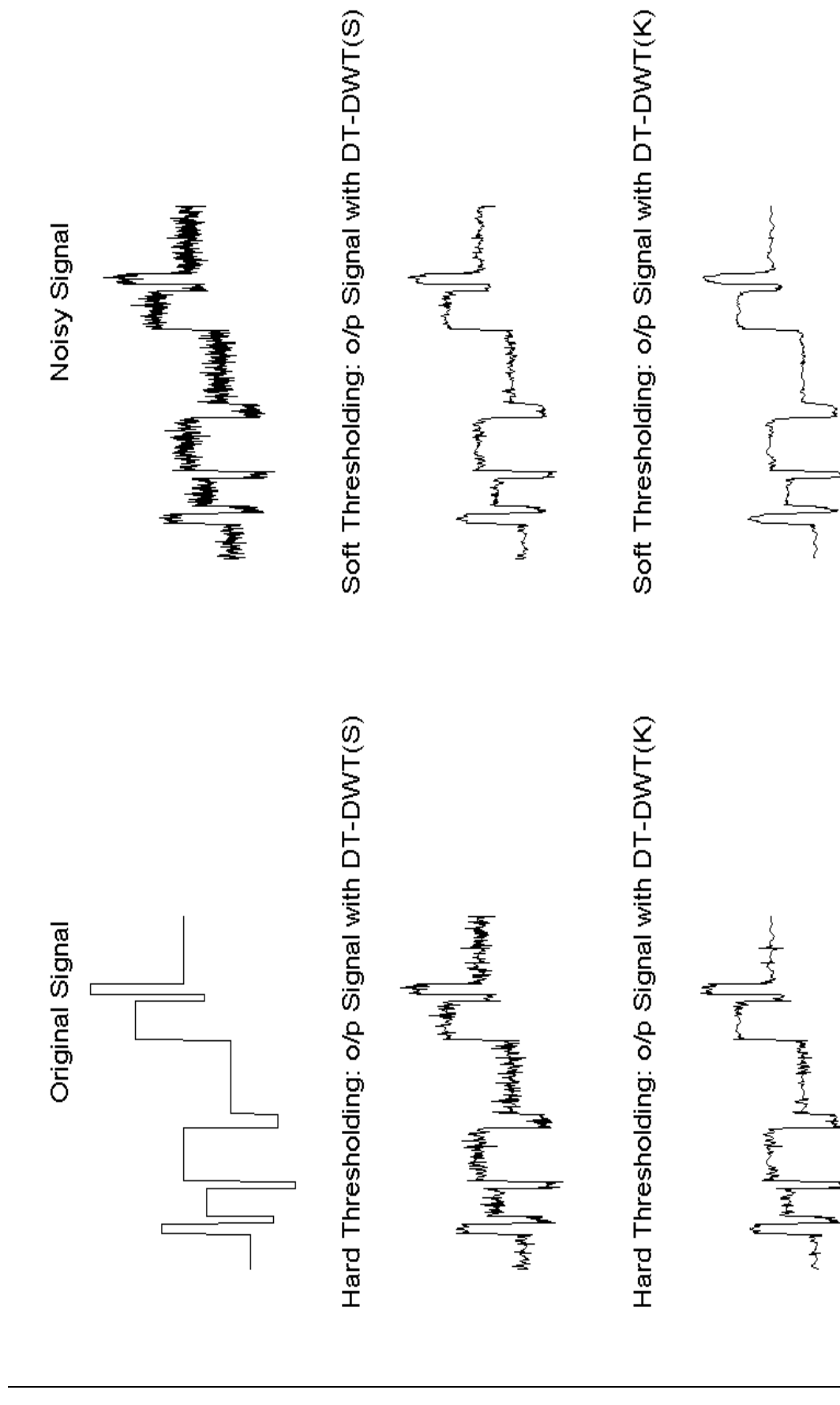


Figure 4.2: (b) Denoising of signal ‘blocks’ with redundant CWT, DT-DWT(S) and DT-DWT(K)

## 4.4 Audio Signal Denoising

### 4.4.1 WT for Audio Signals

Audio signal denoising is a special 1-D application. Traditionally audio signal processing is based on time-frequency (STFT) representation rather than time-scale. The choice of wavelets for audio signal processing is due to its multiresolution properties with constant-Q filterbank, which is a suitable model for the internal auditory processing of inner ear. The CWTs are more closely related to Fourier techniques (due to their complex valued representation) than the real valued WTs. The basic approach of denoising audio signal with redundant CWT (namely DT-DWT(K)) mentioned in this section is taken from [143]. Various other approaches to wavelet based audio signal processing can be found in [144-146].

### 4.4.2 Denoising Model

The traditional Fourier based model for noise reduction in many audio signals of interest (e.g. speech, music) is known as STSA (Short Time Spectrum Attenuation) [147]. The variant of STSA derived in wavelet domain is STWA (Short Time Wavelet Attenuation) as shown in figure (4.3).

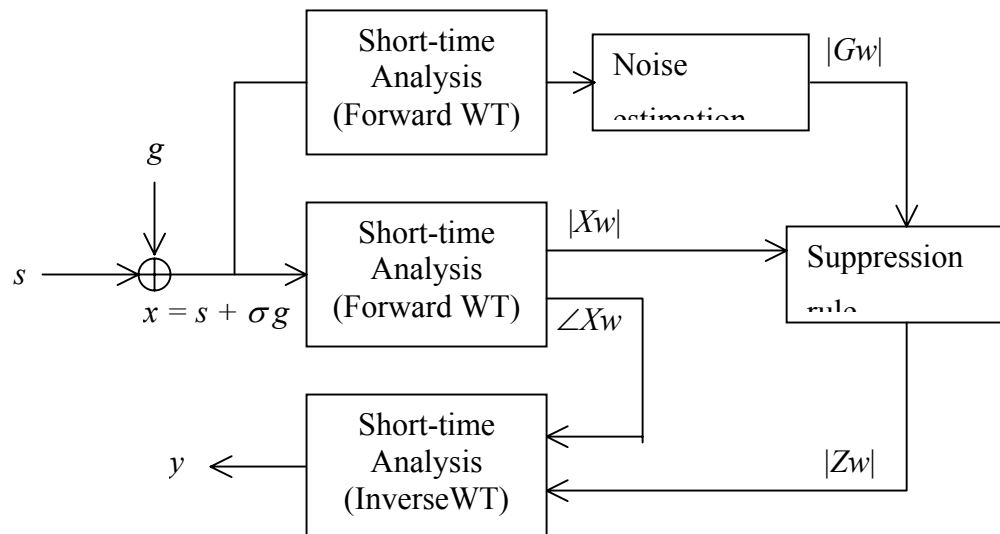


Figure 4.3: Block diagram of STWA (short time wavelet attenuation) method

STWA is equivalent to applying a real valued gain between 0 and 1 with threshold based offset to the wavelet coefficients at each level of the noisy (observed) short time audio signal  $x(n)$  based on a predefined thresholding strategy in order to get an estimated wavelet coefficients  $Zw$  for the recovered signal  $y(n)$ . The formula governing this wavelet attenuation is termed as ‘noise suppression rule’; it depends in general on the power of signal  $P_{Xw}$  and power of noise  $P_{Gw}$  in wavelet domain. The observed signal magnitude is termed as  $|Xw|$  and the estimate of noise magnitude is as  $|Gw|$ . The noise estimate is assumed to be accurate as it can be derived in the absence of actual audio signal (assuming noise remains stationary between such observation intervals).

#### 4.4.3 Shrinkage Strategies

The noise suppression rule in wavelet domain is based on heuristic thresholding in order to optimise quantitative measures like MSE and SNR (defined in equation 4.4) or qualitative human perceptual (through eyes and ears). The global thresholding is optimised to minimise the artifacts or residual noise, which is known as bird noise, warble, clicks, whistles or musical noise.

The approach of denoising audio signal mentioned in this section compares the performance of standard DWT and redundant CWT. Processing of wavelet coefficient processing is investigated with 4 different thresholding rules namely hard, soft, Wiener filtering and raised-cosine-law. In all cases, wavelet coefficients above predetermined threshold are unchanged but the coefficients below threshold are attenuated in different ways with [147]

$$P_{Xw} = \sum |Xw|^2 \text{ and } P_{Gw} = \sum |Gw|^2 \text{ as:}$$

Hard thresholding:      Threshold value ( $\lambda$ ) =  $2\sqrt{P_{Gw}}$

$$Zw = Xw \quad \text{for } \forall |Xw| \geq \lambda$$

$$Zw = 0 \quad \text{for } \forall |Xw| < \lambda$$

Soft thresholding: Threshold value ( $\lambda$ ) =  $4\sqrt{P_{Gw}}$

$$Zw = Xw \quad \text{for } \forall |Xw| \geq \lambda$$

$$Zw = \left( |Xw| - \frac{1}{4}\lambda \right) e^{j\angle[Xw]} \quad \text{for } \forall |Xw| < \lambda$$

Wiener filtering: Threshold value ( $\lambda$ ) = no specific threshold

$$Zw = \frac{(P_{Xw} - P_{Gw})}{P_{Xw}} Xw \quad \text{for } \forall Xw$$

Raised-cosine-law: Threshold value ( $\lambda$ ) =  $7\sqrt{P_{Gw}}$

$$Zw = Xw \quad \text{for } \forall |Xw| \geq \lambda$$

$$Zw = \frac{1}{2} \left[ 1 - \cos\left(\frac{\pi}{\lambda} |Xw|\right) \right] Xw \quad \text{for } \forall |Xw| < \lambda$$

(4.5)

#### 4.4.4 Performance Measure

The performance of standard DWT and DT-DWT(K) for audio signal denoising is compared quantitatively using MSE and SNR as defined in equation (4.4). The qualitative performance is compared with human perceptual (through eyes and ears). The relevant spectrograms of audio signals are shown in figures (4.4) and (4.5).

#### 4.4.5 Results and Discussion

It is clear from the performance results of tables (4.6), and figures (4.4) and (4.5) that the denoising capability of redundant CWT (namely DT-DWT(K)) is superior than the standard DWT for audio speech with lower initial SNR. In both cases, hard thresholding and Wiener filtering perform poorer whereas soft thresholding and raised-cosine-law perform better.

<b>Methods and Initial Parameters</b>	<b>Standard DWT</b>		<b>DT-DWT(K)</b>	
	<b>MSE</b>	<b>SNR (dB)</b>	<b>MSE</b>	<b>SNR (dB)</b>
<b>Thresholding Rule</b>	<b>MSEi= 824</b>	<b>SNRi= 5.00</b>	<b>MSEi= 824</b>	<b>SNRi= 5.00</b>
<b>Hard</b>	343	8.81	212	10.90
<b>Soft</b>	237	10.40	175	11.72
<b>Wiener</b>	625	6.20	630	6.17
<b>Raised-cosine</b>	205	11.04	161	12.10

Table 4.6: *The MSE and SNR of denoised audio signal (y) from the observed noisy signal (x) with respect to original signal (s).* The initial value of MSE and SNR for noisy signal are  $\text{MSE}_i = 824$ ,  $\text{SNR}_i = 5.00 \text{ dB}$ . The wavelets used for standard DWT is ‘bior6.8’ and for DT-DWT(K) is ‘near\_sym\_b’ and ‘qshift\_b’. The maximum decomposition level employed is  $J = \log_2(N)$ , where  $N = 65536$  = size of audio signal. The audio signal contains a microphone quality snap shot of a male lecturer’s speech.

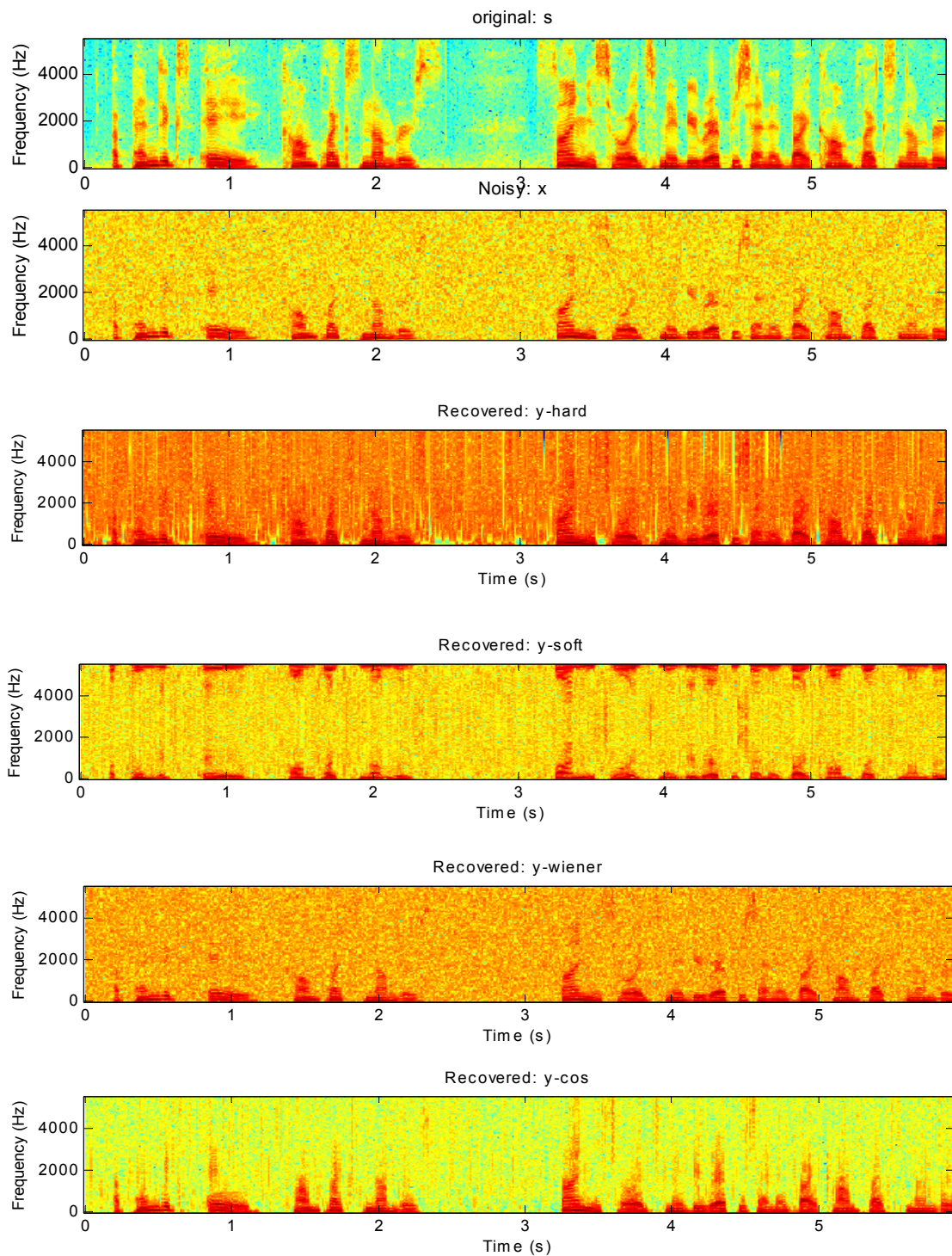


Figure 4.4: Spectrograms of audio signals with standard DWT based denoising

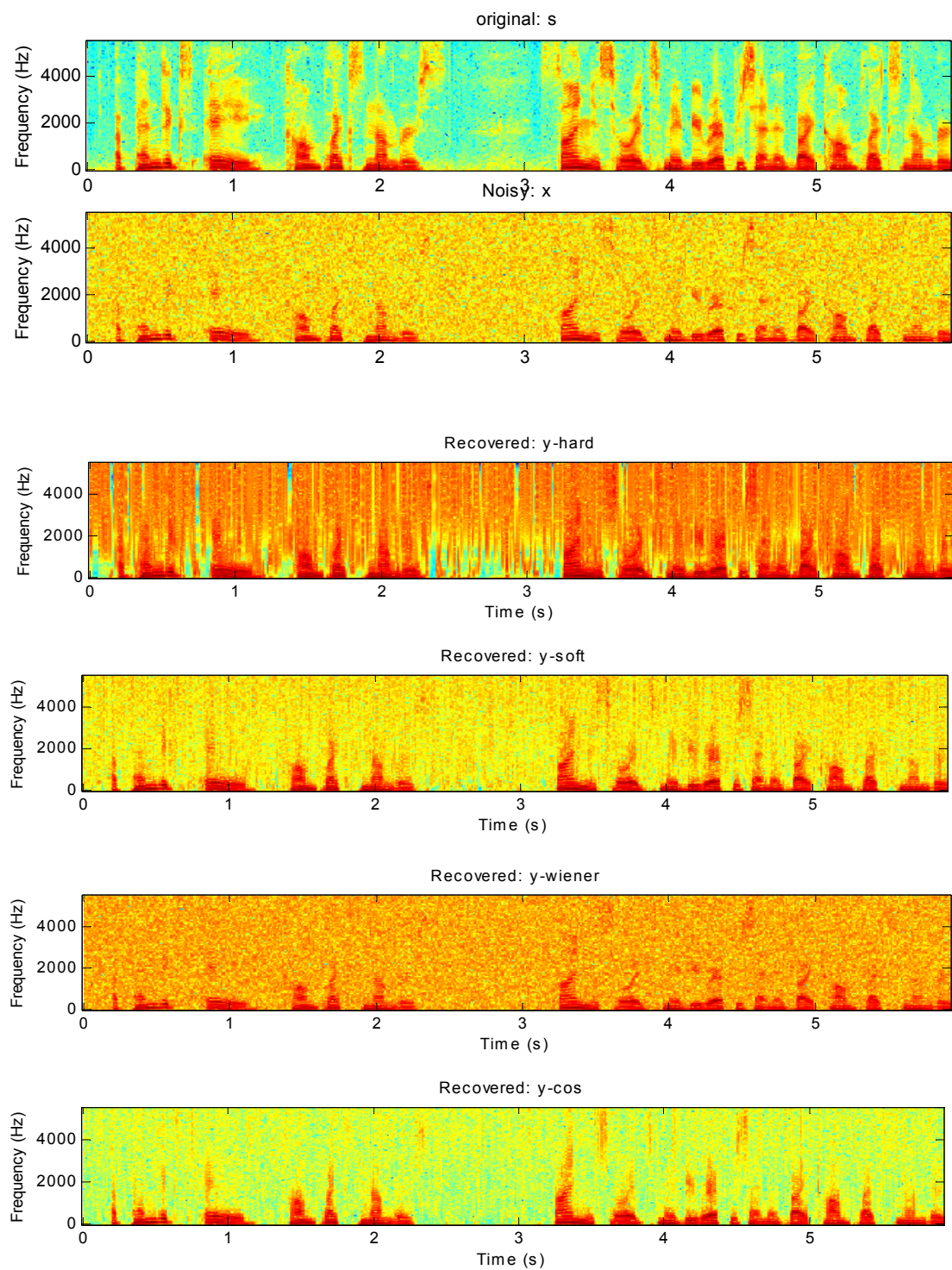


Figure 4.5: Spectrograms of audio signals with DT-DWT(K) based denoising

## 4.5 2-D Denoising

In this section 2-D denoising performance of redundant CWTs (both DT-DWT(K) and DT-DWT(S)) is compared with other wavelet based algorithms such as standard DWT, SWT. The results are also compared with conventional image filtering (denoising/smoothing) methods such as Average (Mean), Median, and Wiener filtering [148-150]. For conventional filtering methods, relevant Matlab (Image processing toolbox) functions are employed [151].

### 4.5.1 Image and Noise Model

The standard test images such as Lenna, Goldhill, Peppers, Airplane and Pattern are taken for experiments (see Appendix C). Original images are corrupted by additive white Gaussian noise.

The image and noise model is given as:

$$x = s + \sigma \cdot g$$

where,  $s$  is an original image and  $x$  is a noisy image corrupted by additive white Gaussian noise  $g$  of standard deviation  $\sigma$ . Both images  $s$  and  $x$  are of size N by M (mostly M=N and always power of 2).

### 4.5.2 Shrinkage Strategy

All wavelet-based algorithms in this section determine the optimum threshold value iteratively with a selected resolution-step size from ‘stpsz’ = {1,2,5,10} to minimize the MSE for both hard and soft thresholding options separately.

### 4.5.3 Algorithm

2-D denoising is an extension of 1-D denoising based on 2-D separable WT implementation (discussed in section 2.5.1). The basic algorithm for wavelet shrinkage denoising remains same as listed in section 4.3.3 but is applied to the matrix of 2-D data.

For all conventional filtering methods, 3-by-3 filter kernel is taken for convolution. For all wavelet based methods, decomposition is performed up to  $J$  levels. For standard DWT and SWT the arbitrary wavelet basis employed is ‘wtype’. Filters for DT-DWT(K) (‘wtype-k’), and DT-DWT(S) (‘wtype-s’), are given in Appendix A and B respectively.

#### 4.5.4 Performance Measure

The quantitative measures for 2-D denoising, namely MSE (Mean Square error) and PSNR (Peak Signal to Noise Ratio) are determined as:

$$\text{MSE} = \frac{1}{NM} \sum_{n=1}^N \sum_{m=1}^M [s(n,m) - y(n,m)]^2$$

$$\text{PSNR} = 10 \log_{10} \left( \frac{255}{\sqrt{\text{MSE}}} \right) \quad (4.7)$$

where,  $s$  is an original image and  $y$  is a recovered image from a noisy image  $x$ .

The qualitative performance is evaluated through human visual system by observing the recovered images with various algorithms.

#### 4.5.5 Results and Discussion

A few sample results of denoising performance (using various methods) based on quantitative measure are presented in tables (4.7) to (4.12) and the qualitative performance based on human visual system for various algorithms are shown in figures (4.6) to (4.15).

The performance results of various algorithms can be evaluated for low and high noise conditions as follows:

- 
1. Under low noise conditions ( $\sigma=10$ ), conventional filtering methods namely Median and Weiner perform better than standard DWT. Though the performance of Mean filter is poorer than standard DWT.
  2. The denoising capability ( $\sigma=10$ ) of both DT-DWTs is better than SWT and standard DWT for all natural images as well as for synthetic ‘Pattern’ image. The performance of both DT-DWTs is nearly same with DT-DWT(K) slightly better than DT-DWT(S).
  3. Under high noise conditions ( $\sigma=40$ ), all conventional filtering methods give poor denoising results than even standard DWT. For all images, performance of both DT-DWTs is better than SWT and standard DWT. The performance of DT-DWT(K) is the best using both hard and soft thresholding.
  4. The lowest values of optimum threshold (for both hard and soft thresholding) for DT-DWT(K) in all noise conditions ( $\sigma= 10$  or  $40$ ) suggest its superior denoising capabilities with improved feature preservation (with less blurring).
  5. The effect of improved directionality on denoising for redundant CWT (both DT-DWTs) compared to less directional standard DWT is quite clear for ‘pattern’ image for all noise conditions.
  6. From human visual perspective, the performance of various algorithms for high noise conditions is quite clear. The performance of DT-DWTs is distinguishably superior to standard DWT. But under low noise conditions, minute differences are very difficult to perceive hence all wavelet based methods seem to have nearly same visual effects.

<b>Performance Measure for Denoising Methods</b>	<b>Images with <math>\sigma = 10</math></b>				
	<b>Lenna</b>	<b>Goldhill</b>	<b>Peppers</b>	<b>Airplane</b>	<b>Pattern</b>
<b>Initial MSE (MSEi)</b>	100	100	100	100	99
	<b>(a) MSE (Conventional filtering)</b>				
<b>Mean</b>	68	75	57	64	153
<b>Median</b>	60	65	41	44	69
<b>Wiener</b>	40	42	30	28	67
	<b>(b) MSE (Hard thresholding)</b>				
<b>Standard DWT</b>	56	65	43	45	79
<b>SWT</b>	39	41	28	26	42
<b>DT-DWT(K)</b>	35	39	27	24	29
<b>DT-DWT(S)</b>	35	38	26	23	30
	<b>(c) MSE (Soft thresholding)</b>				
<b>Standard DWT</b>	44	48	38	40	63
<b>SWT</b>	36	39	28	28	47
<b>DT-DWT(K)</b>	33	37	27	27	35
<b>DT-DWT(S)</b>	33	37	27	27	38

Table 4.7: *MSE for various denoising methods ( $\sigma = 10$ ) for different images: (a) Conventional filtering (b) Hard thresholding (c) Soft thresholding with parameters  $J=3$ ,  $\text{stpsz} = 1$ ,  $\text{wtype} = \text{'db2'}$ ,  $\text{wtype-k} = \text{'near_sym_b'}$  and  $\text{'qshift_b'}$ ,  $\text{wtype-s} = \text{'FSfilt'}$  and  $\text{'otherfilt'}$ .*

<b>Performance Measure for Denoising Methods</b>	<b>Images with <math>\sigma = 10</math></b>				
	<b>Lenna</b>	<b>Goldhill</b>	<b>Peppers</b>	<b>Airplane</b>	<b>Pattern</b>
<b>Initial PSNR (PSNRi in dB)</b>	28.12	28.15	28.12	28.12	28.15
<b>(a) PSNR in dB (Conventional filtering)</b>					
<b>Mean</b>	29.82	29.34	30.57	30.02	26.26
<b>Median</b>	30.35	29.99	32.02	31.71	29.69
<b>Wiener</b>	32.08	31.87	33.33	33.62	29.82
<b>(b) PSNR in dB (Hard thresholding)</b>					
<b>Standard DWT</b>	30.63	29.99	31.71	31.52	29.15
<b>SWT</b>	32.24	31.95	33.65	33.93	31.88
<b>DT-DWT(K)</b>	32.65	32.19	33.75	34.25	33.49
<b>DT-DWT(S)</b>	32.64	32.25	33.84	34.38	33.28
<b>(c) PSNR in dB (Soft thresholding)</b>					
<b>Standard DWT</b>	31.65	31.28	32.23	32.10	30.14
<b>SWT</b>	32.59	32.18	33.60	33.53	31.39
<b>DT-DWT(K)</b>	32.91	32.37	33.77	33.77	32.65
<b>DT-DWT(S)</b>	32.87	32.33	33.77	33.76	32.27

Table 4.8: *PSNR for various denoising methods ( $\sigma = 10$ ) for different images:* (a) Conventional filtering (b) Hard thresholding (c) Soft thresholding with parameters  $J=3$ ,  $stpsz = 1$ ,  $wtype = 'db2'$ ,  $wtype-k = 'near_sym_b'$  and  $'qshift_b'$ ,  $wtype-s = 'FSfilt'$  and  $'otherfilt'$ .

<b>Denoising Methods</b>	<b>Images with <math>\sigma = 10</math></b>				
	<b>Lenna</b>	<b>Goldhill</b>	<b>Peppers</b>	<b>Airplane</b>	<b>Pattern</b>
	<b>(a) Optimum threshold value (<math>\lambda_h</math>)</b> <b>for Hard thresholding</b>				
<b>Standard DWT</b>	30	27	30	28	22
<b>SWT</b>	28	27	31	30	30
<b>DT-DWT(K)</b>	16	15	17	17	17
<b>DT-DWT(S)</b>	32	30	35	34	35
	<b>(b) Optimum threshold value (<math>\lambda_s</math>)</b> <b>for Soft thresholding</b>				
<b>Standard DWT</b>	11	10	12	11	7
<b>SWT</b>	12	11	14	13	11
<b>DT-DWT(K)</b>	7	7	8	8	7
<b>DT-DWT(S)</b>	15	14	16	16	14

Table 4.9: *Optimum threshold value for various denoising methods ( $\sigma = 10$ )* for different images: (a) Hard Thresholding  $\lambda_h$  (b) Soft thresholding  $\lambda_s$ . with parameters  $J=3$ ,  $stpsz = 1$ ,  $wtype = 'db2'$ ,  $wtype-k = 'near_sym_b'$  and ' $qshift_b$ ',  $wtype-s = 'FSfilt'$  and ' $otherfilt$ '.

<b>Performance Measure for Denoising Methods</b>	<b>Images with <math>\sigma = 40</math></b>				
	<b>Lenna</b>	<b>Goldhill</b>	<b>Peppers</b>	<b>Airplane</b>	<b>Pattern</b>
<b>Initial MSE (MSEi)</b>	1593	1600	1605	1593	1595
<b>(a) MSE (Conventional filtering)</b>					
<b>Mean</b>	234	242	223	231	317
<b>Median</b>	322	325	304	310	388
<b>Wiener</b>	317	322	305	301	342
<b>(b) MSE (Hard thresholding)</b>					
<b>Standard DWT</b>	177	224	199	242	609
<b>SWT</b>	124	162	114	141	294
<b>DT-DWT(K)</b>	113	155	108	135	212
<b>DT-DWT(S)</b>	116	161	110	139	225
<b>(c) MSE (Soft thresholding)</b>					
<b>Standard DWT</b>	186	224	207	240	521
<b>SWT</b>	133	172	137	168	376
<b>DT-DWT(K)</b>	121	159	125	156	252
<b>DT-DWT(S)</b>	124	168	129	159	275

Table 4.10: *MSE for various denoising methods ( $\sigma = 40$ ) for different images:* (a) Conventional filtering (b) Hard thresholding (c) Soft thresholding with parameters  $J=4$ ,  $\text{stpsz} = 1$   $\text{wtype} = \text{'db2'}$ ,  $\text{wtype-k} = \text{'near_sym_b'}$  and  $\text{'qshift_b'}$ ,  $\text{wtype-s} = \text{'FSfilt'}$  and  $\text{'otherfilt'}$

<b>Performance Measure for Denoising Methods</b>	<b>Images with <math>\sigma = 40</math></b>				
	<b>Lenna</b>	<b>Goldhill</b>	<b>Peppers</b>	<b>Airplane</b>	<b>Pattern</b>
<b>Initial PSNR (PSNRi in dB)</b>	16.11	16.09	16.10	16.10	16.10
<b>(a) PSNR in dB (Conventional filtering)</b>					
<b>Mean</b>	24.45	24.28	24.60	24.50	23.10
<b>Median</b>	23.05	23.00	23.30	23.20	22.20
<b>Wiener</b>	23.12	23.06	23.30	23.40	22.80
<b>(b) PSNR in dB (Hard thresholding)</b>					
<b>Standard DWT</b>	25.66	24.63	25.10	24.30	20.30
<b>SWT</b>	27.12	26.03	27.60	26.60	23.40
<b>DT-DWT(K)</b>	27.62	26.23	27.80	26.80	24.90
<b>DT-DWT(S)</b>	27.48	26.06	27.70	26.70	24.60
<b>(c) PSNR in dB (Soft thresholding)</b>					
<b>Standard DWT</b>	25.44	24.63	25.00	24.30	21.00
<b>SWT</b>	26.88	25.75	26.80	25.90	22.40
<b>DT-DWT(K)</b>	27.30	26.09	27.10	26.20	24.10
<b>DT-DWT(S)</b>	27.29	25.88	27.00	26.10	23.70

Table 4.11: *PSNR for various denoising methods ( $\sigma = 40$ ) for different images:* (a) Conventional filtering (b) Hard thresholding (c) Soft thresholding with parameters  $J=4$ ,  $stpsz = 1$ ,  $wtype = 'db2'$ ,  $wtype-k = 'near_sym_b'$  and  $'qshift_b'$ ,  $wtype-s = 'FSfilt'$  and  $'otherfilt'$ .

<b>Denoising Methods</b>	<b>Images with <math>\sigma = 40</math></b>				
	<b>Lenna</b>	<b>Goldhill</b>	<b>Peppers</b>	<b>Airplane</b>	<b>Pattern</b>
<b>(a) Optimum threshold value (<math>\lambda_h</math>)</b>					
<b>for Hard thresholding</b>					
<b>Standard DWT</b>	146	147	140	137	117
<b>SWT</b>	133	131	131	128	122
<b>DT-DWT(K)</b>	78	75	78	75	71
<b>DT-DWT(S)</b>	153	147	148	142	141
<b>(b) Optimum threshold value (<math>\lambda_s</math>)</b>					
<b>for Soft thresholding</b>					
<b>Standard DWT</b>	75	73	71	68	50
<b>SWT</b>	76	71	73	69	55
<b>DT-DWT(K)</b>	45	43	43	41	36
<b>DT-DWT(S)</b>	88	83	85	80	70

Table 4.12: *Optimum threshold value for various denoising methods ( $\sigma = 40$ )* for different images: (a) Hard Thresholding  $\lambda_h$  (b) Soft thresholding  $\lambda_s$  with parameters  $J=4$ ,  $\text{stpsz} = 1$ ,  $\text{wtype} = \text{'db2'}$ ,  $\text{wtype-k} = \text{'near\_sym\_b'}$  and  $\text{'qshift\_b'}$ ,  $\text{wtype-s} = \text{'FSfilt'}$  and  $\text{'otherfilt'}$ .

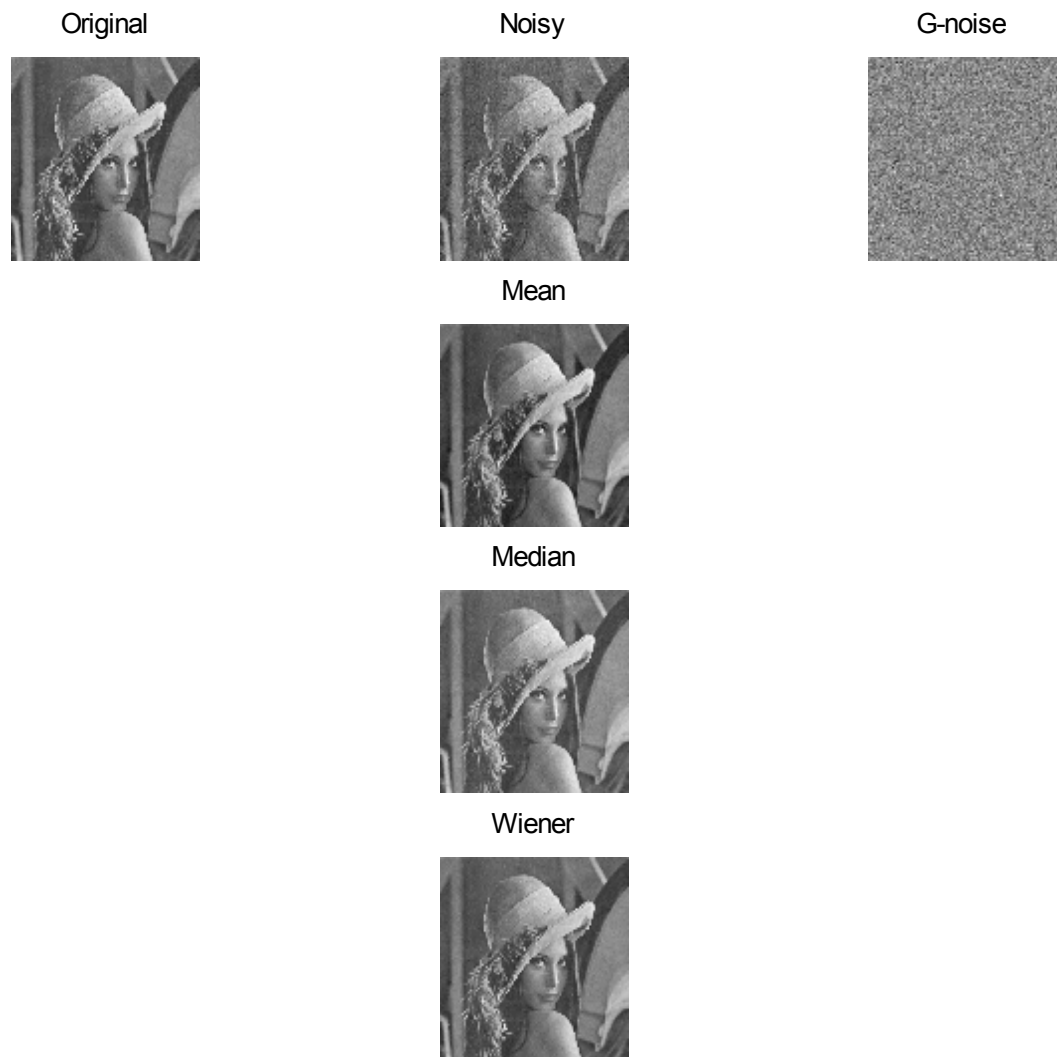
$\sigma=10$ 

Figure 4.6: Conventional filtering methods for denoising of ‘Lenna’ image with reference to tables (4.7) and (4.8).

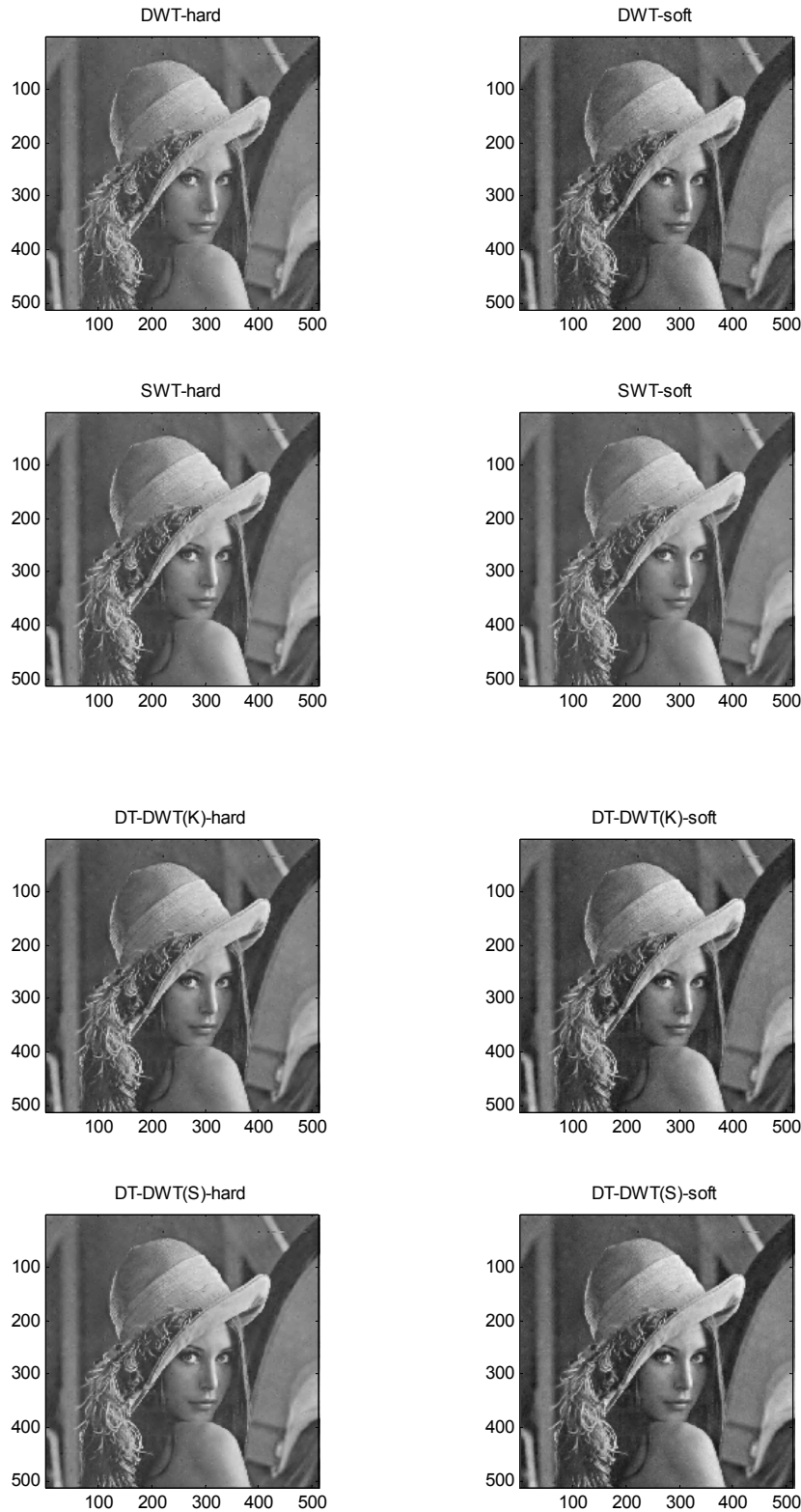
$\sigma = 10, J=3$ 

Figure 4.7: Wavelet Transform based methods for denoising of ‘Lenna’ image with reference to tables (4.7) to (4.9).

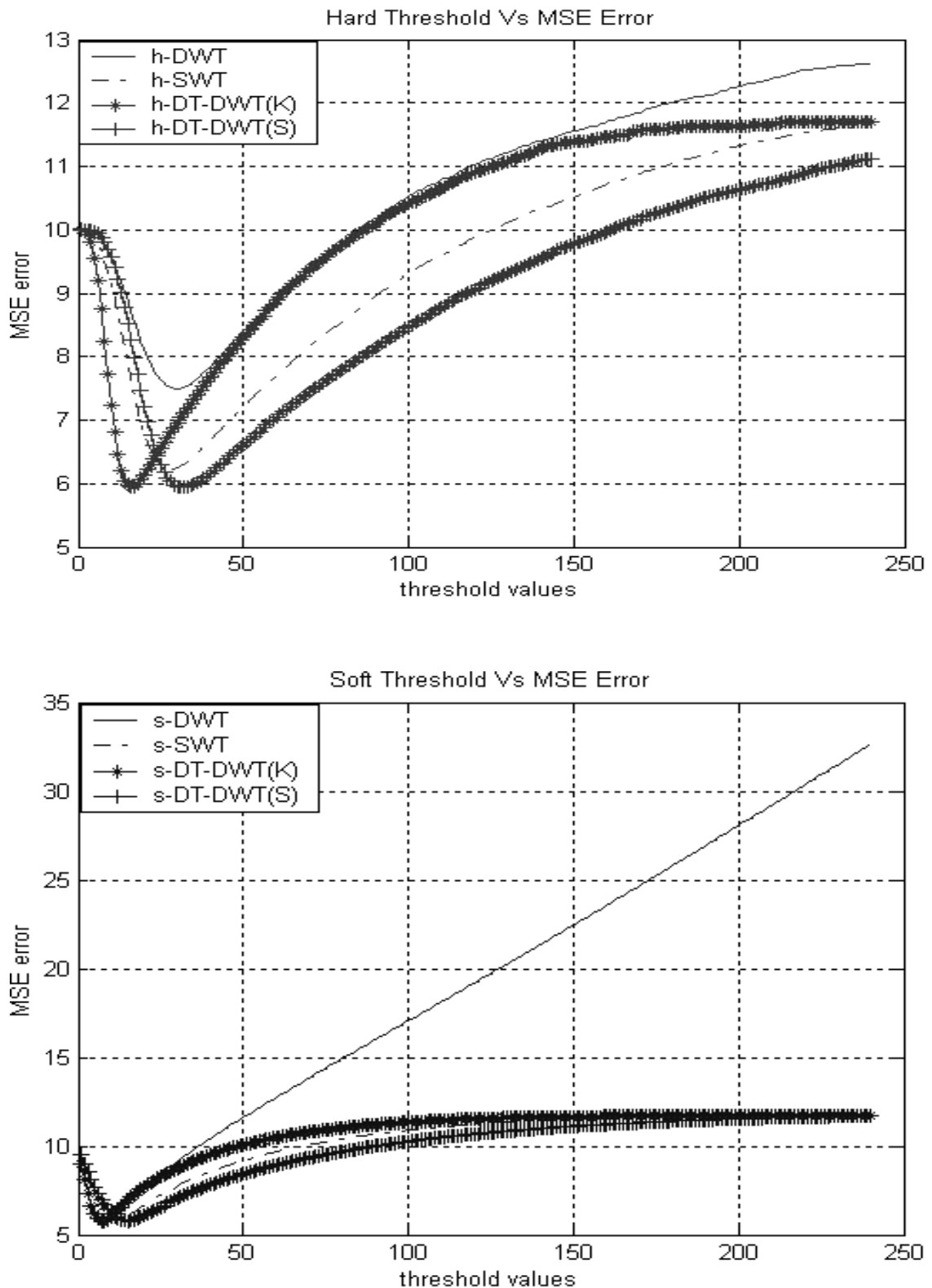
$\sigma = 10, J=3$ 

Figure 4.8: Threshold Vs MSE for determination of optimum threshold value for all wavelet based methods. Image for denoising is ‘Lenna’ with reference to table (4.9).

$$\sigma = 40$$

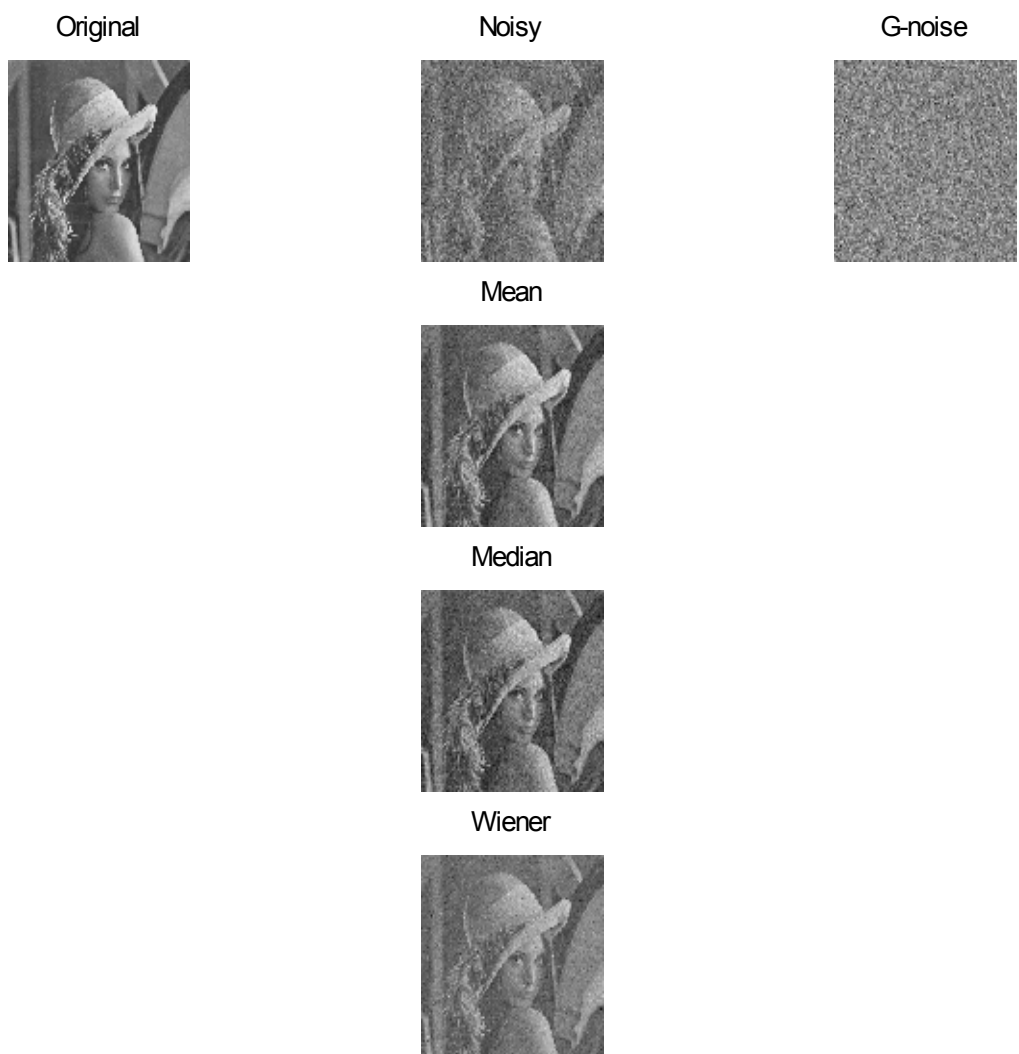


Figure 4.9: Conventional filtering methods for denoising of ‘Lenna’ image with reference to tables (4.10) and (4.11).

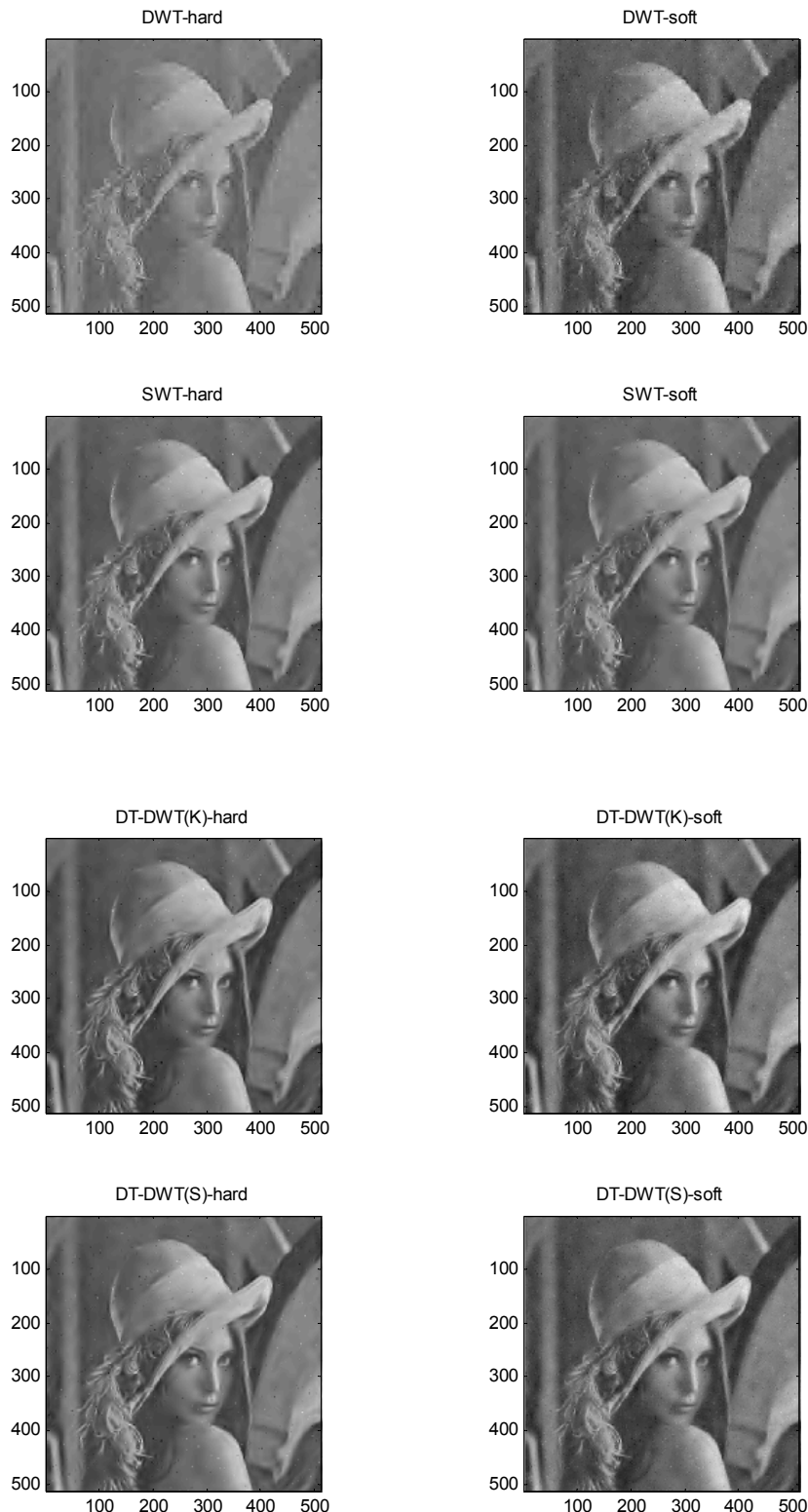
$\sigma = 40, J=4$ 

Figure 4.10: Wavelet Transform based methods for denoising of ‘Lenna’ image with reference to tables (4.10) to (4.12).

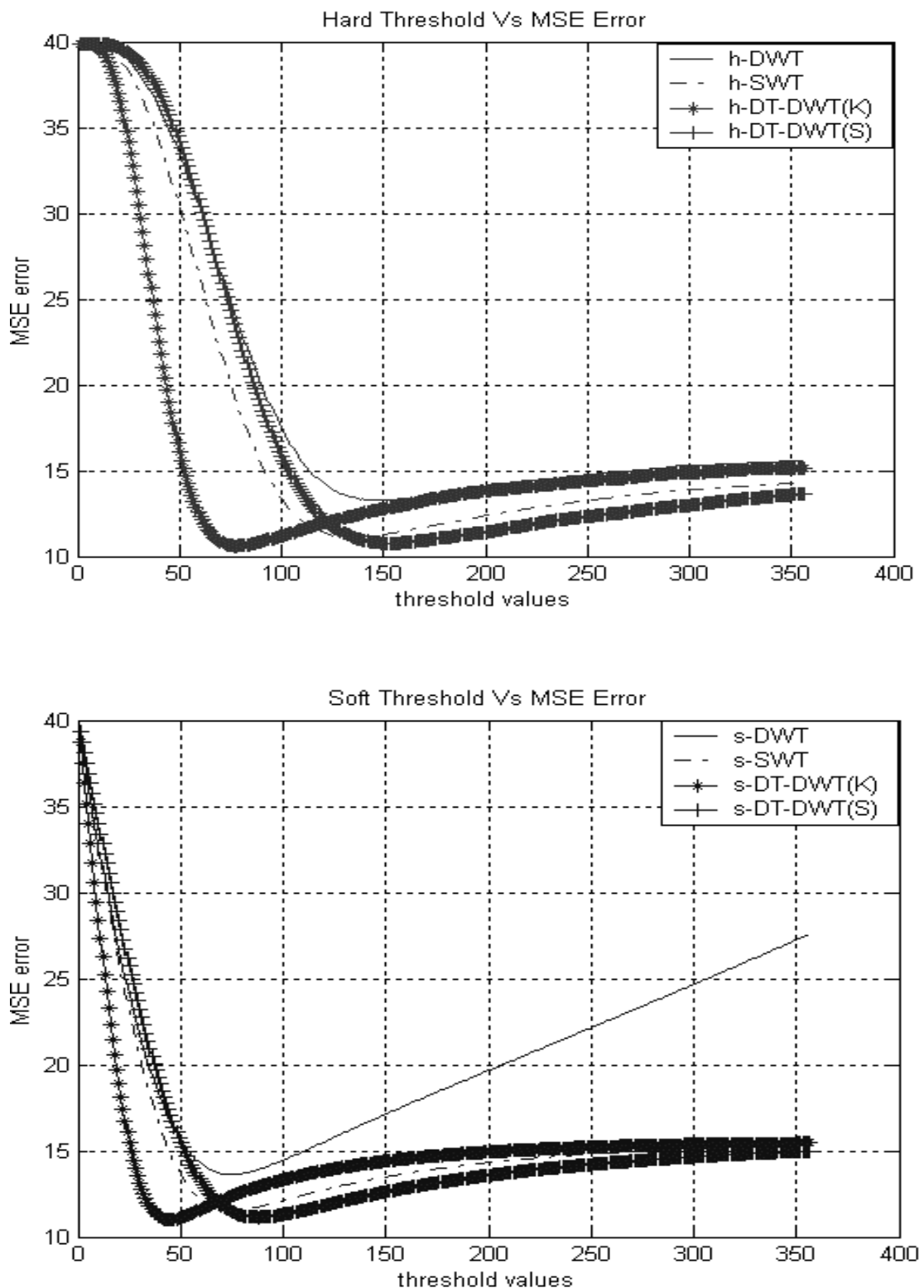
$\sigma = 40, J=4$ 

Figure 4.11: Threshold Vs MSE for determination of optimum threshold value for all wavelet based methods. Image for denoising is ‘Lenna’ with reference to table (4.12).



Figure 4.12: DWT based denoising of ‘Lenna’ image using hard and soft thresholding with reference to tables (4.10) to (4.12).



Figure 4.13: SWT based denoising of ‘Lenna’ image using hard and soft thresholding with reference to tables (4.10) to (4.12).

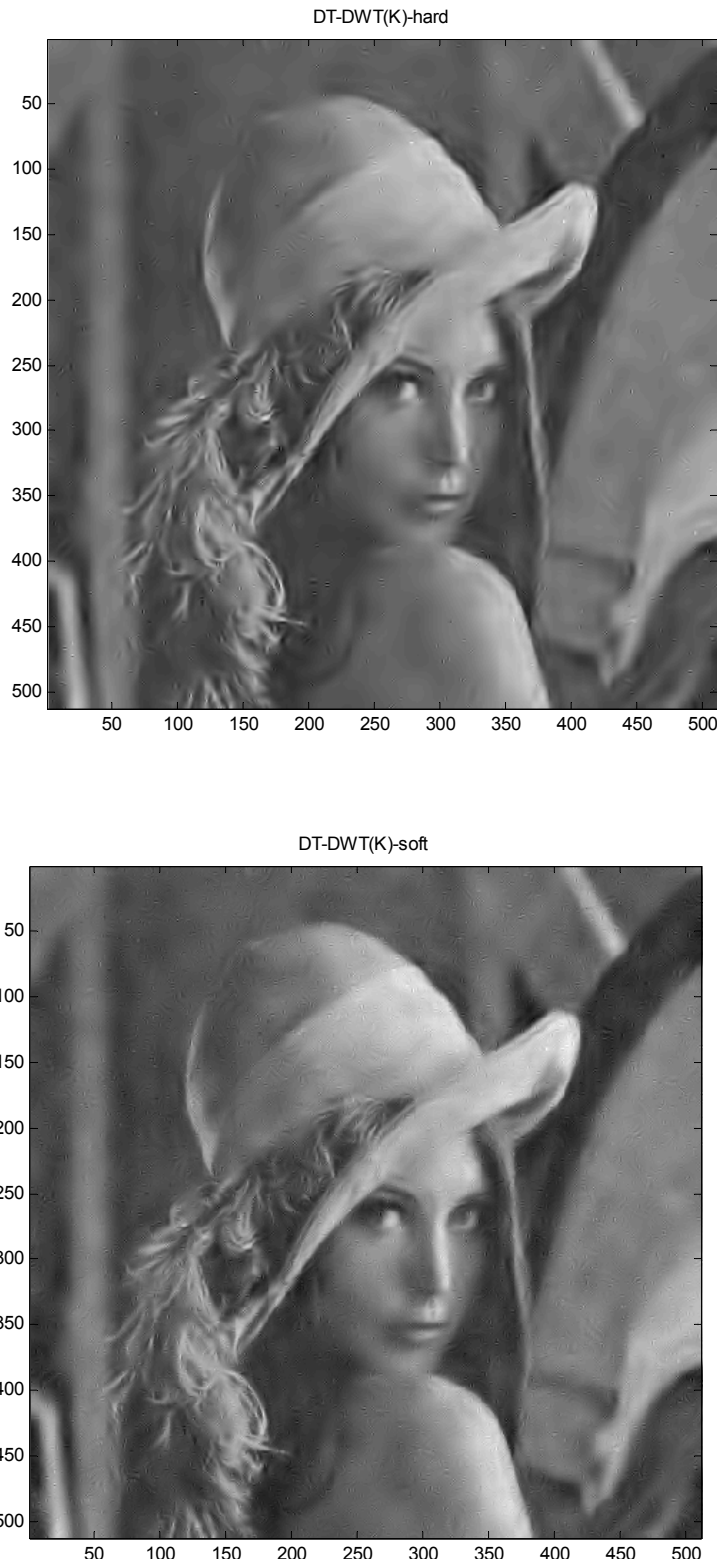


Figure 4.14: DT-DWT(K) based denoising of ‘Lenna’ image using hard and soft thresholding with reference to tables (4.10) to (4.12).



Figure 4.15: DT-DWT(S) based denoising of ‘Lenna’ image using hard and soft thresholding with reference to tables (4.10) to (4.12).

## 4.6 Conclusion

It is concluded that DT-DWTs are superior to standard DWT for all 1-D and 2-D denoising application. The choice of shrinkage (thresholding) strategy, and selection of optimum threshold value are very crucial for wavelet shrinkage denoising using any form of WT. DT-DWTs are especially efficient in higher noise conditions. Entropy based WP is not suitable for generalised denoising applications in poor SNR conditions. Almost equal performance of limited redundant DT-DWT with other advantages makes it a promising choice over highly redundant SWT for signal and image denoising applications.

# **Chapter 5:**

## **Application II- Edge Detection**

### **5.1 Introduction**

For many natural signals the vital information about its originating source, external environment, processing, and the characterisation of important features is closely linked with the transients (or local singularities, edges) in those signals under consideration [148,150,152-154]. For 1-D signal, edge is considered as a distinct observable variation in the smoothness or continuity. For 2-D, image intensity is often proportional to scene radiance, physical edges (corresponding to the significant variations in reflectance, illumination, orientation and depth of scene surfaces) are represented in the image by changes in the intensity function.

Due to wealth of information associated with edges, edge detection is an important task for many applications related to computer vision and pattern recognition [154,155]. There are various categories of edges such as step, ramp, exponential or certain non-deterministic singularities with varying degree of sharpness [156]. Steps (and its combinations) are the most common type of edge encountered. This type of edges result from various phenomena; for example when one object hides another, or when there is shadow on a surface. It generally occurs between two regions having almost common, but different grey levels.

Chapter 5 is organised into five sections. Section 5.1 is an introduction. Section 5.2 presents the survey of various classical edge detection approaches and highlights a few important multiscale approaches. Section 5.3 is about 1-D edge detection in higher noise environment using multiscale algorithms. In this section, existing algorithms are critically reviewed and compared with individually developed new algorithms. In section 5.4, a very simple 2-D edge detection methodology is presented to compare edge detection performance of the extensions of DWT with DT-DWT(K). Section 5.5 is the conclusion of the study of edge detection.

## 5.2 Edge Detection Approaches

### 5.2.1 Classical Approaches

In a function, singularities can be characterised as discontinuities where derivative(s) or gradient approaches infinity. However, if the signal data is discrete, then the edges are often defined as the local maxima of the derivative(s). Essentially an edge detector is a high pass filter (operator) that can be applied to extract the edge points in a signal [118,148,150]. The classical 2-D gradient operators such as Roberts, Prewitt, Sobel and Fri-Chen for edge detection reduce to an FIR filter with impulse response [-1,0,1] in 1-D [148]. All these operators being high pass filters are sensitive to noise (especially widely used AWGN) [157].

To combat with noise, more general robust extensions, so-called filtered derivate methods (e.g. *Marr and Hildreth*) are devised [158-160]. These pre-smoothing approaches combine various smoothing operators (e.g Gaussian) with gradient estimation are more effective in higher noise conditions and are attractive due to low complexity linear implementation. The weakness of all above approaches is that the optimal result may not be obtained by using a fixed size operator. Attempting to achieve simultaneously detection and localisation of an edge results in a tradeoff between the level of smoothing and the accuracy of estimated edge location. The tradeoff is also sensitive to category of edge (sharp or smooth) and SNR of the signal. *Canny* [161] in his computational approach to edge detection

showed exploited such tradeoff and derived an improved edge detector for noisy environment by different size kernels in filtered derivative method with non-maximum suppression and dual thresholding.

Various attempts for edge detection in noisy conditions are based on combinations of many different explicit and heuristic models (e.g. liner filtering, covariance models, dispersion of gradient, regularisation, statistics, neural networks, genetic algorithms, fuzzy reasoning etc.) in order to closely approximate the uncertainty of noise distributions. Most of these attempts compare the results with well-known detectors such as Sobel, Canny, DoG, and LoG. Because of only qualitative performance comparisons (without well accepted objective performance measure based on ground-truth calibration), there is a belief that edge detection algorithms are reaching an asymptotic level of performance [162].

### **5.2.2 Multiscale Approaches**

The developments in the field of multi-resolution wavelet transforms with their ability to detect and characterise singularities, attracted many researchers to explore the optimal edge detection problem in higher noise conditions [163-166,176,177]. The advantage with multiscale approach is its inherent implementation, with variable size derivative operators at various scales, to tradeoff between detection and localisation of local singularities. The indirect inter-dependence of wavelet coefficients at different scales opens the possibility to explore the hidden association of information at various scales (levels).

The important investigations of multiscale edge detection include MZ-MED (*Mallat and Zong's Multiscale Edge Detection*) based on modulus maxima evolution from coarse to fine scales [164], multiscale products by *Xu et.al.* [165] based on *Rosenfeld's* idea of cross-scale correlation [166]. A few other multiscale singularity detection approaches are as [167-170].

Usefulness of wavelet based singularity detection in natural signals (e.g. Speech, ECG and Seismic) is evident from [173-175]. All these multiscale edge detection methods use fast implementation of non-decimated, non-orthogonal dyadic wavelet transform based on ‘a-trous’ algorithm with a cubic spline kernel. Higher redundant non-decimated wavelet transform is a practical approximation (in discrete domain) to continuous wavelet transforms that is more appropriate for accurate localisation of detected edge. The spline kernel has simplicity of iterative MRA implementation. The spline kernel generates wavelets similar to derivative of Gaussian, optimal in noisy environment [171,172].

### 5.3 1-D Edge Detection

#### 5.3.1 Review of Existing Approaches

The existing multiscale edge detection research (at Signal Processing Group of University of Strathclyde) in higher noise environment include *Setarehdan* and *Soraghan*’s FMED (Fuzzy Multiscale Edge Detection) approach of fuzzy-based modulus maxima across scales [176], and *Akbari* and *Soraghan*’s FWOMED (Fuzzy-based Weighted Offset MED) across scales [177].

In this section, 1-D edge detection is critically reviewed with existing multiscale methods for single step-edge detection with varying slope and noise. The standard FMED (Fuzzy Multiscale Edge Detection) algorithm is explored with different wavelet basis (e.g ‘cubic spline’, ‘db3’), and new FMED (‘db3’) and DB-FMED (Dual-Basis FMED) algorithms are developed. Also redundant CWT (based on DT-DWT(K)) is employed for edge detection, and a new and an original CMED (Complex Multiscale Edge Detection) algorithm is developed. The performance (in terms of RMSE of detected edge localisation in terms of sample points) of new algorithms is compared with the available results from relevant existing techniques.

### 5.3.2 Edge Model

The single step-edge model with varying slopes and noise levels is taken for all simulations. The standard time shifted unit step ( $s$ ) is a step edge model with slope of 1 (in discrete domain) is denoted as  $\Delta = 0$ . One or more samples ( $\Delta$ ) in between the sharp step edge create a linear slope of  $1:(\Delta+1)$ . For simplicity as slope is represented with  $\Delta$ . The AWGN (additive white Gaussian noise) of arbitrary standard deviation ( $\sigma$ ) is superimposed on a given step edge to generate the noisy step edge ( $x = s + g_n$ ). The sample size of step edge profile is ( $n = 1$  to  $N$ ) with only a single positive going edge located at  $n \geq En$ . A discrete signal is generated by first  $En$  zeros followed by  $\Delta$  samples forming a linear slope and lastly  $(N-\Delta-En)$  number of ones. The generalised step edge model with different parameters of slope and noise is shown in figure (5.1).

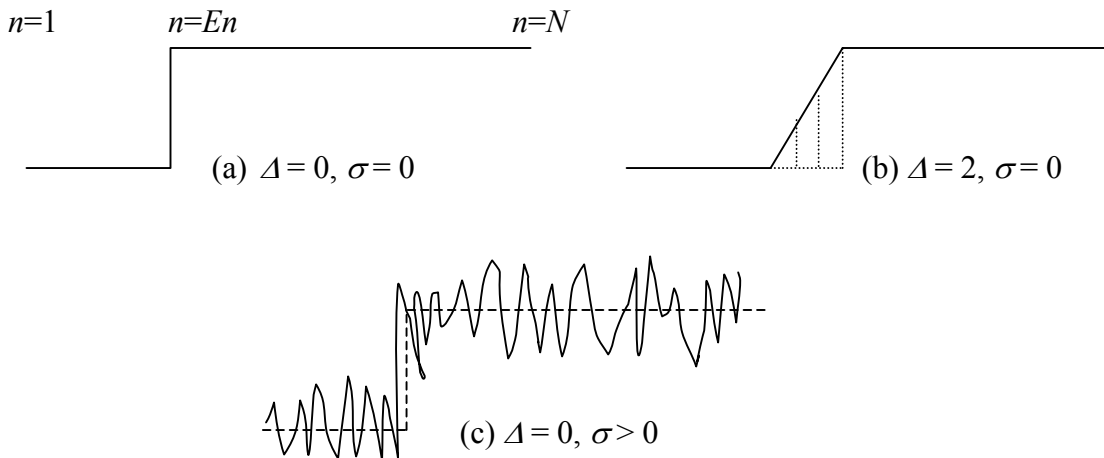


Figure 5.1: *Generalised step edge model*: (a) with no slope and no noise, (b) with slope of 2 samples and no noise (c) with no slope and noise of arbitrary standard deviation [0: 0.1:1]

### 5.3.3 Multiscale Decomposition

Many 1-D multiscale edge detection algorithms such as MZ-MED and variants of FMED except CMED employs non-decimated wavelet transform based on ‘a-trous’ algorithm (i.e. SWT). The redundancy created by equal size wavelet coefficients at

all levels is important for correct detection and localisation of the step edge without any loss of information.

Using SWT,  $N$  point edge profile is decomposed up to  $J = \log_2(N)$  levels. The filterbank implementation of classical MZ-MED and standard FMED uses a lowpass and highpass filters derived from cubic spline kernel (approximately Gaussian) and its scale dependent derivatives as shown in figure (5.2).

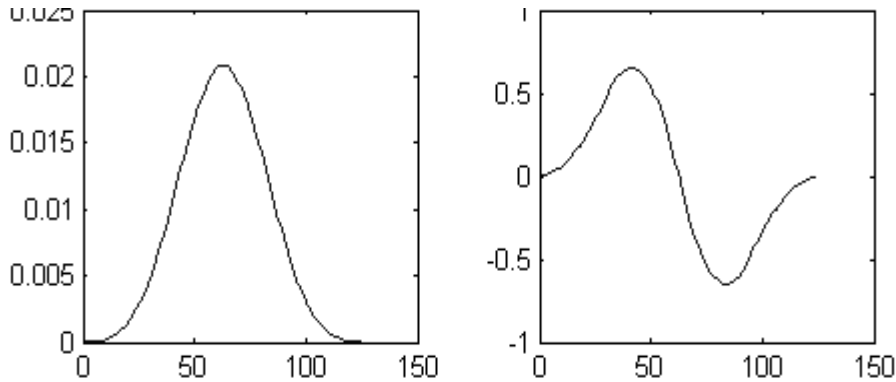


Figure 5.2: Cubic spline smoothing function  $\phi(t)$  and its derivative  $\psi(t) = d/dt(\phi(t))$ .  $\psi_j(t) = (1/j)\psi(t/j)$  is a wavelet yielding a filter bank that estimates the derivative at a level  $j$ .

Singularity information at various scales (levels) is used in different ways by different algorithms to determine the correct edge location.

### 5.3.4 FMED (Fuzzy Multiscale Edge Detection) Algorithms

Novel implementations of existing standard FMED (Fuzzy Multiscale Edge Detection) algorithm include FMED ('db3'), which uses multiscale decomposition with 6-tap 'db3' wavelet, and DB-FMED (Dual-Basis FMED), which uses the combination of 'cubic-spline' scaling kernel and 'db3'. The implementation steps for all FMED based algorithms are described as:

1. Non-decimated WT is computed for edge profile  $x$  using SWT (Matlab function `swt`) up to  $j = 1$  to  $J = \log_2(N)$  levels. FMED ('cubic') uses cubic spline scaling kernel, FMED ('db3') uses wavelet basis 'db3' for  $J$  level

decomposition while DB-FMED uses two parallel SWT decomposition trees, one with ‘db3’ and other with ‘cubic spline’ kernel. For cubic spline implementation, lowpass filter taken is  $h_0 = [1,4,6,4,1]/16$  and other analysis and synthesis filters are computed with matlab function ‘orthfilt’.

$$w(j,n) = \text{WT}(x(n)), j=1 \text{ to } J, n= 1 \text{ to } N$$

2. For DB-FMED, coefficients of both trees at each level are combined with wavelet fusion averaging rule resulting in only one decomposition tree.

$$w(j,n) = \text{average}\{w(j,n)(\text{'db3'}) + w(j,n)(\text{'cubic spline'})\}$$

3. Depending on size of edge profile ( $x$ ), slope, and on the wavelet basis selection, there is a localisation error (in terms of samples) of true edge from fine to coarse level in multiscale propagation. This error is reduced with predetermined offset ( $\pm n_{\text{off}}$ ) by proper amount and in correct direction (+ for right and - for left) through cyclic shift of wavelet coefficients at each level.

$$w_o(j,n) = \text{offset} \{ w(j,n), \pm n_{\text{off}} \}$$

In simulations the relevant offsets for all  $J$  levels are selected as:

$$\text{FMED('cubic spline'): } n_{\text{off}} = 0 (\Delta=0) \text{ and } n_{\text{off}} = -(\Delta-1) (\Delta>0)$$

$$\text{FMED('db3'): } n_{\text{off}} = -(\Delta-2) \text{ (for all } \Delta>0)$$

$$\text{DB-FMED: } n_{\text{off}} = +1 (\Delta=0) \text{ and } n_{\text{off}} = -(\Delta-2) (\Delta>0)$$

Wavelet coefficients at each level (scale) are zero clipped  $w^+$  such that only positive coefficients are selected for positive going edge model (considered as per figure (5.1)) and negative  $w^-$  coefficients if negative going edge model is considered.

$$w^+(j,n) = +\text{Ve\_clip}\{w_o(j,n)\}, \quad w^-(j,n) = -\text{Ve\_clip}\{w_o(j,n)\}$$

- 
4. Coefficients at each level are normalised between [0,1] to be consistent with fuzzy membership axioms and set operations [178]. Now wavelet coefficients at each level  $j$  can be viewed as fuzzy subset  $F_j$  of  $(\mu_{Fj}(n), n)$ , where  $\mu$  is the membership value associated with each of  $n$  wavelet coefficients at level  $j$ .

$$F_j = (\mu_{Fj}(n), n) = \text{Normalised } \{w^+(j,n) \text{ or } w^-(j,n)\}$$

5. Each local maximum of normalised wavelet coefficients (at each level) is a potential representative of actual step edge in a given signal. Hence at each scale, a membership value  $(\mu_{Fj}(n), n)$  with local maxima (modulus maxima) is identified and boosted by assigning the highest fuzzy membership value 1.

$$(\mu_{Fj}(n), n) = 1, \text{ if } (\mu_{Fj}(n), n) \text{ is a local maximum}$$

6. At finer levels the amount of noise is higher and also the chances of false edge detection are more while at courser levels, the amount of noise is less but the localisation of true edge is ambiguous. So depending on the edge location  $E_n$  (in original edge profile) and noise variance, heuristically some arbitrary number of levels (fuzzy subsets) is selected to compute a minimum fuzzy set ( $F_{min}$ ) in vertical direction for optimal edge detection.

$$F_{min} = \text{Minimum } \{F_j\} \text{ such that}$$

$$(\mu_{Fmin}(n), n) = \text{Minimum} \{ (\mu_{Fj}(n), n) \}$$

$$\text{for } j = k_1 \text{ to } k_2 \in \{1 \text{ to } J\}, n = 1 \text{ to } N$$

In the presented experiments with FMED algorithms, number of levels considered are  $j = 2$  to  $J$ .

7. The final step of the algorithm is to find the position (index) of a sample having maximum membership value (horizontal operation) from the computed minimum fuzzy set ( $F_{min}$ ). The detected position (index) reveals the true position of an edge in a given noisy edge profile.

---


$$\text{Detected Edge } (D_n) = \text{Position}\{\text{Maximum}\{F_{\min}\}\}$$

8. Performance of FMED algorithm is judged by minimisation of RMSE between the true edge  $E_n$  and detected edge  $D_n$ .

### 5.3.5 CMED (Complex Multiscale Edge Detection) Algorithms

Basic CMED (Complex Multiscale Edge Detection) algorithm is based on redundant CWT using DT-DWT(K) to exploit the limited redundancy with improved denoising ability for 1-D edge detection. DT-DWT(K) is a kind of two standard DWT trees working in parallel, so at each subsequent decomposition there is a data size reduction by a factor of 2.

Due to quadrature nature of DT-DWT(K), the wavelet coefficients of two trees pick up the same singularity with some offset and polarity inversion between respective real and imaginary levels. The novelty of the CMED algorithm is in the proper alignment of wavelet coefficients of both real and imaginary trees from fine to coarse level for efficient edge detection under noisy conditions.

The key steps of basic CMED algorithm are as follows:

1. A given noisy single step-edge profile ( $x$ ) is decomposed using multi-scale DT DWT(K) up to  $J$  levels in two trees.
2. To compensate for offset and polarity discrepancies, real-tree coefficients are left shifted (cyclically) by 1-sample ( $n_{\text{off}} = -1$ ) for all levels ( $j = 1$  to  $J$ ) and polarity of real-tree coefficients are reversed (for  $j = 2$  to  $J$ ).
3. For maintaining the same size of coefficients at all levels, both real and imaginary trees coefficients are interpolated with right amount of level dependent zeros ( $2^j - 1$ ) at each level ( $j = 1$  to  $J$ ) before each coefficient.

- 
4. All coefficients at each level of both trees are zero clipped (keeping only +ve values) to account for positive going edge.
  5. All the coefficients are normalised between [0,1].
  6. Coefficients of both real and imaginary trees at each level are combined using the formula of complex magnitude and phase. The magnitude tree is used for further processing.
  7. Depending on the true location of edge, optimum level  $j_{\text{opt}} = \log_2(En)$  is selected for edge detection with minimum RMSE.
  8. The position of maximum magnitude coefficient at a selected optimum level gives the location of detected edge.

The basic CMED algorithm is not fuzzy based and it works only at a unique level for optimum edge detection using combined real and imaginary trees. Variants of CMED algorithm such as CMED algorithm with only imaginary tree (IMED), and CMED algorithm with fuzzy union of various scales are also investigated (FCMED). The other variant of CMED namely SFCMED (Spatial Fuzzy CMED) is also explored through fuzzy combination of reconstructions (of decimated coefficients) at different scales in spatial domain.

### 5.3.6 Performance Measure

Root Mean Square Error (RMSE) and percentage Hit (% Hit) are taken for evaluating the performance of single positive going step edge with different slope conditions ( $\Delta$ ) under varying degree of SNR. Related definitions and equations are given as:

$$\text{RMSE (in terms of samples)} = \sqrt{(Ed - En)^2} \quad (5.1)$$

where,  $Ed$  = Position of detected edge,  $En$  = Position of correct edge

The percentage Hit is defined in two forms, first is percentage Accurate Hit (%AHit) that is the percentage of detected edge  $Ed$  exactly at the true edge location  $En$  (detected without noise), and the second form is percentage Interval Hit (%IHit) that is the percentage of detected edge  $Ed$  within  $[En-1 \text{ to } En+\Delta+1]$ , in the portion of transition of step edge profile. In other words,

%AHit  $\rightarrow Ed$  at  $En$  (where  $En$  is dependent on basis function and slope) and  
 %IHit  $\rightarrow Ed$  is within  $[En-1 \text{ to } En+\Delta+1]$  samples. (5.2)

$$\text{SNR(dB)} = 10 \log_{10} \left[ \frac{E\{(s - \bar{s})^2\}}{\sigma^2} \right] \quad (5.3)$$

where,  $E(\cdot)$  is an expectation operation,  $s$  is an original single step-edge profile without noise,  $\bar{s}$  is the mean value of signal  $s$ , and  $\sigma^2$  is the variance of AWGN super imposed on signal  $s$ .

Slope ( $\Delta$ ) = number of samples within the transition of step-edge profile. (5.4)

### 5.3.7 Results and Discussion

The results of MZ-MED and FWOMED are taken from [177], results of FMED ('cubic') are taken from an individual implementation of the standard FMED algorithm developed in [176]. Other novel implementations of standard FMED with different basis such as FMED('db3') and DB-FMED are developed individually during the studies of standard FMED. An original CMED algorithm is developed using DT-DWT(K). A quantitative comparison of various algorithms for a selected step-edge profile, with different parameters is given in tables (5.1) to (5.5), uniformly iterated 50, 000 times for all algorithms using Monte-Carlo simulations.

Implementation of FMED ('cubic') for a noisy and sloppy single edge step-edge profile (with nearly accurate detection of the edge as a result) is shown in figure (5.3). Wavelet coefficients at  $J$  levels and their zero clipped +ve parts are shown in figure (5.4).  $J$  level fuzzy subsets of clipped coefficients and their interactions (at

level 2 to  $J$ ) to form a minimum fuzzy set are shown in figure (5.5). Processing steps related to basic CMED algorithm are highlighted through figures (5.6) to (5.10).

From the results in tables (5.1) to (5.5), it can be concluded that for all noise and slope conditions, the FWOMED algorithm is better than well known MZ-MED algorithm and FMED ('cubic') algorithm in terms of RMSE error. Two FMED based algorithms namely FMED ('db3') and DB-FMED perform better than all other non-decimated multiscale edge detection algorithms in varying slope and noise conditions. Performance of FMED ('db3') is optimum in lower slope conditions ( $\Delta = 0,1$ ), where as DB-FMED is optimum for moderate to higher slope conditions ( $\Delta = 3,5$ ). Basic CMED algorithm is comparable to other FMED algorithms in lower noise conditions ( $\sigma \leq 0.4$ ) for all slope conditions.

CMED algorithm is significantly poorer in higher noise conditions. Also the other major disadvantage of basic CMED algorithm is its limitation to detect the edges located only at power of two indices. The other variants such as IMED, FCMED and SFCMED are even poorer than basic CMED. The limitations of basic CMED algorithm are because of the use of decimated DT-DWT(K) and single level detection strategy. But the promising %Hit results (table 5.5) with accurate localisation of edge at courser levels (at level 4 and 5 in figure (5.9)) with DT-DWT(K) suggest its potential for further investigations to generalise the basic CMED algorithm.

It is proposed that by developing new non-decimated version of DT-DWT(K) with multilevel fuzzy reasoning might generalise a basic CMED to NFCMED (Non-decimated Fuzzy CMED) for detection of any arbitrary edge (not exactly at power of 2 locations). NFCMED being equally redundant at all levels and having all the benefits of CWT might prove to be a challenging research for comparable performance against the variants of FMED algorithms.

Noise Parameters		Step edge having $\Delta=0, N=128$ (initial 32 zeros + $\Delta+N-32-\Delta$ ones)						
		$n_{\text{off}} = 0$ for FMED('cubic_spline'), $n_{\text{off}} = -(\Delta-2)$ for FMED('db3'), $n_{\text{off}} = +1$ for DB-FMED, $n_{\text{off}} = -1, j_{\text{opt}} = 5$ for CMED						
		RMSE (after 50 000 iterations)						
SNR (dB)	$\sigma$	MZ-MED	FWOMED	FMED (‘cubic’)	FMED (‘db3’)	DB-FMED	CMED	
$\infty$	0	0	0	0	0	0	0	0
12.73	0.1			0.30	0.17	0.21	0	
6.71	0.2	0.26	0.86	0.48	0.35	0.38	0	
3.19	0.3			0.67	0.65	0.61	0.20	
0.69	0.4	1.29	1.33	1.23	0.96	1.07	1.32	
-1.25	0.5			1.96	1.68	1.69	3.37	
-2.83	0.6	2.98	2.45	2.94	2.35	2.41	6.30	
-4.17	0.7			3.86	2.93	3.18	8.63	
-5.33	0.8	5.81	4.83	5.23	3.82	3.99	10.65	
-6.35	0.9			5.71	4.48	4.85	12.79	
-7.27	1.0	9.31	7.83	6.45	5.36	5.70	14.48	

Table 5.1: RMSE of various 1-D edge detection algorithms with  $\Delta=0$  in varying AWGN noise conditions.

Noise Parameters		Step edge having $\Delta=1, N=128$ (initial 32 zeros + $\Delta+N-32-\Delta$ ones)						
		$n_{\text{off}} = -(\Delta-1)$ for FMED('cubic_spline'), $n_{\text{off}} = -(\Delta-2)$ for FMED('db3'), $n_{\text{off}} = -(\Delta-2)$ for DB-FMED, $n_{\text{off}} = -1, j_{\text{opt}} = 5$ for CMED						
		RMSE (after 50 000 iterations)						
SNR (dB)	$\sigma$	MZ-MED	FWOMED	FMED (‘cubic’)	FMED (‘db3’)	DB-FMED	CMED	
$\infty$	0	0	0	0	0	0	0	0
6.71	0.2	0.75	0.57	0.26	0.25	0.31	0.01	
0.69	0.4	1.56	1.24	1.16	1.09	1.10	1.25	
-2.83	0.6	3.27	2.44	2.86	2.39	2.44	6.07	
-5.33	0.8	5.89	4.73	4.76	3.90	3.98	10.78	
-7.27	1.0	9.67	7.93	6.37	5.49	5.64	14.40	

Table 5.2: RMSE of various 1-D edge detection algorithms with  $\Delta=1$  in varying AWGN noise conditions.

Noise Parameters		Step edge having $\Delta=3, N=128$ (initial 32 zeros + $\Delta + N-32-\Delta$ ones)						
		$n_{\text{off}} = -(\Delta-1)$ for FMED('cubic_spline'), $n_{\text{off}} = -(\Delta-2)$ for FMED('db3'), $n_{\text{off}} = -(\Delta-2)$ for DB-FMED, $n_{\text{off}} = -1, j_{\text{opt}} = 5$ for CMED						
		RMSE (after 50 000 iterations)						
SNR	$\sigma$	MZ-MED	FWOMED	FMED (‘cubic’)	FMED (‘db3’)	DB- FMED	CMED	
$\infty$	0	0	0	0	0	0	0	0
6.71	0.2	1.11	0.95	1.02	1.05	0.86	0.01	
0.69	0.4	1.92	1.51	2.00	1.87	1.71	1.67	
-2.83	0.6	3.51	2.64	3.66	3.13	3.05	6.37	
-5.33	0.8	6.08	4.97	5.41	4.63	4.59	11.24	
-7.27	1.0	9.41	8.03	7.03	6.12	6.24	14.90	

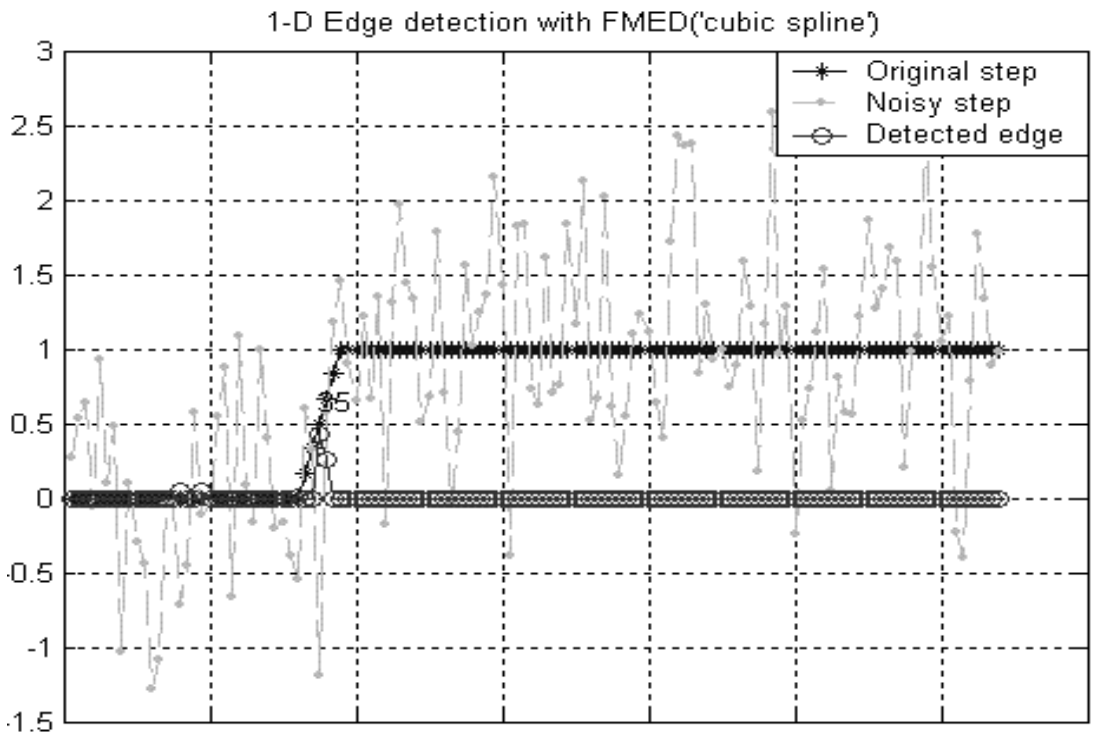
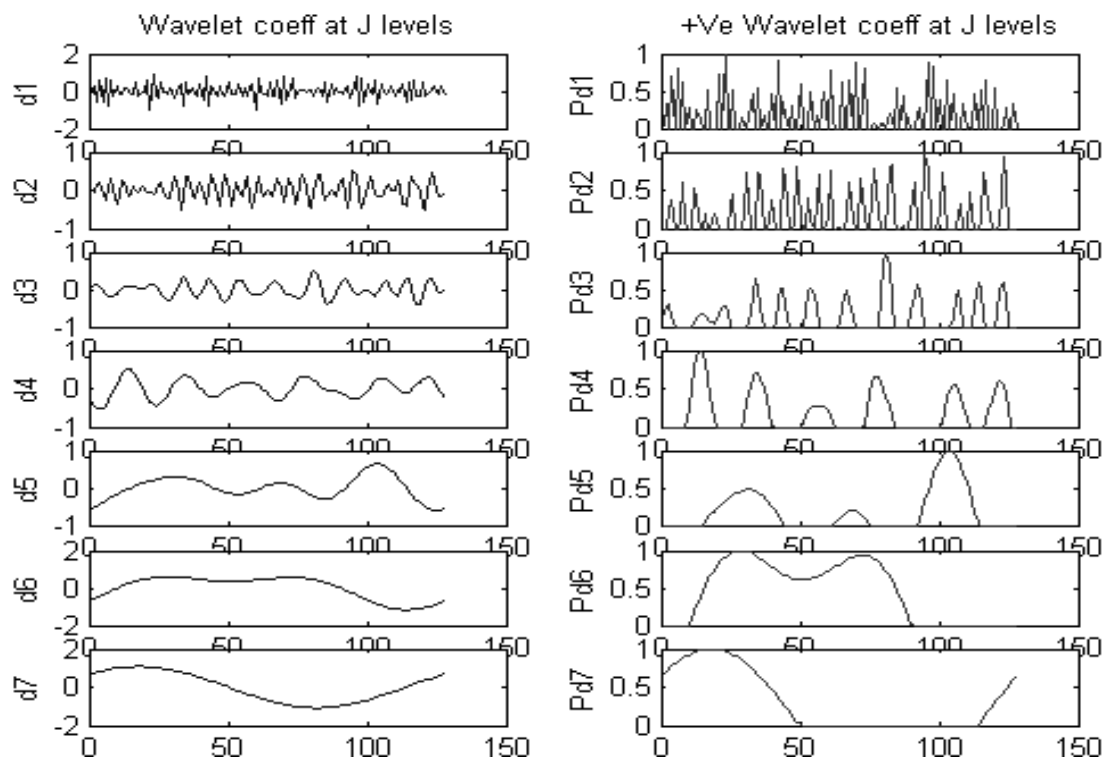
Table 5.3: RMSE of various 1-D edge detection algorithms with  $\Delta=3$  in varying AWGN noise conditions.

Noise Parameters		Step edge having $\Delta=5, N=128$ (initial 32 zeros + $\Delta + N-32-\Delta$ ones)						
		$n_{\text{off}} = -(\Delta-1)$ for FMED('cubic_spline'), $n_{\text{off}} = -(\Delta-2)$ for FMED('db3'), $n_{\text{off}} = -(\Delta-2)$ for DB-FMED, $n_{\text{off}} = -1, j_{\text{opt}} = 5$ for CMED						
		RMSE (after 50 000 iterations)						
SNR (dB)	$\sigma$	MZ-MED	FWOMED	FMED (‘cubic’)	FMED (‘db3’)	DB- FMED	CMED	
$\infty$	0	0	0	0	0	0	0	0
6.71	0.2	1.63	1.34	2.00	2.01	1.82	0.01	
0.69	0.4	2.39	1.85	3.02	2.82	2.61	2.62	
-2.83	0.6	3.78	2.91	4.70	4.09	3.96	7.61	
-5.33	0.8	6.22	5.14	6.38	5.47	5.44	12.10	
-7.27	1.0	9.60	8.14	8.05	7.04	7.03	16.04	

Table 5.4: RMSE of various 1-D edge detection algorithms with  $\Delta=5$  in varying AWGN noise conditions.

Noise and Slope		Step edge having $N=128$ (initial 32 zeros + $\Delta$ + $N-32-\Delta$ ones)							
		% AHit (after 50 000 iterations)				% IHit (after 50 000 iterations)			
$\sigma$	$\Delta$	FMED (‘cubic’)	FMED (‘db3’)	DB- FMED	CMED	FMED (‘cubic’)	FMED (‘db3’)	DB- FMED	CMED
0	0	100	100	100	100	100	100	100	100
	1	100	100	100	100	100	100	100	100
	3	100	100	100	100	100	100	100	100
	5	100	100	100	100	100	100	100	100
0.2	0	54	67	63	100	100	98	100	100
	1	76	78	71	99	98	99	98	99
	3	32	30	39	99	99	99	100	99
	5	17	15	18	99	99	100	100	99
0.4	0	38	48	41	98	83	82	88	98
	1	46	46	46	98	81	85	84	98
	3	20	20	25	97	88	93	94	97
	5	12	12	13	96	89	93	93	96
0.6	0	25	33	27	89	61	63	70	89
	1	29	29	30	90	59	67	67	90
	3	14	15	16	89	72	80	81	89
	5	8	9	10	87	74	82	83	87
0.8	0	17	23	19	81	44	59	54	81
	1	19	20	21	81	44	53	53	81
	3	10	11	12	80	59	68	69	80
	5	7	7	8	79	63	71	72	79
1.0	0	13	17	14	73	34	38	44	73
	1	14	16	15	74	34	44	43	74
	3	8	9	10	73	48	58	58	73
	5	6	6	7	71	54	62	62	71

Table 5.5: % Hit of various 1-D edge detection algorithms in varying slope and AWGN noise conditions.

Figure 5.3: 1-D edge detection with FMED ('cubic') with  $\sigma=0.6$  and  $\Delta=5$ .Figure 5.4:  $J$  level wavelet coefficients (left) and their only positive parts (right) with FMED('cubic') under the noise of  $\sigma=0.6$  and slope of  $\Delta=5$ .

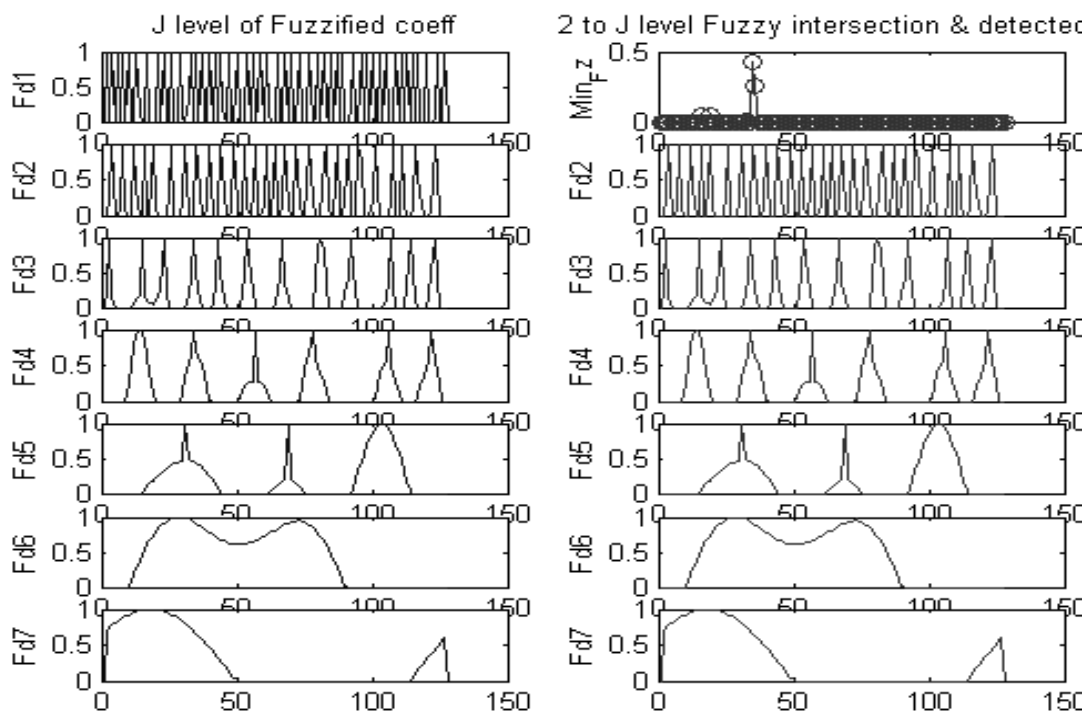


Figure 5.5:  $J$  level fuzzy subsets (left) and their corresponding 2 to  $J$  level fuzzy intersection (right) for the computation of minimum fuzzy set (right top) employing FMED ('cubic') under the noise of  $\sigma=0.6$  and slope of  $\Delta=5$

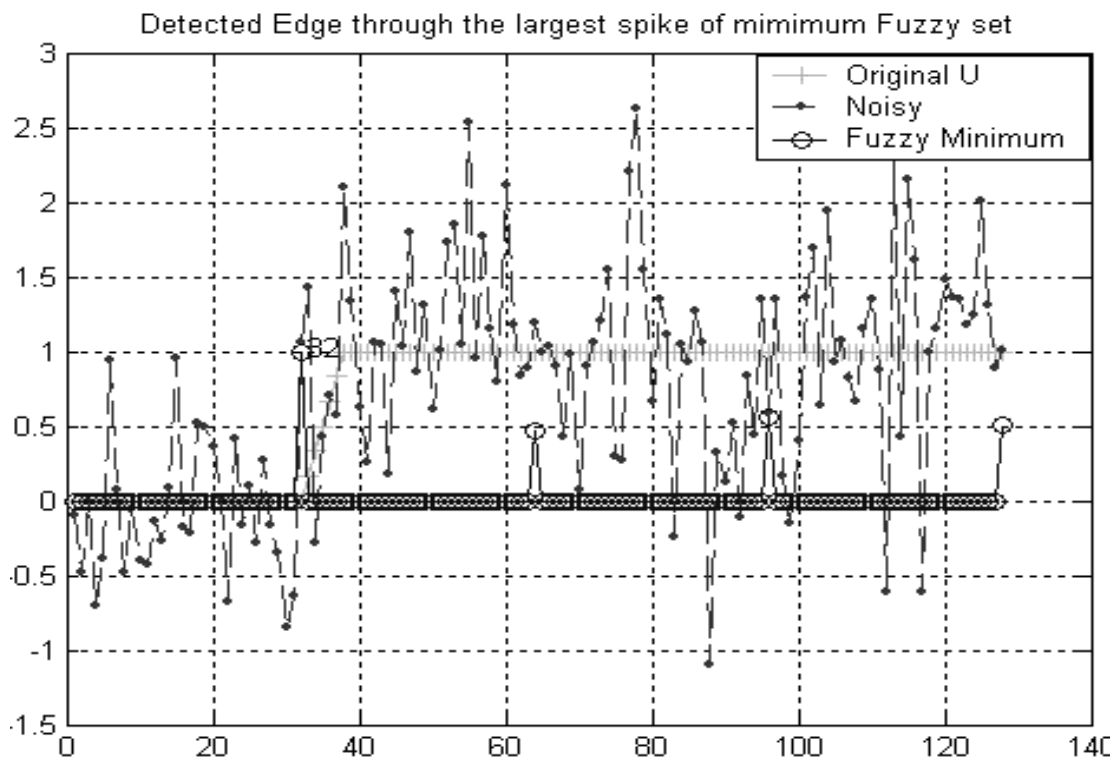


Figure 5.6: 1-D edge detection with CMED:  $\sigma=0.6$  and  $\Delta=5$

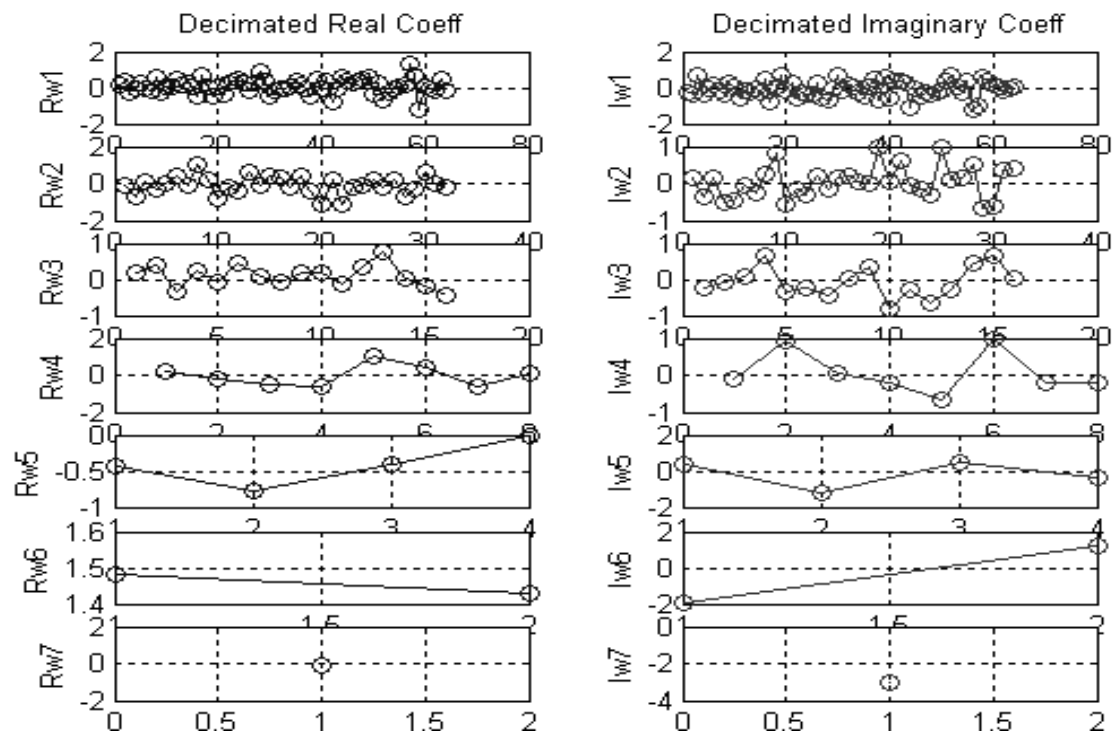


Figure 5.7:  $J$  level of decimated real and imaginary coefficients with CMED:  $\sigma=0.6$  and  $\Delta=5$

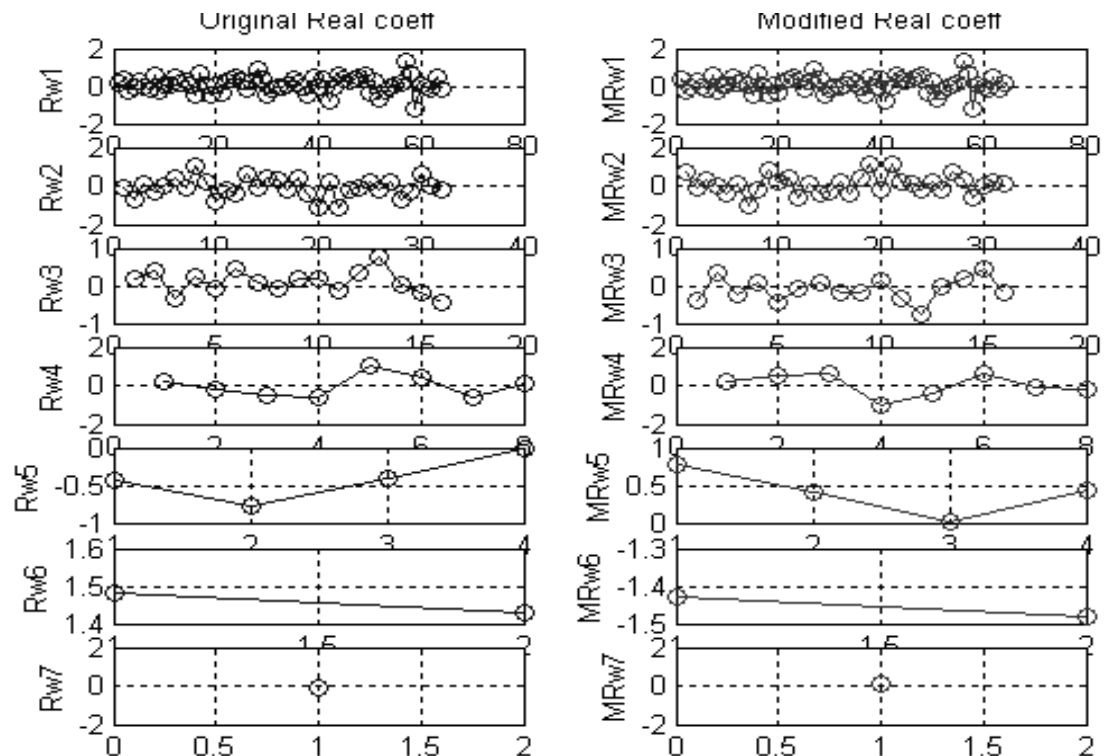


Figure 5.8:  $J$  level of decimated original and modified (inverted and left cyclic shift of 1 sample for levels 2 to  $J$ ) real coefficients with CMED:  $\sigma=0.6$  and  $\Delta=5$

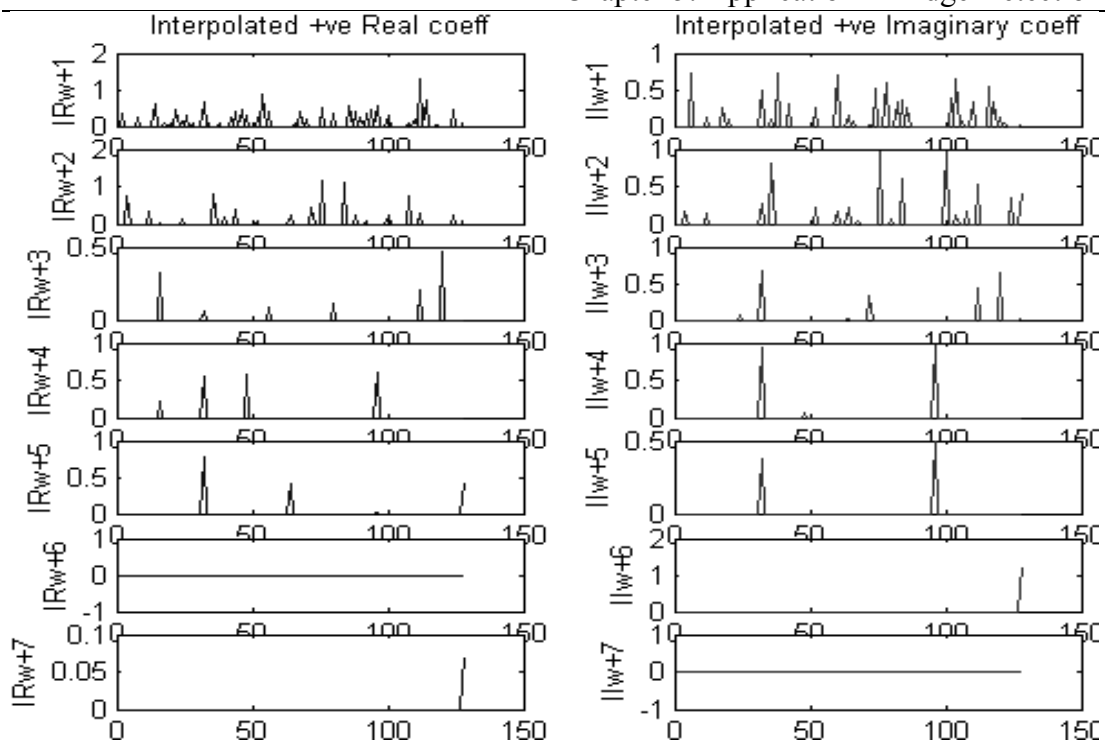


Figure 5.9:  $J$  level of interpolated modified real and original imaginary coefficients with CMED:  $\sigma=0.6$  and  $\Delta=5$

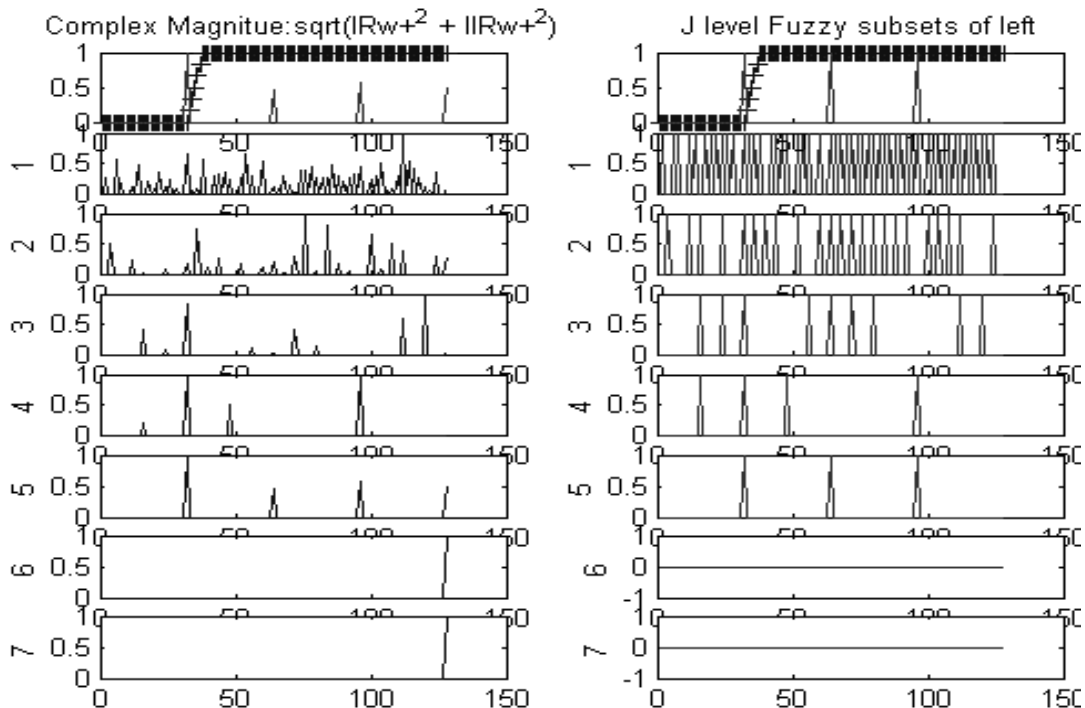


Figure 5.10:  $J$  level of complex magnitude coefficients (left) and fuzzy subsets of complex magnitudes (right). Top left shows detected edge with complex magnitude (at level 5) and top right shows detected edge with fuzzy subset (at level 5) employing CMED:  $\sigma=0.6$  and  $\Delta=5$

## 5.4 2-D Edge Detection

As discussed in the introduction of section 5.1, edge information is very precious for various image-processing applications. Review of many conventional algorithms and methods based on edge detection for image processing can be found in [179-181]. Though *Canny*'s operator is a robust edge detector in a noisy environment [161], some less noticed and unconventional methods for edge in noisy conditions can be found in [182,183].

### 5.4.1 Basic Approach

Multiscale methods based on non-orthogonal (and redundant) wavelet transform [163,164] showed promising performance for edge detection in noisy environment, and are widely employed in many applications. Object segmentation, Motion estimation, Image fusion, Image registration and CBIR (Content Based Image Retrieval) are just a few examples utilising the multiscale edge information for image processing [184-190]. More recently many researchers have combined advanced techniques such as Fuzzy reasoning [191-193], HMM (Hidden Markov Models) [194,195], Neural networks [196,197], and Genetic algorithms [198] for improved multiscale image segmentation, registration and object extraction in wide range of applications.

Though redundancy and Gaussian like wavelet basis are common in many multiscale edge-detection applications, viewpoint of our research is different for 2-D edge detection. Central theme of this research is to investigate the effects of redundancy, shift-invariance and directionality of different types of wavelet transforms in edge detection. In this section, 2-D edge detection is investigated using various wavelet based, and conventional algorithms. 2-D separable wavelet-based algorithms employ standard DWT, SWT and redundant CWT (namely DT-DWT(K) and DT-DWT(S)), whereas conventional algorithms are based on 2-D edge operators such as Prewitt, Sobel, and Canny.

### **5.4.2 Algorithms**

Conventional 2-D edge detection is performed using Matlab (image processing toolbox) function ‘edge’ with default settings. The wavelet-based algorithms employ a simple strategy (without any advanced optimisation techniques to combat with noise) to verify the subtle differences of edge detection performance of various wavelet transforms.

#### **5.4.2.1 WT based Algorithm**

*With standard DWT and SWT*

1. A given image (2-D signal) is decomposed to  $J$  levels using standard DWT or SWT with suitable wavelet basis.
2. The lowpass subband is filled with zeros and all high-pass subbands are unchanged.
3. A  $J$  level reconstruction is performed with relevant inverse wavelet transform.
4. From recovered image, 2-D edge thinning mask is computed using local maxima approach.
5. The recovered image is thresholded by a suitable heuristic threshold to eliminate features below certain intensities.
6. Final edge detection is achieved by multiplying the thresholded image with thinning mask.

#### **5.4.2.2 CWT based Algorithm**

*With DT-DWT(K) and DT-DWT(S)*

1. An image (of size in power of 2 in both directions) is taken.

- 
2. The image is decomposed with the redundant CWT (using DT-DWT(K) or DT-DWT(S)) to the depth of  $J$  levels.
  3. All lowpass subbands (four) of last levels are set to zeros.
  4. Any highpass subbands of real or imaginary trees are not altered
  5.  $J$  level inverse transform is taken to reconstruct the image.
  6. A 2-D thinning mask from reconstructed image is computed by finding local maximum (horizontal and vertical). Comparative neighbour-hood approach is used to form this mask.
  7. Reconstructed image is thresholded with heuristic threshold value using hard or soft thresholding to form a binary image.
  8. A refined image with sharp edges is obtained by multiply a thinning mask with binary output image.

### 5.4.3 Performance Measure

In general it is quite challenging to compare the performance of edge detection algorithms in quantitative manner. Even though the definition of edge is also difficult to quantify objectively, there are a few proposed measure to quantify the performance of edge detectors such as conditional probabilities  $P(\frac{nd}{nt})$ ,  $P(\frac{nd}{nt})$ , MSD (Mean Squared Distance) and FOM (Figure of Merit) as suggested in [199,200].

$$\text{MSD} = \frac{1}{nd} \sum_{i=1}^{nd} di^2$$

$$\text{FOM} = \frac{1}{\max\{nd, nt\}} \sum_{i=1}^{nd} \frac{1}{1 + 0.9 di^2} \quad (5.5)$$

where,  $nd$  = no. of detected edge pixels,  $nt$  = no. of true edge pixels,  $di$  = edge deviation of  $i^{\text{th}}$  detected pixel from its true position.

These quantitative measures may be reasonable for predetermined and simple test images but not practical for natural images, and are not widely used. Hence in this research, the results are presented for qualitative comparisons relying on the human visual system.

#### 5.4.4 Results and Discussion

The results of various edge detectors for a test image are shown in figures (5.11) and (5.12).

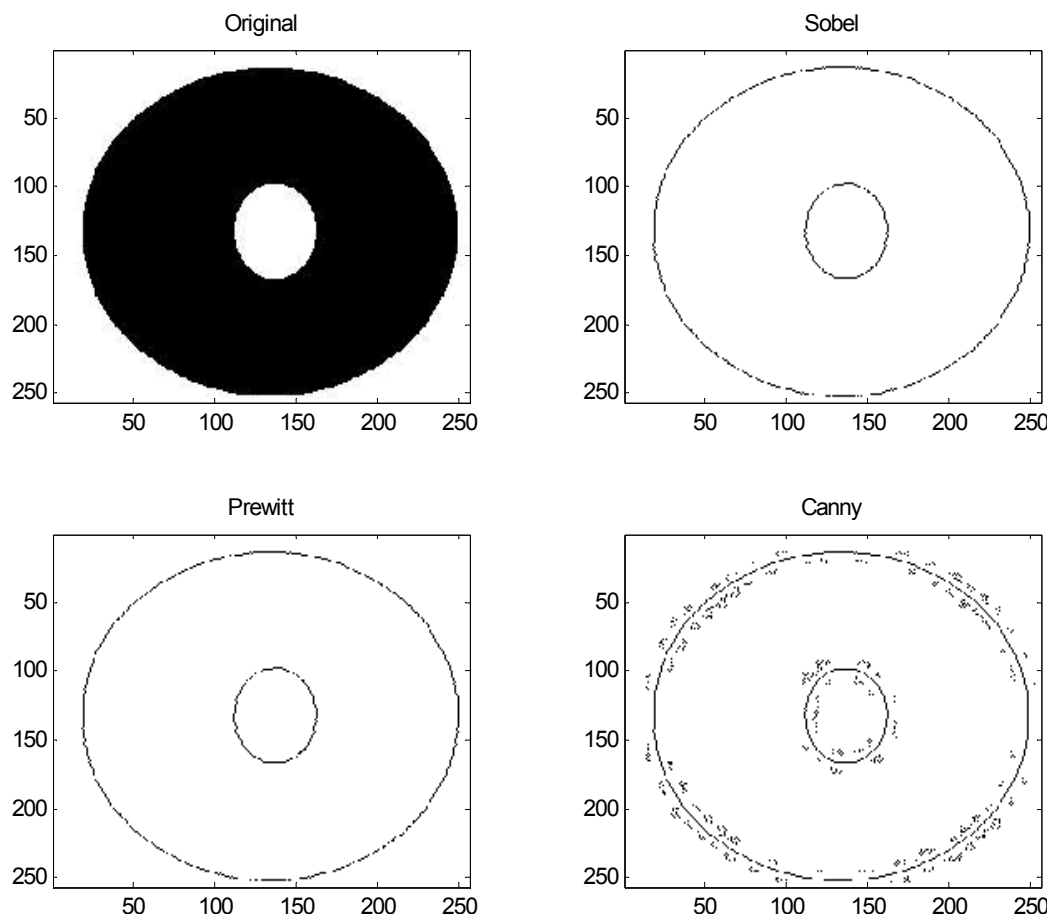


Figure 5.11: 2-D edge detection with conventional edge operators

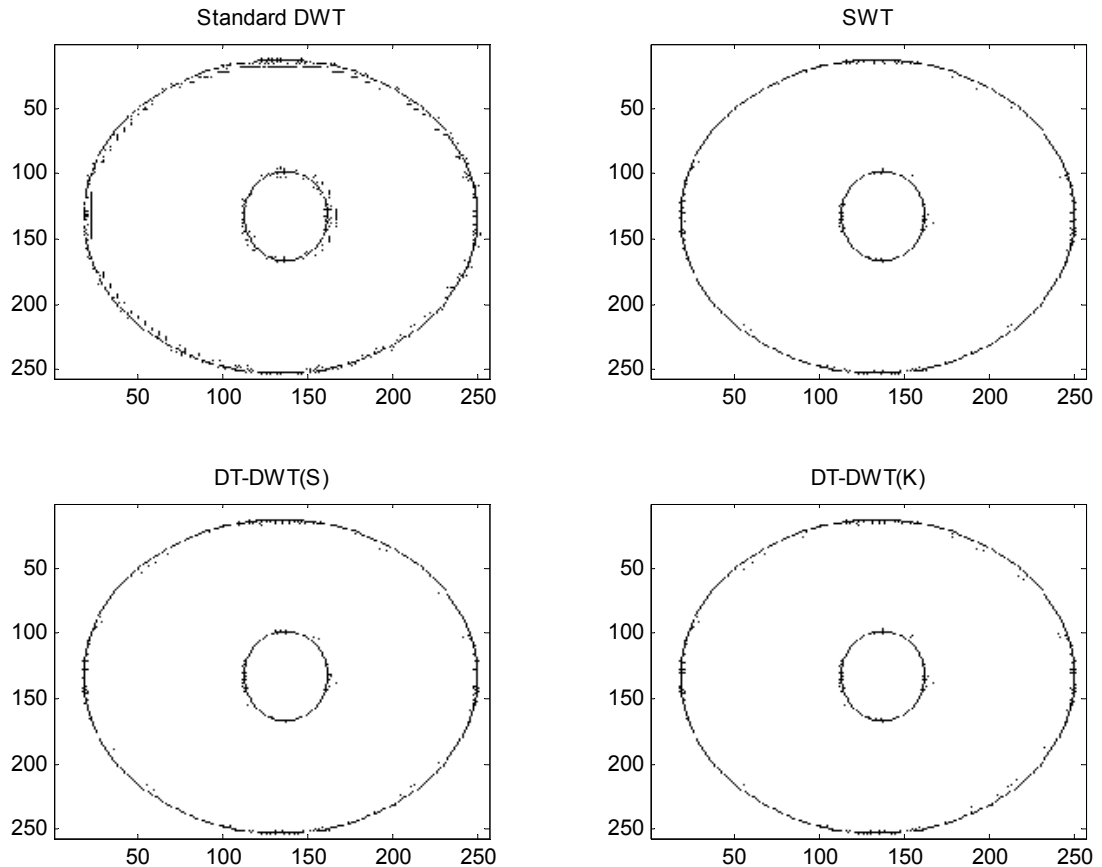


Figure 5.12: 2-D edge detection with wavelet based methods. For all method, test image is  $256 \times 256$  ‘ring.jpg’,  $J=2$  and threshold value = 35. For standard DWT and SWT wavelet basis is ‘db2’. The wavelet filters used for DT-DWT(K) are ‘near\_sym\_b’ and ‘qshift\_b’ as given in appendix A and the filters for DT-DWT(S) are as given in appendix B.

From the figures (5.11) and (5.12), it is clear that conventional 2-D edge detectors (of matlab) with default thresholding schemes are better than simple implementation of wavelet based detectors for detection boundaries with very good sharpness and resolutions without noise as well and in noisy conditions. Canny edge detector with its defaults settings is more liberal (and more leaky) than Prewitt and Sobel but flexibility makes it more robust in blurred images.

The results in figure (5.12) show that the performance of both DT-DWT methods is superior to the standard DWT due to its (4:1) redundancy, and improved directionality (with more spatial orientations). The superior performance of SWT

compared to standard DWT lies in its highly redundant representation. Visually, performance of SWT is comparable to both DT-DWTs. The results presented here are without the presence of noise.

A set of experiments show that the redundancy is of prime importance for improved edge detection in wavelet domain. Improved directionality also plays an important role in images with large number of randomly oriented edges. More sophisticated techniques may be employed in wavelet domain to combat with noise utilizing the directionality and/or redundancy of the transforms for improvement over conventional edge detectors.

## 5.5 Conclusion

It is concluded that redundancy of the transform is very important for efficient Edge detection with multiscale approaches. Directionality of the transform also plays an important role in fidelity of Edge detection in multi dimensions.

Multiscale algorithms (FMED extensions) with non-decimated SWT having Gaussian like kernel are promising for single edge, 1-D Edge detection in higher noise environment over other classical Edge detection approaches (Canny, Prewitt etc.). Limited redundant DT-DWT, being a decimated extension, is not very promising for 1-D Edge detection in its original form with CMED. The accuracy of edge localisation at lower resolution scales is higher with DT-DWT (using CMED algorithm) than with SWT (using FMED algorithms) suggests its potential for further investigations using its non-decimated extension.

For 2-D Edge detection, performance of DT-DWT is superior to standard DWT but almost similar to SWT. Integration of advanced noise removal, and multi-edge detection techniques with non-decimated DT-DWT might be suitable for efficient Edge detection in images corrupted by higher noise.

# **Chapter 6:**

## **Conclusions and Future Scope**

### **6.1 Conclusions**

In this thesis, Wavelet Transforms (WT) is reviewed in detail. The history, evolution, and various forms of WTs are investigated. Advantages, applications, and limitations of popular standard DWT and its extensions are realised. Complex Wavelet Transforms (CWT), a powerful extension to real valued WT is thoroughly investigated to reduce the major limitations of standard DWT and its extensions in certain signal processing applications.

The history, basic theory, recent trends, and various forms of CWTs with their applications are collectively and comprehensively analysed. Recent developments in CWTs are critically compared with existing forms of WTs. Potential applications are investigated and suggested that can be benefited with the use of different variants of CWTs.

Individual software codes are developed for simulation of selected applications such as Denoising and Edge detection using both WTs and CWTs. The performance is statistically validated and compared to determine the advantages and limitations of CWTs over well-established WTs. Promising results are obtained using individual implementation of existing algorithms incorporating novel ideas into well-established frameworks.

---

In chapter 2, the background for analysing the CWTs is presented. WTs are reviewed in detail with individual investigations and simulations. Complex mathematical formulations and important properties of WTs are studied. Evolution and advantages of WTs as an alternative to FT for non-stationary signals are studied. 1-D and 2-D implementations of various versions of WTs are realised with software simulations. Applications of various forms of WTs are surveyed. It is realised that WT is an important tool for non-stationary signal processing applications. WT has a great potential for singularity detection, denoising and compression and it presents a novel framework of time-scale for analysing and characterising many natural signals with the wealth of time-varying information. Chapter 2 concludes with three major disadvantages of widely used standard DWT, namely; Shift-sensitivity, Poor-directionality, and Lack of Phase-information. These disadvantages severely limit the applications of WTs in certain signal processing applications. It ends with motivation to reduce these disadvantages of WTs through a complex extension known as CWTs.

Thorough analysis of CWTs is presented in chapter 3. The limitations of the earlier work on CWTs (with the motivation to utilise both the magnitude and phase information in more effective manner than real valued WTs) are presented. Recent developments in the field of CWTs, with the motivation to reduce all three limitations of standard DWT, are critically analysed. CWTs are classified into two important categories namely RCWT (Redundant CWT) and NRCWT (Non-redundant CWT). RCWT include DT-DWT(S) (*Selesnick's* Dual-Tree DWT) and DT-DWT(K) (*Kingsbury's* Dual-Tree DWT). Theory, filterbank structure and properties of both DT-DWTs are critically investigated and compared. Similarly for NRCWT, *Fernandes's* PCWT (Projection based CWT), and *Spaendonck's* non-redundant OHCWT (Orthogonal Hilbert Transform filterbank based CWT) are investigated.

Implementation for both DT-DWTs and PCWT is realised through Matlab simulations based on the theories of sections 3.5 and 3.5. Comparative summary of all CWTs are presented in table (3.2). Depending upon the redundancy and properties, potential applications are suggested (based on literature review, thorough

investigations, and after primary level implementations) that can be benefited by further investigations with various forms of CWTs as an alternative to existing DWT extensions.

In chapter 4, individual implementations of WTs and CWTs (explicitly DT-DWTs) with Matlab simulations are presented for an important signal/image processing application namely Denoising. In chapter 4, 1-D and 2-D CWTs are implemented for signals and images in exiting framework of wavelet shrinkage denoising algorithms. Some novel modifications are made in threshold selections and thresholding strategies. The results are compared with variants of WT based algorithms and other conventional filtering techniques such as Mean, Median and Wiener Filtering. It is observed that in general for higher noise environment, CWTs perform better than WTs and other conventional techniques for different 1-D and 2-D signals. Effects of number of wavelet parameters are investigated. 1-D CWTs are also investigated with certain novel ideas for audio denoising (with initially poor SNR), producing some promising results over standard DWT.

In chapter 5, for Edge Detection application, the background research in the Signal Processing Group of University of Strathclyde is explored further with the novel ideas in existing frameworks. The existing WT based 1-D edge-detection algorithms such as MZ-MED, FMED and FWOMED are reviewed. Individual implementation of cubic spline base FMED algorithm culminated in newer FMED ('db3') and DB-FMED algorithms with their novel implementation using different bases. The newer algorithms showed an improved performance over both FMED and FWOMED in higher noise and slope conditions. Experiments with CWT for 1-D edge detection resulted in a basic CMED algorithm. CMED algorithm is still in its primary stage, with promising edge localisation property at lower resolution scales, compared to other WT based multiscale algorithms. For 2-D edge detection, a very basic strategy of neglecting the lowpass subband is applied to investigate the advantage of CWT over standard DWT. Other conventional edge detectors such as Prewitt and Canny are also implemented for comparison. The result of 2-D edge detection shows the improved performance of CWTs over standard DWT because of

its improved directionality and limited redundancy. The performance of redundant WT (i.e. SWT) compared to DT-DWT based CWT suggests the importance of higher redundancy in edge detection.

## 6.2 Future Scope

It is concluded that CWT (having separable implementation, perfect reconstruction, limited (or no) redundancy, and improved properties over real-valued WTs) has a potential for many signal and image processing applications yet to be explored.

Due to limited academic time span, NRCWT such as *Fernandes's* PCWT and *Spaendonck's* OHCWT have yet to be explored for denoising applications. It is assumed that the properties of PCWT-CR similar to DT-DWTs will result in a comparable performance. Even non-decimated DT-DWTs might even improve the denoising performance over existing DT-DWTs.

The initial simulations for 1-D edge detection show potential scope of further investigation to enhance basic CMED algorithm in higher noise conditions. The suggested NFCMED (Non-decimated Fuzzy CMED) algorithm should be explored for improved 1-D edge detection in higher noise conditions. The extension of NFCMED in 2-D incorporating multiple edge detection and other techniques suitable for higher noise might yield a robust and optimum algorithm for object extraction and segmentation from noisy video clips. *Fernandes's* PCWT with redundant projections (PCWT-CR) should also be explored in similar manner that gives fully redundant projection based CWT suitable for edge detection applications.

DT-DWTs with their good shift invariance should be considered for potential investigations in applications such as Motion estimation in video coding, SAR remote sensing, Texture segmentation, and Image fusion. The non-redundant NRCWT (explicitly PCWT-NR and OHCWT) has a strong potential for further

investigations in directional compression leading toward an improved moderate to low bit-rate video codecs.

Potential applications for further investigations with CWTs are summarised in table (3.2). There is also a potential challenge for improvement in filter designs to further minimising the aliasing of subbands for immunity towards shift-sensitivity, and merging the standard DWT strategies to add two more orientations at  $0^\circ$  and  $90^\circ$  to the available orientations of CWT for further improved directionality. Many researchers perceived that though wavelets showed tremendous applications in signal processing, they are still not optimum in dealing with sparse singularities in natural images. Curvelets, Contourlets, and Piecewise approximations are the newer basis emerging beyond wavelets. It would be interesting to explore the possibility of similar complex extensions to such newer basis and analyse their properties in signal processing context.

# Appendix A

Filters used to implement DT-DWT(K) uses Kingsbury's Dual-Tree Complex Wavelet Transform available from: [ngk@eng.cam.ac.uk](mailto:ngk@eng.cam.ac.uk) ,  
<http://www-sigproc.eng.cam.ac.uk/~ngk/>

**First stage Filters:**

Antonini, Legall, near\_sym\_a and near\_sym\_b.

**Q-shift Filters (after first stage):**

qshift\_06, qshift\_a, qshift\_b, qshift\_c, and qshift\_d.

**For example ‘near\_sym\_b’ filters:**

	<b>Real-tree Analysis Filter</b>	
	<b>Lowpass Filter (<math>h_0</math>)</b>	<b>Highpass Filter (<math>h_1</math>)</b>
1	-0.00175781250000	-0.00007062639509
2	0	0
3	0.02226562500000	0.00134190150670
4	-0.04687500000000	-0.00188337053571
5	-0.04824218750000	-0.00715680803571
6	0.29687500000000	0.02385602678571
7	0.55546875000000	0.05564313616071
8	0.29687500000000	-0.05168805803571
9	-0.04824218750000	-0.29975760323661
10	-0.04687500000000	0.55943080357143
11	0.02226562500000	-0.29975760323661
12	0	-0.05168805803571
13	-0.00175781250000	0.05564313616071
14		0.02385602678571
15		-0.00715680803571
16		-0.00188337053571
17		0.00134190150670
18		0
19		-0.00007062639509

Table (A1): First stage filters (for near\_sym\_b): Imaginary-tree analysis filters are one sample delayed than the real-tree filters. Synthesis filters are obtained by negating odd-indexed coefficients and swapping bands.

## Appendix A (Contd.)

**For example ‘qshift\_b’ filters:**

<b>Analysis Filters</b>				
	Lowpass Filters		Highpass Filters	
	$h_{0a}$ (real)	$h_{0b}$ (imaginary)	$h_{1a}$ (real)	$h_{1b}$ (imaginary)
1	0.00325314276365	-0.00455689562848	-0.00455689562848	-0.00325314276365
2	-0.00388321199916	-0.00543947593727	0.00543947593727	-0.00388321199916
3	0.03466034684485	0.01702522388155	0.01702522388155	-0.03466034684485
4	-0.03887280126883	0.02382538479492	-0.02382538479492	-0.03887280126883
5	-0.11720388769912	-0.10671180468667	-0.10671180468667	0.11720388769912
6	0.27529538466888	0.01186609203380	-0.01186609203380	0.27529538466888
7	0.75614564389252	0.56881042071212	0.56881042071212	-0.75614564389252
8	0.56881042071212	0.75614564389252	-0.75614564389252	0.56881042071212
9	0.01186609203380	0.27529538466888	0.27529538466888	-0.01186609203380
10	-0.10671180468667	-0.11720388769912	0.11720388769912	-0.10671180468667
11	0.02382538479492	-0.03887280126883	-0.03887280126883	-0.02382538479492
12	0.01702522388155	0.03466034684485	-0.03466034684485	0.01702522388155
13	-0.00543947593727	-0.00388321199916	-0.00388321199916	0.00543947593727
14	-0.00455689562848	0.00325314276365	-0.00325314276365	-0.00455689562848

Table (A2): Q-shift filters (after first stage) of type ‘qshift\_b’

<b>Synthesis Filters</b>				
	Lowpass Filters		Highpass Filters	
	$g_{0a}$ (real)	$g_{0b}$ (imaginary)	$g_{1a}$ (real)	$g_{1b}$ (imaginary)
1	-0.00455689562848	0.00325314276365	-0.00325314276365	-0.00455689562848
2	-0.00543947593727	-0.00388321199916	-0.00388321199916	0.00543947593727
3	0.01702522388155	0.03466034684485	-0.03466034684485	0.01702522388155
4	0.02382538479492	-0.03887280126883	-0.03887280126883	-0.02382538479492
5	-0.10671180468667	-0.11720388769912	0.11720388769912	-0.10671180468667
6	0.01186609203380	0.27529538466888	0.27529538466888	-0.01186609203380
7	0.56881042071212	0.75614564389252	-0.75614564389252	0.56881042071212
8	0.75614564389252	0.56881042071212	0.56881042071212	-0.75614564389252
9	0.27529538466888	0.01186609203380	-0.01186609203380	0.27529538466888
10	-0.11720388769912	-0.10671180468667	-0.10671180468667	0.11720388769912
11	-0.03887280126883	0.02382538479492	-0.02382538479492	-0.03887280126883
12	0.03466034684485	0.01702522388155	0.01702522388155	-0.03466034684485
13	-0.00388321199916	-0.00543947593727	0.00543947593727	-0.00388321199916
14	0.00325314276365	-0.00455689562848	-0.00455689562848	-0.00325314276365

Table (A3): Q-shift filters (after first stage) of type ‘qshift\_b’

## Appendix B

Filters used to implement DT-DWT(S) uses Selesnick's Dual-Tree DWT available from: selesi@taco.poly.edu, <http://taco.poly.edu/selesi/>

	<b>Analysis Filters</b>			
	Real Tree		Imaginary Tree	
	Lowpass	Highpass	Lowpass	Highpass
1	0	0	0.01122679215254	0
2	-0.08838834764832	-0.01122679215254	0.01122679215254	0
3	0.08838834764832	0.01122679215254	-0.08838834764832	-0.08838834764832
4	0.69587998903400	0.08838834764832	0.08838834764832	-0.08838834764832
5	0.69587998903400	0.08838834764832	0.69587998903400	0.69587998903400
6	0.08838834764832	-0.69587998903400	0.69587998903400	-0.69587998903400
7	-0.08838834764832	0.69587998903400	0.08838834764832	0.08838834764832
8	0.01122679215254	-0.08838834764832	-0.08838834764832	0.08838834764832
9	0.01122679215254	-0.08838834764832	0	0.01122679215254
10	0	0	0	-0.01122679215254

Table (B1): First stage analysis filters

	<b>Synthesis Filters</b>			
	Real Tree		Imaginary Tree	
	Lowpass	Highpass	Lowpass	Highpass
1	0	0	0	-0.01122679215254
2	0.01122679215254	-0.08838834764832	0	0.01122679215254
3	0.01122679215254	-0.08838834764832	-0.08838834764832	0.08838834764832
4	-0.08838834764832	0.69587998903400	0.08838834764832	0.08838834764832
5	0.08838834764832	-0.69587998903400	0.69587998903400	-0.69587998903400
6	0.69587998903400	0.08838834764832	0.69587998903400	0.69587998903400
7	0.69587998903400	0.08838834764832	0.08838834764832	-0.08838834764832
8	0.08838834764832	0.01122679215254	-0.08838834764832	-0.08838834764832
9	-0.08838834764832	-0.01122679215254	0.01122679215254	0
10	0	0	0.01122679215254	0

Table (B2): First stage synthesis filters

## Appendix B (Contd.)

	<b>Analysis Filters</b>			
	Real Tree		Imaginary Tree	
	Lowpass	Highpass	Lowpass	Highpass
1	0.03516384000000	0	0	-0.03516384000000
2	0	0	0	0
3	-0.08832942000000	-0.11430184000000	-0.11430184000000	0.08832942000000
4	0.23389032000000	0	0	0.23389032000000
5	0.76027237000000	0.58751830000000	0.58751830000000	-0.76027237000000
6	0.58751830000000	-0.76027237000000	0.76027237000000	0.58751830000000
7	0	0.23389032000000	0.23389032000000	0
8	-0.11430184000000	0.08832942000000	-0.08832942000000	-0.11430184000000
9	0	0	0	0
10	0	-0.03516384000000	0.03516384000000	0

Table (B3): Remaining stage (after first stage) analysis filters

	<b>Synthesis Filters</b>			
	Real Tree		Imaginary Tree	
	Lowpass	Highpass	Lowpass	Highpass
1	0	-0.03516384000000	0.03516384000000	0
2	0	0	0	0
3	-0.11430184000000	0.08832942000000	-0.08832942000000	-0.11430184000000
4	0	0.23389032000000	0.23389032000000	0
5	0.58751830000000	-0.76027237000000	0.76027237000000	0.58751830000000
6	0.76027237000000	0.58751830000000	0.58751830000000	-0.76027237000000
7	0.23389032000000	0	0	0.23389032000000
8	-0.08832942000000	-0.11430184000000	-0.11430184000000	0.08832942000000
9	0	0	0	0
10	0.03516384000000	0	0	-0.03516384000000

Table (B4): Remaining stage (after first stage) synthesis filters

## Appendix C

Test images for 2-D denoising. All images are 512 by 512 except  
'Pattern' image, which is 256 by 256

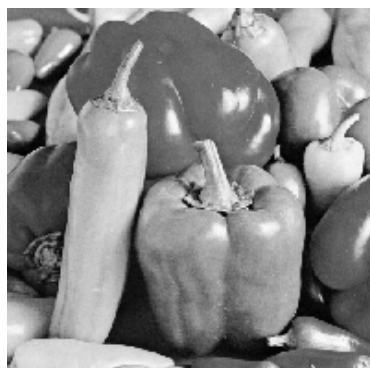
Lenna



Goldhill



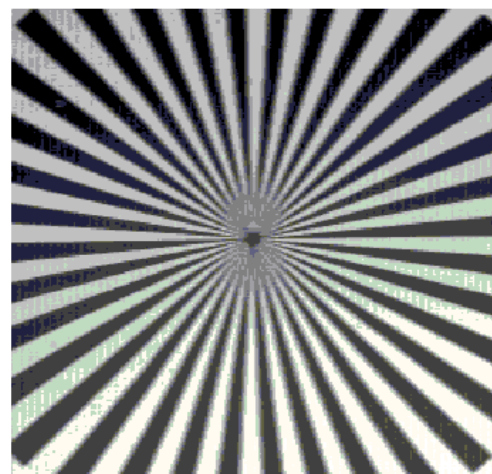
Peppers



Airplane



Pattern



## References

- 1 C Sidney Burrus, R A Gopinath, and Haitao Guo, ‘Introduction to Wavelets and Wavelet Transforms: A Primer’, Prentice Hall, NJ, 1998
- 2 Stephane Mallat, ‘A Wavelet Tour of Signal Processing’, 2/ed, Academic Press, 1999
- 3 J Littlewood, and R Paley, ‘Theorems on Fourier Series and Power Series’, Proc. London Math. Soc., 42, 52-89, 1937
- 4 A Calderon, ‘Intermediate Spaces and Interpolation, the Complex Method’, Studia Math., 24, 113-190, 1964
- 5 J Morlet et al., ‘Wave Propagation and Sampling Theory’, Geophysics, 47, 203-236, 1982
- 6 A Grossmann, and J Morlet, ‘ Decomposition of Hardy Functions into Square Integrable Wavelets of Constant Shape’, SIAM J. Math. Anal., 15, 723-736, 1984
- 7 Y Meyer, ‘Orthonormal Wavelets’ in Wavelets: Time-Frequency Methods and Phase Spaces (J M Combes, A Grossmann and Ph Tchamitchian, editors), 2/ed, Springer Verlag, NY, 21-37, 1989
- 8 I Daubechies, ‘Where do Wavelets Come From?- A Personal Point of View’, Proc. IEEE, 84(4), 510-513, 1996
- 9 Barbara B Hubbard, ‘The World According to Wavelets’, A K Peters Ltd., Wellesley, MA, 1996
- 10 G Strang, ‘Wavelets and Dilation Equations: A Brief Introduction’, SIAM Review, 31(4), 614-627, 1989
- 11 O Rioul, and M Vetterli, ‘Wavelets and Signal Processing’, IEEE Sig. Proc. Mag., 14-38, 1991
- 12 Amara Graps, ‘Introduction to Wavelets’, IEEE Computational Sciences and Engineering, 2(2), 50-61, 1995,  
URL:<http://www.cis.udel.edu/~amer/CISC651/IEEEwavelet.pdf>
- 13 Robi Polikar, ‘The Story of Wavelets’, In physics and Modern topics in Mechanical and Electrical Engineering (ed. N Mastorakis), 192-197, World

- Scientific and Eng. Society Press,  
URL:<http://engineering.rowan.edu/%7epolikar/WAVELETS/WTtutorial.htm>
- 14 G Strang, and T Nguyen, ‘Wavelets and Filter Banks’, Wellesley-Cambridge Press, 1996
- 15 M Vetterli, and J Kovacevic, ‘Wavelets and Subband Coding’, Prentice Hall, NJ, 1995
- 16 R M Rao, and A S Bopardikar, ‘Wavelet Transforms: Introduction to Theory and Applications’, Prentice Hall PTR, 1998
- 17 J S Walker, ‘A Primer on Wavelets and their Scientific Applications’, CRC Press, 1999
- 18 Jaideva C Goswami, and A K Chan, ‘Fundamentals of Wavelets: Theory, Algorithm and Applications’, John Wiley & Sons, 1999
- 19 A Jensen, and A la Cour-Harbo, ‘Ripples in Mathematics’, Springer Verlag, 2001
- 20 C K Chui, ‘Wavelets: A Tutorial in Theory and Applications’, Academic Press, NY, 1992
- 21 C K Chui, S J Liu, and A K Chan, ‘Wavelets in a Box’, Academic Press, 1998
- 22 G Kaiser, ‘A Friendly Guide to Wavelets’, Birkhauser, Boston, 1994
- 23 D Lokenath, ‘Wavelets Transforms and their Applications’, Birkhauser, Boston, 2002
- 24 I Daubechies, ‘Ten Lectures on Wavelets’, 61, SIAM Publications, 1992
- 25 The Mathworks, ‘Wavelet Toolbox (ver 2.2) User’s Guide’, 2002,  
URL: [www.mathworks.com](http://www.mathworks.com)
- 26 I Daubechies, ‘Orthonormal Bases of Compactly Supported Wavelets’, Comm. Pure and Applied Math., 41, 909-996, 1988
- 27 S G Mallat, ‘A Theory for Multiresolution Signal Decomposition: The Wavelet Representation’, IEEE Trans. Pattern Reco. and Machine Int., 11(7), 674-693, 1989
- 28 P P Vaidyanathan, ‘Multirate Systems and Filter Banks’, Prentice Hall, 1993

## References

- 29 A Cohen, I Daubechies, and J C Feauveau, ‘Biorthogonal Bases of Compactly Supported Wavelets’, Communications of Pure and Applied Math., 45(5), 485-560, 1992
- 30 W Sweldens, ‘The Lifting Schemes: A Custom Design Construction of Biorthogonal Wavelets’, Applied and Communicational Harmonic Analysis, 3(2), 186-200, 1996
- 31 R R Coifman and D L Donoho, ‘Translation Invariant De-noising’, in A Antoniadis (editor): Wavelets and Statistics, Springer Verlag, 1995
- 32 M Vetterli, and C Herley, ‘Wavelets and Filterbanks: Theory and Design’, IEEE Trans. ASSP, 2207-2232, 1992
- 33 A K Soman, P P Vidyanathan, and T Q Nguyen, ‘Linear Phase Paraunitary Filterbanks: Theory, Factorization and Designs’, IEEE Trans. Sig. Proc., 41(12), 3480-3496, 1993
- 34 IEEE93, ‘Special Issue on Wavelets and Signal Processing’, IEEE Trans. Sig. Proc., 41(12), 3213-3600, 1993
- 35 IEEE92, ‘Special Issue on Wavelet Transform and Multiresolution Signal Analysis’, IEEE Trans. Info. Theory, 38(2, PartII), 529-924, 1992
- 36 A Brice, D L Donoho, and H Y Gao, ‘Wavelets Analysis’, IEEE Spectrum, 33(10), 26-35, 1996
- 37 F Hlawatsch, and G F Boudreux-Bartles, ‘Linear and Quadratic Time-Frequency Signal Representations’, IEEE Sig. Proc. Magazine, 9 (2), 21-67, 1992
- 38 I Daubechies, ‘The Wavelet Transform, Time-Frequency Localization and Signal Analysis’, IEEE Trans. Info. Theory, 36, 961-1005, 1990
- 39 L Cohen, ‘Time-Frequency Distributions- A Review’, Proc. of IEEE, 77(7), 941-981, 1989
- 40 D Gabor, ‘Theory of Communication’, Journal of the IEE, 93, 429-457, 1946
- 41 J B Allen, and L R Rabinar, ‘A Unified Approach to Short-Time Fourier Analysis and Synthesis’, Proc. IEEE, 65, 1558-1564, 1977
- 42 M R Portnoff, ‘Time-Frequency Representation of Digital Signals and Systems Based on Short-Time Fourier Analysis’, IEEE Trans. ASSP, 28, 55-69, 1980

## References

- 43 R Bracewell, ‘The Fourier Transform and its Applications’, 2/ed, McGraw-Hill, NY, 1986
- 44 W M Siebert, ‘Circuits, Signals and Systems’, MIT Press and McGraw-Hill, 1986
- 45 J O Stromberg, ‘A Modified Franklin System and Higher Order Spline Systems on  $\mathbb{R}^N$  as Unconditional Bases for Hardy Spaces’, in W Beckner(editor): Proc. of Conf. In Honour of A Zygmund, 475-493, Wadsworth Mathematics Series, 1992
- 46 G Battle, ‘A Block Spin Construction of Ondeletts; Part I: Lamarie Functions’, Commu. Math. Phys., 110, 601-615, 1987
- 47 G Battle, ‘A Block Spin Construction of Ondeletts; Part I: The QFT Connection’, Commu. Math. Phys., 114, 93-102, 1988
- 48 Y Meyer, ‘Ondeletts, Ondeletts et Operateurs’, Paris: Hermann, 1990
- 49 S Mallat, ‘Multiresolution Approximations and Wavelet Orthonormal Bases of  $L_2(\mathbb{R})$ ’, Trans. American Math. Soc., 315, 69-87, 1989
- 50 B Jawerth, and W Sweldens, ‘An Overview of Wavelet Based Multiresolution Analysis’, SIAM Review, 36, 377-412, 1994
- 51 M Vetterli, ‘Filterbanks Allowing Perfect Reconstruction’, Sig. Proc., 10(3), 219-244, 1986
- 52 N J Fligde, ‘Multirate Digital Signal Processing’, John Wiley & Sons, 1994
- 53 M J Smith, and T P Barnwell, ‘Exact Reconstruction Techniques for Tree-Stured Subband Coders’, IEEE Trans. ASSP, 34, 434-441, 1986
- 54 O Rioul, ‘Regular Wavelets: A Discrete-Time Approach’, IEEE Trans. Sig. Proc., 41(12), 3572-3579, 1993
- 55 H Volkemer, ‘On Regularity of wavelets’, IEEE Trans. Info. Theory, 38(2), 872-876, 1992
- 56 S Mallat, and WL Hwang, ‘Singularity Detection and Processing with Wavelets’, IEEE Trans. Info. Theory, 38, 617-643, 1992
- 57 G Karlson, and M Vetterli, ‘Theory of Two-Dimensional Multirate Filterbanks’, IEEE Trans. Sig. Proc., 38 (6), 925-937, 1990
- 58 ISO/IEC JTC 1/SC 29/WG1 N943, ‘JPEG2000 Requirements and Profiles’, International Organization of Standardization, Copenhagen, 1999

## References

- 
- 59 J Kovacevic, and M Vetterli, ‘Nonseparable Multidimensional Perfect Reconstruction Filterbank and Wavelet Bases for  $R^n$ ’, IEEE Trans. Info. Theory, 38(2), 533-555, 1992
- 60 M Vetterli, and J Kovaevic, ‘Wavelets and Subband Coding’, Englewood Cliffs, NJ: Prentice Hall, 1995
- 61 Y P Lin, and P P Vidyanathan, ‘Theory and Design of Two Dimensional Filter Banks: A Review’, Multidimensional Systems and Signal Processing, 7, 263-30, 1996
- 62 D Stanhill, and Y Y Zeevi, ‘Two-Dimensional Orthogonal Filterbanks and Wavelets with Linear Phase’, IEEE Trans. Signal processing, 46(1), 183-190, 1998
- 63 R Andrew, and D T Nguyen, ‘Separable Versus Quincunx Wavelet Transforms for Image Compression’, 6<sup>th</sup> IEEE int. Workshop on Signal Processing and Communication Systems, Melbourne, Australia, 1998
- 64 O S Haddadin, V J Mathews, and T G Stockham, ‘Subband Vector Quantization of Images using Hexagonal Filterbanks’, In J.A. Storer and M. Cohn, editors, Proceedings Data Compression Conference, IEEE Computer Society Press, 2-11, Snowbird, Utah, March 1992
- 65 K Ramchandran, and M Vetterli, ‘Best Wavelet Packet Bases in a Rate-Distortion Sense’, IEEE Trans. Image processing, 2(2), 160-175, 1993
- 66 R R Coifman, and M V Wickerhauser, ‘Entropy Based Algorithms for Best Bases Selection’, IEEE Trans. Info. Theory, 38(2), 713-718, 1992
- 67 M V Wickerhauser, ‘Adapted Waveform Analysis from Theory to Software’, A K Peters Ltd., 1995
- 68 Harri Ojanen, ‘WAVEKIT: a Wavelet Toolbox for Matlab’, 1998, <http://www.math.rutgers.edu/~ojanen/wavekit/index.html>
- 69 M J Shensa, ‘The Discrete Wavelet Transform: Wedding the ‘A Trou’ and Mallat’s Algorithms’, IEEE Trans. Info. Theory, 40, 2464-2482, 1992
- 70 J C van den Berg (editor), ‘Wavelets in Physics’, Cambridge University Press, 1999
- 71 A Aldroubi, and M Unser (editors), ‘Wavelets in Medicine and Biology’, CRC Press, 1996

## References

- 72 E J Stollnitz et al, ‘Wavelets for Computer Graphics: Theory and Applications’, Morgan Kaufmann, 1996
- 73 Ali N Akansu, and M J Medley (editors), ‘Wavelet, Subband, and Block Transforms in Communications and Multimedia’, Kluwer Academic Publishers, 1999
- 74 Carl Taswell, ‘Handbook of Wavelet Transform Algorithms’, Birkhauser, 2002
- 75 Felix Fernandes, ‘Directional, Shift-insensitive, Complex Wavelet Transforms with Controllable Redundancy’, PhD Thesis, Rice University, 2002
- 76 H Guo, ‘Theory and Applications of Shift-invariant, Time-varying and Undecimated Wavelet Transform’, MS Thesis, Rice University, 1995
- 77 I Cohen, S Raz, and D Malah, ‘Shift-invariant Wavelet Packet Bases’, Proc.. ICASSP-95, Detroit, MI, 1081-1084, 1995
- 78 A Said, and W Pearlman, ‘A New Fast and Efficient Image Codec Based on Set Partitioning in Hierarchical Trees’, IEEE Trans. Cir. and Sys. For Video Tech., 6, 243-250, 1996
- 79 J Li, PY Cheng, and C C J Kuo, ‘An Embedded Wavelet Packet Transform Technique for Texture Compression’, In SPIE, 2569, 602-613, 1995
- 80 L Balmelli, and A Mojsilovic, ‘Wavelet Domain Features for Texture Description, Classification and Reliability Analysis’, Proc. IEEE Int. Conf. On Image Proc. ( ICIP), 4, 440-444, 1999
- 81 M C Morrone, and D C Burr, ‘Feature Detection in Human Vision: A Phase Dependent Energy Model’, Proc. R. Soc. Lond., B 235, 221, 1988
- 82 T D Tran, R L de Queiroz, and T Nguyen, ‘Linear-phase Perfect Reconstruction Filterbank: Lattice Structure, Design and Application in Image Coding’, IEEE Trans. Sig. Proc. 48, 133-147, 2000
- 83 A V Oppenheim, and J S Lim, ‘The Importance of Phase in Signals’, Proc. IEEE, 69, 529-541, 1981
- 84 G P Lorenzetto, and P Kovesi, ‘A Phase Based Image Comparison Technique’, DICTA99, University of Western Australia, 1999

- 85 J Driesen, and R Belmans, ‘Time-Frequency Analysis in Power Measurement Using Complex Wavelets’, IEEE Int. Sympo. on Cir. and Sys. (ISCAS2002), 681-684, 2002
- 86 W Lawton, ‘Applications of Complex Valued Wavelet Transforms to Subband Decomposition’, IEEE Trans. Sig. Proc., 41, 12, 3566-3568, 1993
- 87 J M Lina, ‘Image Processing with Complex Daubechies Wavelets’, J. of Math. Imaging and Vision, 7, 211-223, 1997
- 88 T Bulow, and G Sommer, ‘Hypercomplex Signals- A Novel Extension of the Analytic Signal to the Multidimensional Case’, IEEE Trans. Sig. Proc., 49, 11, 2001
- 89 Adolf Cusmariu, ‘Fractional Analytic Signals’, Signal Processing, Elsevier, 82, 267 – 272, 2002
- 90 X P Zang, M Desai, and Y N Peng, ‘Orthogonal Complex Filter Banks and Wavelets: Some Properties and Design’, IEEE Trans. Sig. Proc., 47 ,4, 1999
- 91 J M Lina, ‘Complex Daubechies Wavelets: Filter Design and Applications’, Proc. ISAAC Conf., University of Delaware, 1997
- 92 B Belzar, J M Lina, and J Villasenor, ‘Complex Linear Phase Filters for Efficient Image Coding’, IEEE Trans. Sig. Proc., 1995
- 93 N G Kingsbury, ‘Image Processing with Complex Wavelets’, Phil. Trans. Royal Society London, 1999
- 94 N G Kingsbury, ‘Shift Invariant Properties of the Dual-Tree Complex Wavelet Transform’, Proc. IEEE Conf. on Acoustics, Speech and Signal Processing, Phoenix, AZ, paper SPTM 3.6, March 16-19, 1999
- 95 N G Kingsbury, ‘Complex Wavelets for Shift Invariant Analysis and Filtering of Signals’, Journal of Applied and Computational Harmonic Analysis, 10, 3, 234-253, 2001
- 96 N G Kingsbury, ‘Design of Q-shift Complex Wavelets for Image Processing using Frequency Domain Energy Minimization’, Preprint, ICIP03
- 97 Homepage of Prof. N G Kingsbury, <http://www-sigproc.eng.cam.ac.uk/~ngk/>
- 98 I W Selesnick, ‘Hilbert Transform Pairs of Wavelet Bases’, IEEE Sig. Proc. Letters, 8,6,170-173, 2001

- 99 I W Selesnick, ‘The Design of Hilbert Transform Pairs of Wavelet Bases via the Flat Delay Filter’, Proc. of ICASSP, Salt lake City, UT, 2001
- 100 Homepage of Prof. Selesnick, <http://taco.poly.edu/selesi/>
- 101 F Fernandes, ‘Directional, Shift-Insensitive, Complex Wavelet Transforms with Controllable Redundancy’, PhD Thesis, Rice University, 2002
- 102 F Fernandes, R van Spaendonck, M Coates, and C S Burrus, ‘Directional Complex Wavelet Processing’, in Wavelet Applications VII, Proc. of SPIE, 2000
- 103 R Spaendonck, T Blue, R Baraniuk, and M Vetterli, ‘Orthogonal Hilbert Transform Filterbanks and Wavelets’, ICASSP03, April 6-10, 2003
- 104 R Spaendonck, F Fernandes, M Coates, and C Burrus, ‘Non-redundant, Directionally Selective, Complex Wavelets’, IEEE Proc. of Int. Conf. Image Proc., 379-382, 2000
- 105 F Fernandes, I W Selesnick, R Spaendonck, and C Burrus, ‘Complex Wavelets Transforms with Allpass Filters’, Preprint, EURASIP 2003
- 106 S. Hahn, ‘Hilbert Transforms in Signal Processing’, Artech House, Boston, MA, 1996
- 107 I W Selesnick, ‘The Double Density DWT’, ( In A Petrosian and F G Meyer; editors, Wavelets in Signal and Image Analysis: from Theory to Practice’), Kluwar, 2001
- 108 I W Selesnick, ‘The Double Density Dual-Tree Discrete Wavelet Transforms’, IEEE Trans. Sig. Proc., 2001
- 109 P P Vidyanathan, P Q Hoang, ‘Lattice Structures for Optimal Design and Robust Implementation of Two-channel Perfect Reconstruction QMF Banks’, IEEE Trans. ASSP, 81-94, January, 1988
- 110 A Farris, ‘Wavelet Design using Grobner Bases’, PhD Thesis, Polytechnic University, NY, 2003
- 111 J Magarey, and N G Kingsbury, ‘Motion Estimation using Complex-valued Wavelet Transform’, IEEE Trans. Sig. Proc., 46(4), 1998
- 112 P Hill, N Canagarajah, and D Bull, ‘Image Fusion using Complex Wavelets’, BMVC 2002, Cardiff University, 2-5 Sept 2002.

- 113 S Hatipoglu, S K Mitra, and N. Kingsbury, ‘Image Texture Description using Complex Wavelet Transform’, Proc. Int. Conf. Image Proc., Vancouver, B.C., Canada, vol. II, 530-533, September 2000
- 114 F Fernandes, R Spaendonck, and C Burrus, ‘A New Framework for Complex Wavelet Transforms’, preprint draft for IEEE Trans. Sig. Proc, 2002
- 115 P. Loo, ‘Digital Watermarking Using Complex Wavelets’, PhD thesis, University of Cambridge, 2002
- 116 C Taswell, ‘The What, How and Why of Wavelet Shrinkage Denoising’, IEEE Computing Science and Engineering, 2(3), 12-19, 2000
- 117 A Weeks, ‘Fundamentals of Electronic Image Processing’, SPIE Optical Engineering Press and IEEE press, 1996
- 118 R C Gonzalez, and R E Woods, ‘Digital Image Processing’, 2/ed, Addison Wesley, 1992
- 119 A Murat Tekalp, ‘Digital Video processing’, Prentice Hall, 1996
- 120 R Neelamani, H Choi, and R G Baraniuk, ‘ForWaRD: Fourier-Wavelet Regularized Deconvolution for Ill-Conditioned Systems’, to appear in IEEE Trans. Sig. Proc., 2003.
- 121 J S Lee, ‘Digital Image Enhancement and Noise Filtering by use of Local Statistics’, IEEE PAMI, 2, 165-168, 1980
- 122 W K Pratt, ‘Generalized Wiener Filtering Computation Techniques’, IEEE Trans. Computers, C-21, 636-692, 1972
- 123 D L Donoho, and I M Johnston, ‘Ideal Spatial Adaptation by Wavelet Shrinkage’, Biometrika, 81(3), 425-455, 1994
- 124 D L Donoho, ‘De-noising by Soft Thresholding’, IEEE Trans. Info. Theory, 41(3), 613-627, 1995
- 125 S G Chang, B Yu, and M Vetterli, ‘Adaptive Wavelet Thresholding for Image Denoising and Compression’, IEEE Trans. Image Proc., 9(9), 1532-1546, 2000
- 126 J Qian, ‘Denoising by Wavelet Transform’, Rice University, USA
- 127 J C Woods, and K L Johnston, ‘Wavelet-denoising of Magnetic Resonance Images: Importance of Rician Statistics’, Magnetic Resonance in Medicine, 41, 631-635, 1999

- 128 L Gagnon, and A Jounan, ‘Speckle Filtering of SAR images- A Comparative Study between Complex-wavelet-based and Standard Filters’, SPIE Proc., 3169, 80-91, 1997
- 129 H Guo et.al., ‘Wavelet based Speckle Reduction with Application to SAR Based ATD/R’, 1, 75-79, ICIP, 1994
- 130 G Cincotti, G Loi, and M Pappalardo, ‘Frequency Decomposition and Compounding of Ultrasound Medical Images with Wavelet Packets’, IEEE Trans. on Medical Imaging, 20(8), 2001
- 131 R Nowak, and R Baraniuk, ‘Wavelet-domain Filtering for Photon Imaging Systems’, IEEE Trans. on Image Proc., 8(5), 666-678, 1999
- 132 R Nowak, ‘Wavelet-based Rician Noise Removal for Magnetic Resonance Imaging’, IEEE Trans. on Image Proc., 8(10), 1408-1419, 1999
- 133 R R Coifman, and D L Donoho, ‘Translation Invariant De-noising’, in Wavelets and Statistics, 125-150, Springer Verlag, 1995
- 134 J Stark, F Murtagh, and A Bijaoui, ‘Image Processing and Data Analysis: The Multiscale Approach’, Cambridge University Press, 1998
- 135 M Lang, H Guo, J Odegard, and C S Burrus, ‘Noise Reduction using an Undecimated Wavelet Transforms’, IEEE Sig. Proc. Letters, 1996
- 136 N G Kingsbury, ‘Image Processing with Complex Wavelets’, Phil. Trans. Royal Society London, 1999
- 137 J Romberg, H Choi, R Baraniuk, and N G Kingsbury, ‘Hidden Markov Tree Models for Complex Wavelet Transforms’, IEEE Trans. Sig. Proc., 2002
- 138 J Liu, and P Moulin, ‘Complexity Regularized Image Denoising’, IEEE Trans. on Image Proc., 10(6), 841-851, 2001
- 139 L Sendur, and I W Selesnick, ‘Bivariate Shrinkage Functions for Wavelet Based Denoising Exploiting Interscale Dependency’, IEEE Trans. Sig. Proc., 50(11), 2744-2756, 2002
- 140 E J Candes, and D L Donoho, ‘Ridgelets: A Key to Higher-dimensional Intermittency’, Phil. Trans. Royal Soc. London, 2495-2509, 1999
- 141 J Starck, E J Candes, and D L Donoho, ‘The Curvelet Transform for Image Denoising’, IEEE Trans. on Image Proc., 11(6), 2002

- 142 M N Do, and M Vetterli, ‘The Contourlet Transform: An Efficient Directional Multiresolution Image Representation’, Submitted to IEEE Trans. Image Proc., 2003
- 143 P Wolfe, and S J Godsill, ‘Audio Signal Processing Using Complex Wavelets’, Conference of Audio Engineering Society, 2003
- 144 M D Hazas, ‘Processing of Non-stationary Audio Signals’, M S Thesis, University of Cambridge, 1999
- 145 N A Whitmal, J C Rutledge, and J Cohen, ‘Wavelet Based Noise Reduction’, Proc. IEEE ICASSP-95, 5, 3003-3006, 1995
- 146 P K Ramarapu, and R C Maher, ‘Methods for Reducing Audible Artifacts in a Wavelet-based Broadband Denoising Systems’, Journal of Audio Engineering Society, 46(3), 178-190, 1998
- 147 J B Allen, ‘Short Term Spectral Analysis, Synthesis, and Modification by Discrete Fourier Transform’, IEEE Trans. on ASSP, 25(3), 235-238, 1977
- 148 A K Jain, ‘Fundamentals of Digital Image Processing’, Prentice Hall, NJ, 1990
- 149 J S Lim, ‘Two Dimensional Signal and Image Processing’, Prentice Hall, NJ, 1990
- 150 K R Castleman, ‘Digital Image Processing’, Prentice Hall, NJ, 1996
- 151 Image Processing Toolbox User’s Guide, MathWorks Inc., URL: [www.mathworks.com](http://www.mathworks.com)
- 152 V Torre, and T Poggio, ‘On Edge Detection’, IEEE Trans. on PAMI, 8, 147-163, 1986
- 153 L S Davis, ‘A Survey of Edge Detection Techniques’, CGIP, 4, 248-270, 1975
- 154 V S Nalwa, ‘A Guided Tour of Computer Vision’, Addison-Wesley, 1993
- 155 L G Shapiro, and G Stockman, ‘Computer Vision’, Prentice Hall, 2001
- 156 J Ponce, and M Brady, ‘Towards a Surface Primal Sketch’, in Three Dimensional Vision, editor: T Kanade, Academic press, NY, 1985
- 157 B Berter, T A Poggio, and V Torre, ‘Ill-posed Problems in Early Vision’, Proc. IEEE, 76, 869-889, 1998
- 158 D Marr, and E C Hildreth, ‘Theory of Edge Detection’, Proc. R. Soc. London, B207, 187-217, 1980

- 159 R M Haralick, 'Digital Step Edges from Zero Crossings of Second Directional Derivatives', IEEE Trans. PAMI, 6(1), 58-68, 1984
- 160 K S Shanmugam, F M Dickey, and J A Green, 'An Optimal Frequency Domain Filter for Edge Detection in Digital Pictures', IEEE Trans. PAMI, 1, 37-43, 1979
- 161 J Canny, 'A computational Approach to Edge Detection', IEEE Trans. PAMI, 8, 679-698, 1986
- 162 M Heath, S Sarkar, T Sanoki, and K W Bowyer, 'A Robust Visual Method for Assessing the Relative Performance of Edge Detection Algorithms', IEEE Trans. PAMI, 19 (12), 1338-1359, 1997
- 163 S Mallat, and W L Hwang, 'Singularity Detection and Processing with Wavelets', IEEE Trans. Info. Theory, 38, 617-643, 1992
- 164 S Mallat, and S Zong, 'Characterization of Signals form Multiscale Edges', IEEE Trans. PAMI, 14, 710-732, 1992
- 165 Y Xu, J Weaver, D Healy, and J Lu, 'Wavelet Transform Domain Filters: A Spatially Selective Noise Filtration Technique', IEEE Trans. Image Proc., 3, 747-758, 1994
- 166 A Rosenfeld, and M Thurston, 'Edge and Curve Detection for Visual Scene Analysis', IEEE Trans. Computer, 20, 562-569, 1970
- 167 B M Sadler, T Pham, and L C Sadler, 'Optimal and wavelet based Shock Wave Detection and Estimation', J Acoust. Soc. Am., 104(2), 955-963, 1998
- 168 D Ziou, and S Tabbone, 'A Multiscale Edge Detector', PR, 26(9), 1305-1314, 1993
- 169 D J Park, K N Nam, and R H Park, 'Multiresolution Edge Detection Techniques', Pattern Recognition, 28(1), 211-219, 1995
- 170 C L Du, and W L Hwang, 'Singularity Detection and Characterisation with Complex Valued Wavelets and Their Applications', -----
- 171 M Unser, 'Ten Good Reasons for Using Spline Wavelets', Proc. SPIE, 3169, wavelet Applications in Signal and Image Proc., 5, 422-433, 1997
- 172 Yu P Wong, and S L Lee, 'Scale-space Derived from B-Splines', IEEE Trans. PAMI, 20(10), 1040-1055, 1998

- 173 S Kadambe, G Faye, and B Bartel, ‘Application of the Wavelet Transform for Pitch Detection of Speech Signals’, IEEE Trans. Info. Theory, 38(2), 917-924, 1992
- 174 C Li, C Zeng, and C Tai, ‘Detection of ECG Characteristic Points Using Wavelet Transforms’, IEEE Trans. Biomed. Eng., 42, 21-28, 1995
- 175 K Anant, and F Dowla, ‘Wavelet Transform Methods for Phase Identification in Three Component Seismograms’, Bull. Seism. Soc. Am., 87(6), 1598-1612, 1997
- 176 S K Setarehdan, and J J Soraghan, ‘Automatic Cardiac LV Boundary Detection and Tracking Using Hybrid Fuzzy Temporal and Fuzzy Multiscale Edge Detection’, IEEE Trans. Biomed. Eng., 46(9), 1111, 1999
- 177 A S Akbari, and J J Soraghan, ‘Fuzzy-based Multiscale Edge Detection’, IEE Electronic Lett., 39(1), 30-31, 2003
- 178 D Dubois, and H Prade, ‘Fuzzy Sets and Systems: Theory and Applications’, Academic and Harcourt Brace Jovanovich, NY, 1980
- 179 R Derich, ‘Fast Algorithms for Low-level Vision’, IEEE Trans. PAMI, 2, 78-87, 1990
- 180 D Ziou, and S Tabbone, ‘Edge Detection Techniques – An Overview’, Int. J. of Pat. Rec. and Image. Analysis, 8(4), 537-559, 1998
- 181 T McInerney, D Terzopoulos, ‘Deformable Models in Medical Image Analysis: A Survey’, Med. Img. Ana., 1(2), 91-108, 1996
- 182 I Pollak, A S Willsky, and H Krim, ‘Image Segmentation and Edge Detection with Stabilised Inverse Diffusion Equations (SIDE)’, IEEE Trans. Image Proc., 9(2), 2000
- 183 C Hao, M Qi, O Heute, and C Moraga, ‘New Method for Fast Edge Detection Based on Subband Decomposition’, Image Anal. Stereol, 20, 53-57, 2001
- 184 L S Rogers, and C Johnston, ‘SAR Image Despeckling using Multiscale Edge Representation’, IEEE IGARSS98, 10-12, 1998
- 185 B Zhu, A H Tewifik, M A Colestock, O N Grel, and P E Cetin, ‘Image Coding with Wavelet Representation, Edge Information and Visual Masking’, 1(1), ICIP95, 1995

- 186 H Li, B S Manjunath, and S K Mitra, 'Multisensor Image Fusion using Wavelet Transform', *Graphical Models and Image Proc.*, 57(3), 235-245, 1995
- 187 C T Hsu, and R A Beuker, 'Multiresolution Feature Based Image Registration', *Proc. SPIE*, 4067, 1490-1498, 2000
- 188 S Kulkarni, and B Verma, 'An Intelligent Hybrid Approach For Content Based Image Retrieval', *Int. J. of Computational Intelligence and Applications*, World Scientific Publishing, 2(2), 173-184, 2003
- 189 C Busch, 'Wavelet Based Texture Segmentation on Multimodal Tomographic Images', *Comp. And Graphics*, 21(3), 347-358, 1997
- 190 M A Mohimeed, and C C Li, 'Motion Estimation and Compensation Based on Almost Shift-invariant wavelet Transform for Image Sequence Coding', *IEEE Trans. Cir. Syst. For Video Tech.*, 214-229, 1998
- 191 A S Akbari, and J J Soraghan, 'Multiscale Fuzzy Reasoning (MFR) for Object Extraction', *IEEE Int. Workshop NNSP2003*, 2003
- 192 K Rieth, and J Geikler, 'FRED: Fuzzy Reasoning Edge Detection', Nasa's Technology Transfer Program, NASA Technology Applications Team KSC, Fax: 919-541-6221, 2003
- 193 M R Rezaee et al, 'A Multiresolution Image Segmentation Technique Based on Pyramidal Segmentation and Fuzzy Clustering', *IEEE Trans. Image Proc.*, 9(7), 1238-1248, 2000
- 194 C W Shaffey, N G Kingsbury, and I H Jermyn, 'Unsupervised Image Segmentation via Markov Trees and Complex Wavelets', *IEEE ICIP02*, 2002
- 195 H Choi, and R G Baraniuk, 'Multiscale Image Segmentation using Wavelet Domain Hidden Markov Models', *IEEE Trans. Image Proc.*, 10(9), 1309-1321, 2001
- 196 M Thuillard, 'A Review of Wavelet Networks, Wavenets, Fuzzy Wavenets and Their Applications', ESIT 2002, Germany, 2002
- 197 M Gendron, 'Wavelet Multiscale Edge Detection Using an ADALINE Neural Network to Match-up Edge Indicators', *Int. Conf. on Industry, Eng. and Management Systems*, Florida, (NRL/PP/7440-01-1016), 2002

References

- 198 P Chalermnot, and T El-Ghazawi, ‘Multiresolution Image Registration using Genetics’, 452-456, Proc. ICIP99, 1999
- 199 I E Abdou, and W K Pratt, ‘Quantitative Design and Evaluation of Enhancement/Thresholding Edge Detectors’, Proc. IEEE, 67(5), 753-763, 1979
- 200 V Ramesh, and R M Haralick, ‘Performance Characterization of Edge Detectors’, SPIE 1708, 252-266, 1992